STABILITY INVESTIGATION OF THERMALLY INDUCED FLOW OSCILLATIONS IN CRYOGENIC HEAT EXCHANGERS

FINAL REPORT

October 1967

J. C. Friedly
J. L. Manganaro
P. G. Kroeger
Research and Development Center
General Electric Company
Schenectady, New York

Contract NAS8-21014

Prepared for

GEORGE C. MARSHALL SPACE FLIGHT CENTER
NATIONAL AERONAUTICS AND SPACE ADMINISTRATION
HUNTSVILLE, ALABAMA

ABSTRACT

An analytical model describing thermally induced flow oscillations in heat exchangers for supercritical fluids has been compared with experimental data. The model is basically that developed previously by Dr. Novak Zuber. The effect of the heat transfer rate to the tube wall has been added. The model and the data are shown to be consistent and reasonably close in agreement on the appearance of the oscillations. It is found that the rate of heat transfer plays an important role in stabilizing the system.

From the full model a greatly simplified stability criterion is derived. The criterion is a single equation stating that for stability a ratio of stabilizing to destabilizing pressure drops must be greater than an expansion factor. All parameters in the criterion are theoretically based and can be predicted in advance; the criterion reduces directly to the correlation used successfully by Thurston. Therefore, it should be useful as a design tool.

ACKNOWLEDGMENTS

The authors are grateful to Professor N. Zuber of New York University for initially suggesting this problem to them. We acknowledge the many helpful discussions held with P. H. Kydd and F. W. Staub. A. Worlund of NASA, R. S. Thurston of Los Alamos, and J. R. Cleveland of Rocketdyne have all been most generous in furnishing information and comments during the course of the work.

TABLE OF CONTENTS

TABLE OF CONTENTS (Cont'd)

LIST OF ILLUSTRATIONS

LIST OF ILLUSTRATIONS (Cont'd)

LIST OF TABLES

Section 1

PROGRAM OBJECTIVES

In heating various cryogenic fluids close to their critical point, as for instance in rocket engine heat exchangers, severe oscillations have been experienced. The cause of these oscillations was the subject of previous research by Zuber,[1] who developed an analytical model for the prediction of thermally induced flow oscillations.

It is the objective of this investigation, performed under National Aeronautics and Space Administration Contract NAS8-21014, to verify the validity of Zuber's model by comparison with experimental data. If needed, modifications and extensions of the analysis are to be made. From a valid model, simple stability criteria are to be provided for use in design and applications.

Section 2

SUMMARY AND CONCLUSIONS

Experiments on flow oscillations in heat exchangers for supercritical fluids were compared with a stability analysis of an analytical model of the system. Data considered were for hydrogen taken by Thurston,[2] and for oxygen, two sets obtained from the National Aeronautics and Space Administration. Some data for subcritical boiling systems were also considered. The model is based on the equations of change for the fluid as originally formulated by Zuber.[1] Dynamics of heat transfer to the tube wall has been added to Zuber's model, requiring use of an approximate solution technique to obtain closed-form solutions. Stability is determined by use of the standard Nyquist stability criterion. Sensivity of the stability predictions to the approximations in the solution technique and to the calculation of model parameters from the data is considered.

A greatly simplified criterion developed from the general behavior of the Nyquist diagrams is in the form of a single inequality, indicating that a ratio of the stabilizing to destabilizing forces or pressure drops must exceed the size of the principal loop of the Nyquist diagram. The criterion includes the effect of upstream and downstream pressure drops, as well as the acceleration and friction pressure drops in the test section. There are no explicit limits on the degree of subcooling of the inlet fluid. Since all parameters in the criterion have a theoretical basis, the criterion can be used to predict stability in advance.

The comparison of the stability predictions made from the full analytical solution with the experimental data was consistent and reasonably good. The model tended to predict that the system was a little more unstable than was reported; there were exceptions, however. Much of the disagreement is believed to be near the limits of the accuracy of the analysis. On the basis of comparison with supercritical data it is concluded that all major effects contributing to the instability phenomenon are included in the model. There may of course be important effects which appear in a different apparatus, but those are not self-evident.

It was found that results obtained using the approximate analytical solution procedure were in adequate agreement with the exact numerical solution of the system equations. The approximate predictions generally tended to be closer to the stability limit. It was concluded that the analytic solution was a useful tool for this stability analysis.

The results were found to be relatively insensitive to an approximate equation of state if applied appropriately. Zuber suggested the use of two straight lines to approximate the specific volume-enthalpy relation for the fluid.[1] This approximation was found to be quite adequate if it permits the total fluid residence time in the exchanger to be closely matched.

The most serious limitation of the analysis is in the prediction of heat transfer coefficients used as parameters. The results are generally particularly sensitive to the heat transfer rate used. With large changes in physical properties, both with tube length and radius, prediction of the film heat transfer coefficient to be used in the analysis does not appear to be on firm ground. Those used were calculated from the Dittus-Boelter equation when experimental data were not available.

The simplified criterion developed from the analytic solution gives good agreement with all three sets of experimental data. It is particularly attractive because it is a simple equation and all parameters have a theoretical basis. The fact that the criterion was derived with no explicit limitations on its range of applicability for this system suggests a general utility. However, more experimental data are needed to investigate its limitations.

The criterion is shown to be of the same form as the correlation equation used successfully by Thurston.[3] However, it is believed to be of more general utility for two reasons: All parameters have a theoretical basis and can be predicted in advance. This criterion specifically includes the effect of inlet and exit pressure drops as well as the test section behavior, whereas Thurston's correlation accounts only for the energy input, flow rate, and fluid properties. Although Thurston's correlation is a reformulation of Zuber's first order equation, it has been found that Zuber's simplified criteria are not satisfactory for the prediction of stability.

Section 3

RECOMMENDATIONS

It is recommended that the model investigated here be used to predict possible unstable behavior in supercritical heat exchangers. The simplified criterion of Table 14, on page 107, should be used as a guideline for design purposes.

It is believed, however, that more experimental data on supercritical systems are needed to thoroughly test the model and the simplified criterion. These should be obtained in controlled laboratory conditions if at all possible. To test the model most efficiently measurements should be taken only at the system stability limit. It is important to measure all system pressure drops and the point heat transfer coefficient. The range of experimentation should be as broad as possible in the fluid residence time and the upstream pressure drop as well as in the usual independent parameters, energy input, flow rate, and pressure.

It is also suggested that more theoretical work be done to determine the effect of those property variations with temperature and pressure which have been ignored here. Special attention should be paid to the heat transfer parameters.

The model used here cannot be recommended for subcritical systems. More theoretical work is needed to define an adequate system model. Zuber's[4] most recent model may be satisfactory, but comparison with experimental data is needed.

Experimental work at subcritical pressures is not recommended until progress has been made toward an adequate model.

Section 4

INTRODUCTION

SIGNIFICANCE OF THE INSTABILITY PHENOMENON

When cryogenic fluids are strongly heated as they pass through a heat exchanger, flow oscillations can be encountered. This instability phenomenon can have detrimental effects on the system operation.

Platt and Wood[5] document instabilities observed in the development of the Saturn booster. Liquid oxygen is bled from the fuel system, heated to a gas, and used to pressurize the oxidizer tank. The instabilities can cause uneven oxidizer flow as well as mechanical failure.

Similar oscillations have been observed with other types of fluids as well. Forced and natural convection boiling liquids can also exhibit these so-called thermal-density flow oscillations. Such behavior can be very serious in a boiling-water reactor. An analogous phenomenon is the instability observed in liquid fuel combustion chambers.[6] There the heat of combustion replaces the external energy source.

Developmental rules of thumb have been formulated to cure an oscillating heat exchanger system if it becomes unstable. There is a need, however, for a simple criterion which will enable a designer to avoid potential unstable designs. It is believed that this can come only from a thorough knowledge of the cause of the instabilities.

PREVIOUS WORK

Zuber recently made a thorough review of the theoretical and experimental work on the instability phenomenon.[1] Most work has been done for subcritical two-phase systems. Zuber noted the similarity between the instability phenomena in subcritical and supercritical fluids and developed a theoretical model applicable both near and above the critical pressure. The model and simplifications derived from it gave good qualitative agreement with reported experimental observations.

Since Zuber's report several additional papers have appeared. Thurston reported extensive data on supercritical hydrogen[2] and suggested means of eliminating the oscillations.[7] Experimental studies by Stenning and Veziroglu[8] on Freon and Rogers[9] on hydrogen have been reported. Both were subcritical. Edeskuty and Thurston[3] published a correlation of several sets of sub- and supercritical data based on a simplified criterion of Zuber.[1] Sanathanan[10] developed an analytic technique which proved useful in modeling flow oscillations in boiling water reactor channels. Recently Zuber has extended his analysis to include slip velocity in two-phase systems.[4] In a study

which is related to but not exactly an instability problem, Hill and McCann[11] developed a feedback control scheme for a heat exchanger for a supercritical fluid.

SCOPE AND SIGNIFICANCE OF THIS WORK

This work takes the basic model of Zuber[1] and applies it primarily to three sets of data on flow oscillations in supercritical fluids. In Section 5, "Analytical Model," the model equations are developed along with modifications required by the data. The equations are solved approximately and the system characteristic equation is obtained. The procedure for determining the stability is outlined in Section 5 under the heading Stability Analysis. Section 6 contains the analysis of the data. The principal assumptions and limitations of the model and how they influence the stability predictions are discussed in more detail in Section 7. Efforts to obtain simplified stability criteria are included in Section 8, which contains a discussion of Zuber's criteria, Thurston's correlation, and a new criterion obtained from the present analysis. Section 9 takes an overall look at the results and conclusions of the entire report.

There are three major contributions in this work. It will be shown that Zuber's model, along with the modifications made to it here, does a consistent and reasonably good job of matching three different sets of experimental data. It will be shown that the rate of heat transfer to the tube wall is a very important stabilizing influence on the system. This has apparently not been pointed out previously. Third, a very simple stability criterion will be developed, based on experience with the full model, which appears attractive for use as a predictive design tool. It is believed to be the most complete simplified criterion now available.

Section 5

ANALYTICAL MODEL

ASSUMPTIONS AND EQUATIONS OF CHANGE

With one important exception the problem will be formulated and solved just as it was done by Zuber[1]. Since the solution which will be obtained here appears far different from Zuber's, it is advisable to reformulate the problem and solve it again; but since the difference is more apparent than real, frequent comparisons will be made between the two problems.

Consider the system shown schematically in Figure 1. The fluid flows through a tube from left to right. Between positions 0 and 1 there is a constriction before the test section is reached. In the test section between positions 1 and 3 the fluid is heated from some external source. Downstream from the test section is a plenum and another constriction. Figure 1 differs from the system considered by Zuber only in the plenum, which was added to be in agreement with Thurston's[2] experimental apparatus.

The dynamic state of the fluid in the test section can be described by a mass balance, as the continuity equation,*

$$\frac{\partial \rho'}{\partial t'} + u' \frac{\partial \rho'}{\partial z'} + \rho' \frac{\partial u'}{\partial z'} = 0 \tag{1}$$

an energy balance

$$\frac{\partial i'}{\partial t'} + u' \frac{\partial i'}{\partial z'} = \left(\frac{1}{\rho'}\right) \frac{q'_w \xi'}{A'_c} \tag{2}$$

written in terms of the fluid enthalpy i', and a momentum balance

$$-\frac{\partial p'}{\partial z'} = \rho' \frac{\partial u'}{\partial t'} + \rho' u' \frac{\partial u'}{\partial z'} + g' \rho' + \frac{f'}{2D'} \rho' u'^2 \tag{3}$$

The term q'_w in Equation 2 is the energy transferred from the wall. Zuber[1] assumed that the wall had zero thickness so that q'_w equalled the energy input into the system q' either by electric heating or transfer from an external hot fluid. As will be shown in Section 7, this is by no means true in all experimental facilities. For example, in Thurston's[2] apparatus the ratio of

*Nomenclature is defined in Section 10. It will be the same as was used by Zuber, with few exceptions. The prime will be adopted as a convention indicating dimensioned variables. The unprimed variables will always be dimensionless.

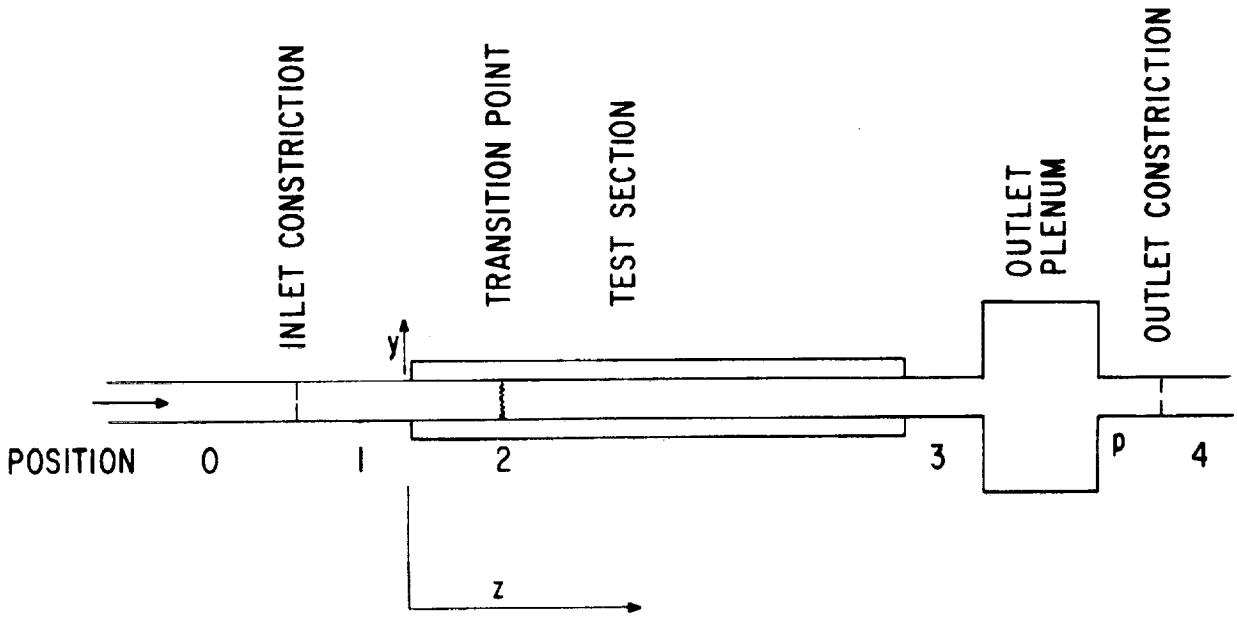

Figure 1. Schematic Diagram of Apparatus

the thermal capacitance of the wall $A'_W \rho'_W c'_W$ to that of the entering fluid $A'_c \rho'_1 c'_p$ is of the order of 10. It would be much higher than that near the exit, where the fluid density is much less. For more generality then, q'_W has been replaced by the standard heat transfer relation.

$$q'_W = h' (T'_W(0) - T') \tag{4}$$

where $T'_W(0)$ is the inside surface temperature of the wall. If the wall curvature is neglected, the energy balance on a wall element with internal energy generation can be written

$$\rho'_W c'_W \frac{\partial T'_W}{\partial t'} = k' \frac{\partial^2 T'_W}{\partial y^2} + \frac{q' \xi'}{A'_W} \tag{5}$$

with the boundary conditions

$$\text{at } y' = 0, \quad k' \frac{\partial T'_W}{\partial y'} = q'_W \tag{6}$$

$$\text{at } y' = \ell'_W, \quad k' \frac{\partial T'_W}{\partial y} = 0 \tag{7}$$

It is in the addition of the dynamics of the heat transfer to the wall that this analysis differs from Zuber's.

It is more convenient to rewrite Equations 1 through 7 in dimensionless form. The following normalizing variables have been used: length, ℓ'; time, $\ell'/\bar{u}'_1$; mass, $\bar{\rho}'_1 \ell'^3$; energy, $\Delta i'_{12}$, and temperature, $\Delta i'_{12}/c_p$. Here $\bar{u}'_1$ and $\bar{\rho}'_1$ represent the velocity and density of the undisturbed inlet fluid and $\Delta i'_{12}$ is the enthalpy increase between positions 1 and 2 of Figure 1. Zuber[1] called position 2 the transition point, and suggested that it be the transposed critical temperature of the fluid. How position 2 is located for the purposes of this analysis is discussed in more detail in Section 7 under the heading Two-region Approximation. Equations 1 to 7 in their dimensionless form, using unprimed variables to indicate the dimensionless quantitities, become

Continuity

$$\frac{\partial \rho}{\partial t} + u \frac{\partial \rho}{\partial z} + \rho \frac{\partial u}{\partial z} = 0 \tag{8}$$

Fluid Energy

$$\frac{\partial i}{\partial t} + \frac{\partial i}{\partial z} = \frac{1}{\rho} \frac{C_W}{\mathcal{J}} (T_W(0) - T) \tag{9}$$

Momentum

$$-\frac{\partial p}{\partial z} = \rho \frac{\partial u}{\partial t} + \rho\, u \frac{\partial u}{\partial z} + g\,\rho + \varphi \rho u^2 \tag{10}$$

Wall energy

$$C_w \frac{\partial T_w}{\partial t} = \frac{C_w}{\mathcal{J}_w}\, \ell_w^2 \frac{\partial^2 T_w}{\partial y^2} + \frac{1}{\tau_{12}} \tag{11}$$

Wall boundary conditions

$$\text{at } y = 0,\ \frac{C_w}{\mathcal{J}_w}\, \ell_w \frac{\partial T_w}{\partial z} = \frac{C_w}{\mathcal{J}} (T_w - T) \tag{12}$$

$$\text{at } y = \ell_w,\ \frac{C_w}{\mathcal{J}_w}\, \ell_w \frac{\partial T_w}{\partial z} = 0 \tag{13}$$

The variables and the parameters in Equations 8 through 13 are defined in the nomenclature. Other than the variables having their dimensional counterparts are the parameters C_w, $\mathcal{J}$, φ, $\mathcal{J}_w$, and τ_{12}. φ, of course, is a dimensionless form of the friction factor. The others have the physcial significance of the heat capacitance of the wall relative to the entering fluid for C_w, the heat transfer time in the fluid for $\mathcal{J}$, the conduction time in the wall for $\mathcal{J}_w$, and the residence time of the entering fluid between positions 1 and 2 for τ_{12}. τ_{12} also equals the fraction of the energy input required between positions 1 and 2. For uniform energy input τ_{12} equals λ_{12}, the length of region 1-2.

The basic assumptions involved in writing Equations 1 to 7 are the following. The problem is one-dimensional; therefore, the fluid properties are assumed to be averaged over the tube cross-section. Fluid expansion work or energy is negligible in the energy equation. The pressure drop due to fluid friction can be written in terms of a friction factor as in the momentum equation. The heat transfer from the wall can be correlated with a heat transfer coefficient h'. The wall is thin enough so that the heat conduction problem can be treated as if the wall were an infinite slab of thickness, ℓ'_w. Equation 5 is also written for heat generation distributed throughout the wall. However, it is not difficult to show that the results in terms of q'_w would be no different if the energy were added externally through the boundary condition Equation 7 instead.

In order to solve Equations 8 to 13 an equation of state must be used in addition. Zuber[1] noted that even for a supercritical fluid, as the fluid temperature or enthalpy gets very far from the critical, the fluid behaves much like a perfect liquid or a perfect gas. Therefore, it was suggested that the equation of state be approximated by two straight lines on the specific volume-enthalpy curve at constant pressure. This is shown in Figure 2. This so-called "two-region approximation" will be adopted here. It will therefore be assumed that the specific volume-enthalpy relation will not be significantly

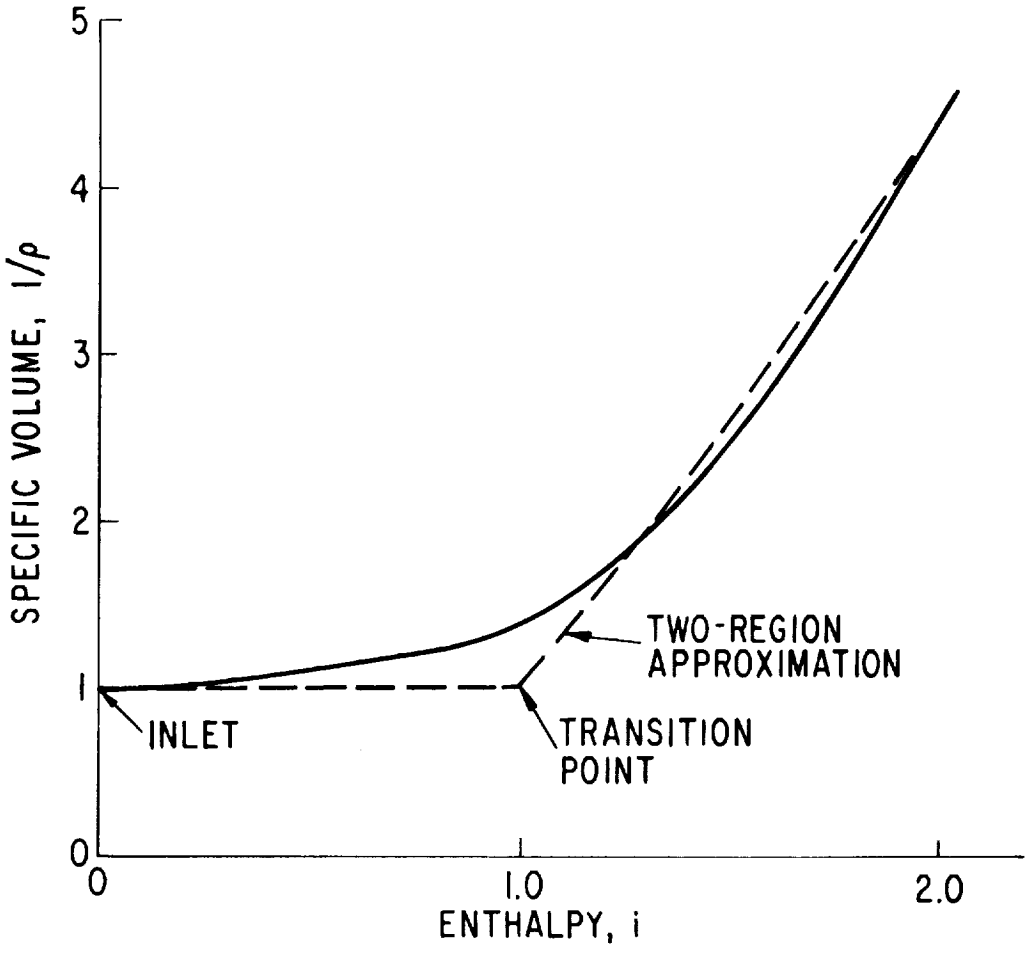

Figure 2. Two-region Approximation

affected by pressure variations and that it can be approximated by two straight lines, as shown in Figure 2. The horizontal line represents liquid-like behavior and that fluid will be called the heavy fluid. The gas-like fluid will be designated the light fluid. The point at which the two lines intersect is called the transition point; and from the definition of the dimensionless enthalpy, the transition enthalpy must be unity if the inlet enthalpy is taken as zero. With the assumption of the two-region approximation the equation of state can be written

$$1/\rho = \begin{cases} 1 & , \ i \leq 1 \\ 1 + \Omega \tau_{12} (i - 1) & , \ i \geq 1 \end{cases} \tag{14}$$

where Ω was designated the reaction frequency by Zuber and is a measure of how much the light fluid expands with or reacts to an enthalpy change. Note that with the assumption of Equation 14, or any other pressure independent relation for the specific volume, the energy and continuity equations have been uncoupled from the momentum equation. The former can be solved first and the momentum equation then solved separately later.

SOLUTION PROCEDURE

Equations 8 to 14 completely define the model for the fluid in the test section. Following the accepted procedure for stability analyses these equations will be solved for small perturbations about the steady-state values of the variables. Then the test section pressures will be related to the pressure drops in the rest of the system of Figure 1. This will give the system response to any external stimulus, say the upstream pressure p_o. A steady-state solution will then be unstable if the perturbation variables increase exponentially as a result of any disturbance.

Zuber[1] has shown that the model can be solved analytically for perturbations when there is no wall capacitance, i.e., $C_W = 0$, and when the two-region approximation Equation 14 is assumed. The same basic solution procedure will be followed here. The variables will be replaced by the sum of a steady-state and a perturbation term,

$$\rho = \bar{\rho} + \delta\rho, \ u = \bar{u} + \delta u, \ i = \bar{i} + \delta i, \ p = \bar{p} + \delta p, \ T_W = \overline{T}_W + \delta T_W,$$

and $T = \bar{T} + \delta T$.

With the introduction of these expressions into Equations 8 to 14, a set of equations is obtained for the steady-state variables and a second set for the perturbations. Omitting the momentum equation for the moment, the steady-state counterparts of Equations 8, 9, and 11 to 13 are as follows.

Continuity

$$\bar{u}\frac{d\bar{\rho}}{dz} + \bar{\rho}\frac{d\bar{u}}{dz} = 0 \tag{15}$$

Fluid Energy

$$\bar{u}\frac{d\bar{I}}{dz} = \frac{1}{\bar{\rho}}\frac{C_w}{\mathcal{J}}\left(\bar{T}_w(0) - \bar{T}\right) \tag{16}$$

Wall Energy

$$0 = \frac{C_w}{\mathcal{J}_w}\ell_w^2\frac{d^2\bar{T}_w}{dy^2} + \frac{1}{\tau_{12}} \tag{17}$$

$$\left.\begin{aligned} &\text{at } y = 0,\ \frac{C_w}{\mathcal{J}_w}\ell_w\frac{d\bar{T}_w}{dy} = \frac{C_w}{\mathcal{J}}\left(\bar{T}_w - \bar{T}\right) \\ &\text{at } y = \ell_w,\ \frac{C_w}{\mathcal{J}_w}\ell_w\frac{d\bar{T}_w}{dy} = 0 \end{aligned}\right\} \tag{18}$$

The steady-state problem is solved as follows. First, integrate Equation 17 across the wall thickness and use the boundary conditions, Equation 18, to obtain

$$\frac{C_w}{\mathcal{J}}\left(\bar{T}_w - \bar{T}\right) = \frac{1}{\tau_{12}} \tag{19}$$

This, of course, is the condition Zuber[1] assumed. Therefore, the steady-state results with and without the heat transfer to the wall will be identical. Equation 15 requires that

$$\bar{\rho}\,\bar{u} = 1 \tag{20}$$

since $\bar{\rho}\bar{u}$ at the inlet is defined to be unity. Combining Equations 19 and 20 then with Equation 16 requires that the enthalpy be

$$\bar{I} = z/\tau_{12} \tag{21}$$

if the energy input, i.e., $1/\tau_{12}$, is constant and if the inlet enthalpy is taken to be zero. Using Equation 21 in the equation of state Equation 14 gives the specific volume

$$1/\bar{\rho} = \begin{cases} 1 & , \ z \le \tau_{12} \\ 1 + \Omega(z - \tau_{12}) & , \ z \ge \tau_{12} \end{cases} \tag{22}$$

From Equation 20, then, the velocity equals the specific volume

$$\bar{u} = \frac{1}{\bar{\rho}} = \left\{ \begin{array}{ll} 1 & , \ z \leq \tau_{12} \\ 1 + \Omega(z - \tau_{12}) & , \ z \geq \tau_{12} \end{array} \right\} \tag{23}$$

Equations 21 to 23 provide the complete steady-state solution for the state of the fluid. It is the same as Zuber's.[1] The enthalpy varies linearly with distance. The transition point, when i = 1, occurs at $z = \lambda_{12} = \tau_{12}$. To the left of the transition point the heavy fluid has a constant density and velocity. To the right the light fluid has a specific volume and velocity which vary linearly with distance. Since the transition point occurs at $z = \tau_{12}$ and the velocity in the heavy region is unity, τ_{12} is the fluid residence time in the heavy region.

The continuity and energy equations for the perturbations are

Continuity

$$s\delta\rho + \bar{u}\frac{d\delta\rho}{dz} + \frac{d\bar{\rho}}{dz}\delta u + \frac{d\bar{u}}{dz}\delta\rho + \bar{\rho}\frac{d\delta u}{dz} = 0 \tag{24}$$

Fluid Energy

$$s\delta i + \bar{u}\frac{d\delta i}{dz} + \frac{d\bar{i}}{dz}\delta u = -\frac{1}{\bar{\rho}^2}\frac{C_w}{\mathcal{J}}(\bar{T}_w(0) - \bar{T})\delta\rho + \frac{1}{\bar{\rho}}\frac{C_w}{\mathcal{J}}(\delta T_w(0) - \delta T) \tag{25}$$

Wall Energy

$$sC_w\delta T_w = \frac{C_w}{\mathcal{J}_w}\ell_w{}^2\frac{d^2\delta T_w}{dy^2} \tag{26}$$

at $y = 0$, $\frac{C_w}{\mathcal{J}_w}\ell_w\frac{d\delta T}{dy} = \frac{C_w}{\mathcal{J}}(\delta T_w - \delta T)$ (27)

at $y = \ell_w$, $\frac{C_w}{\mathcal{J}_w}\ell_w\frac{d\delta T_w}{dy} = 0$ (28)

In Equations 24 to 26 the time derivative has been replaced by the operator s. This operational procedure is equivalent to taking the Laplace transformation of the linear perturbed equations. It is also equivalent to the operational procedure used by Zuber.[1] It will be assumed for the sake of convenience that only the inlet velocity will be disturbed. At z = 0 then, $\delta i = \delta\rho = 0$ and $\delta u = \delta u_1$.

The perturbed problem is solved as follows. The wall temperature profile may be directly solved from Equations 26 to 28 to give

$$\delta T_w = \frac{\delta T}{1 + (\mathcal{J}/\mathcal{J}_w)\sqrt{s\mathcal{J}_w}\ \tanh\sqrt{s\mathcal{J}_w}}$$

Therefore, the perturbation in energy transferred from the wall is

$$\frac{C_w}{\mathcal{J}}(\delta T_w(0) - \delta T) = -\frac{(C_w/\mathcal{J}_w)\sqrt{s\mathcal{J}_w}\tanh\sqrt{s\mathcal{J}_w}}{1+(\mathcal{J}/\mathcal{J}_w)\sqrt{s\mathcal{J}_w}\tanh\sqrt{s\mathcal{J}_w}}\delta T \equiv -W\delta T \tag{29}$$

Equation 29 can be used to eliminate the wall temperature perturbation from the fluid energy equation, Equation 25. Equations 24 and 25 may now be solved along with the perturbed equation of state.

State

$$-\frac{1}{\rho^2}\delta\rho = \begin{cases} 0 & i \le 1 \\ \Omega\tau_{12}\delta i, & i \ge 1 \end{cases} \tag{30}$$

first in the heavy region and then in the light region.

Heavy Region

Combining Equations 30 and 22 with the perturbed continuity equation gives

$$\frac{d\delta u}{dz} = 0 \tag{31}$$

$$\delta u = \delta u_1 \tag{32}$$

Using the steady-state relations, Equations 21 and 23, along with Equations 29 and 30, the energy equation, Equation 25, reduces to

$$s\delta i + \frac{\delta u_1}{\tau_{12}} + \frac{d\delta i}{dz} = -\frac{(C_w/\mathcal{J}_w)\sqrt{s\mathcal{J}_w}\tanh\sqrt{s\mathcal{J}_w}}{1+(\mathcal{J}/\mathcal{J}_w)\sqrt{s\mathcal{J}_w}\tanh\sqrt{s\mathcal{J}_w}}\delta i \equiv -W\delta i \tag{33}$$

In writing Equation 33, δT has been replaced by its equal in these dimensionless terms, δi. The solution to Equation 33 may be written

$$\delta i = -\frac{\delta u_1}{\tau_{12}}\left[\frac{1 - e^{-(s+W)z}}{s+W}\right] \tag{34}$$

where W is the function of the wall heat transfer parameters on the right side of Equation 29. It has been implicitly assumed that C_w, $\mathcal{J}_w$ and $\mathcal{J}$ are constants here.

The perturbed position of the transition point may now be obtained from Equation 34 and the steady-state enthalpy, Equation 21. The transition point is defined as the point at which the dimensionless enthalpy is unity. Letting that point be $z = \tau_{12} + \delta\lambda$, the linearized equation obtained is as follows.

$$1 = \bar{i}\,(\tau_{12} + \delta\lambda) + \delta i\,(\tau_{12}) = 1 + \frac{\delta\lambda}{\tau_{12}} - \frac{\delta u_1}{\tau_{12}}\left[\frac{1 - e^{-(s+W)\tau_{12}}}{s+W}\right] \tag{35}$$

Equation 35 may be solved for the perturbation in the transition position $\delta\lambda$,

$$\delta\lambda = \delta u_1 \frac{1 - e^{-(s+W)\tau_{12}}}{s+W} \tag{36}$$

The contribution of the wall heat transfer in the W term added to the s is evident. Without the W the result is identical with that obtained by Zuber.[1]

Light Region

Using Equations 30 and 21 to eliminate $\delta\rho$ and $d\bar{i}/dz$ and Equations 19 and 29 to eliminate the heat transfer rates the energy equation, Equation 25, can be written as

$$s\delta i + \frac{\delta u}{\tau_{12}} + \bar{u}\frac{d\delta i}{dz} = \left(\Omega - \frac{1}{\bar{\rho}}W\right)\delta i \tag{37}$$

The effect of the wall heat transfer rate here is to decrease the reaction frequency Ω.* Since Ω is proportional to the expansion $\partial v'/\partial i'$ of fluid, the wall heat transfer in effect decreases the ability of the fluid to expand. It does this by limiting the energy which gets into the fluid. It is convenient to label this dimished reaction frequency by the symbol $\mathcal{R}$

$$\mathcal{R} = \Omega - \frac{1}{\rho}W = \Omega - \frac{1}{\rho_{ave}}W \tag{38}$$

The reason for the use of $\bar{\rho}_{ave}$ will be made clear below. Now $\delta\rho$, $d\bar{\rho}/dz$, $d\bar{u}/dz$, and ρ may be eliminated from the continuity equation, Equation 24, using Equations 22, 23, and 30. After some rearranging and collecting terms the continuity equation becomes

$$s\delta i + \frac{\delta u}{\tau_{12}} + \bar{u}\frac{d\delta i}{dz} = \Omega\delta i + \frac{\bar{u}}{\Omega\tau_{12}}\frac{d\delta u}{dz} \tag{39}$$

Equation 39 must be solved simultaneously with Equation 37 for δi and δu. To accomplish this, subtract Equation 37 from Equation 39

$$0 = (\Omega - \mathcal{R})\delta i + \frac{\bar{u}}{\Omega\tau_{12}}\frac{d\delta u}{dz} \tag{40}$$

*This is, of course, not strictly true because W is a function of s and is in general complex. However, the real part of W is positive and does act to diminish the reaction frequency.

With no wall heat transfer effect $\mathcal{R}$ equals Ω, and δu is seen to be independent of distance. With the wall this is no longer true. Proceeding with the solution is made more convenient by defining a new distance variable

$$\zeta \equiv \frac{1n\ \bar{u}}{\Omega} = \frac{1n\ [1+\Omega\ (z\ -\ \tau_{12})]}{\Omega} \tag{41}$$

Physically, ζ is the residence time of the fluid in the light region up to the position z. δu may be eliminated from Equation 37 by taking its derivative with respect to ζ and substituting for $d\delta u/d\zeta$ from Equation 40

$$s\ \frac{d\delta i}{d\zeta} - \Omega\ (\Omega - \mathcal{R}')\ \delta i + \frac{d^2\delta i}{d\zeta^2} = \mathcal{R}\ \frac{d\delta i}{d\zeta} + \frac{d\mathcal{R}}{d\zeta}\ \delta i \tag{42}$$

Equation 42 is a second-order ordinary differential equation which must be solved for δi.

Since the reaction frequency $\mathcal{R}$ has in it $\bar{\rho}$, which varies with distance, Equation 42 has non-constant coefficients. Only in very special cases can these equations be solved in general. Since the equation involves s, it cannot be integrated numerically while still retaining the functional form of s. This difficulty is one which has plagued studies in the dynamics of distributed parameter processes for a long time and it is by no means solved. It is precisely the reason why Zuber[1] was forced to approximate the $1/\rho$ - i curve with straight lines in the first place. Therefore, although Zuber was able to obtain an analytical solution to the problem without the wall heat transfer effect, an exact solution will not be possible here.

There have been numerous attempts to develop methods of solving problems of this general nature, most of them involving the dynamics of distributed parameter chemical reactors.[10, 12, 13-15] Of the two methods which appear to be directly applicable to this problem, the asymptotic method in Reference 12 appears to be the more convenient. The asymptotic approach obtains solutions to equations, like Equation 42, which are valid both for $s = 0$ and as $s \to \infty$. The results obtained for several different types of systems[12] have been found to be good for all values of s. It is clear from the definition of $\mathcal{R}$ that at $s = 0$, $\mathcal{R} \to \Omega$. As $s \to \infty$ the $\mathcal{R}$ approaches a finite value which is small in comparison with the s on the left side of Equation 37.

Therefore, the solution obtained using appropriate average values of $\bar{\rho}$, designated $\bar{\rho}_{ave}$, as well as C_w, $\mathcal{J}_w$, and $\mathcal{J}$ if they vary too, would give solutions which were asymptotically correct. This is the significance of the use of $\bar{\rho}_{ave}$ in Equation 38. Judging from experiences with several other systems,[12] the result may be adequate to approximate the stability of this system.

Assuming, then, that $\mathcal{R}$ is independent of ζ, Equation 42 may be solved to yield

$$\delta i = A\, e^{m_1 \zeta} + B\, e^{m_2 \zeta} \tag{43}$$

where $m_{1,2} = \left(\frac{\mathcal{R} - s}{2}\right) \pm \sqrt{\left(\frac{\mathcal{R} - s}{2}\right)^2 + \Omega(\Omega - \mathcal{R})}$

δu is obtained by putting Equation 43 back into the energy equation, Equation 37.

$$\delta u = \tau_{12} (A\, m_2\, e^{m_1 \zeta} + B\, m_1\, e^{m_2 \zeta}) \tag{44}$$

The constants A and B must be evaluated by matching the solution for the velocity and the enthalpy in the light region at the transition point to that in the heavy region.

at $z = \tau_{12} + \delta\lambda$

$$u_f = 1 + \delta u_1 = u_g = \bar{u}\,(\tau_{12} + \delta\lambda) + \delta u\,(\tau_{12}) \tag{45}$$

$$i_f = 1 = i_g = \bar{i}\,(\tau_{12} + \delta\lambda) + \delta i\,(\tau_{12}) \tag{46}$$

Note that at $z = \tau_{12}$ the variable ζ is zero. Using the steady-state relations of Equations 21 and 23 and the perturbations of Equations 43 and 34, Equations 45 and 46 become

$$\left.\begin{aligned} 1 + \delta u_1 &= 1 + \Omega\delta\lambda + \tau_{12}(A\, m_2 + B\, m_1) \\ 1 &= 1 + \frac{\delta\lambda}{\tau_{12}} + A + B \end{aligned}\right\} \tag{47}$$

Therefore A and B must have the values

$$\left.\begin{aligned} A &= \frac{\delta u_1 - (\Omega - m_1)\,\delta\lambda}{\tau_{12}\,(m_2 - m_1)} \\ B &= -\frac{\delta u_1 - (\Omega - m_2)\,\delta\lambda}{\tau_{12}\,(m_2 - m_1)} \end{aligned}\right\} \tag{48}$$

The density perturbation can be obtained directly from the perturbed equation of state Equation 30 and the enthalpy Equation 43

$$\delta\rho = -\bar{\rho}^2\, \Omega\, \tau_{12}\, (A\, e^{m_1 \zeta} + B\, e^{m_2 \zeta}) \tag{49}$$

It is unfortunate that the perturbation solutions given by Equations 43, 44, and 49 along with Equation 48 are much more complicated than those obtained by Zuber.[1] However, it is possible to obtain some physical understanding for the meaning of the terms. First, it is easy to show that for $C_W = 0$, $\mathcal{R} = \Omega$, and the equations reduce immediately to those used before.[1]

Next, δi and δu are seen to be influenced by both the inlet flow perturbation δu_1 and the transition point perturbation $\delta\lambda$ through the coefficients A and B. Last, it is possible to show that the exponentials in Equations 43 and 44 represent delays of zero and τ_{23} just as occurred in Zuber's solution. This may most easily be seen by looking at the exponentials as $s \to \infty$,

$$\text{as } s \to \infty,\ m_{1,2} \to \frac{\mathcal{R}-s}{2} \pm \left|\frac{\mathcal{R}-s}{2}\right| \to -s \text{ or } 0.$$

Taking the positive root for m_1, $e^{m_1\zeta} \to e^{-s\zeta}$ and $e^{m_2\zeta} \to 1$. Since ζ is defined as $\ln(\bar{u})/\Omega$, this is simply the time it takes the fluid to travel from the transition point to any point z in the light region. If z is taken at the end of the test section, $\zeta = \tau_{23}$. Therefore, the first exponential represents a delay of τ_{23} and the second no delay at all.

The solution for the fluid enthalpy, velocity, and density is complete in the entire test section. The steady-state solutions are given by Equations 21 to 23. The perturbed solutions in the heavy region by Equations 32, 34, and 30. Equation 36 gives the perturbation in the transition point between the heavy and light region. Then Equations 43, 44, and 49, along with Equation 48 gives the perturbed solution in the light region. These solutions can now be inserted into the momentum equation to obtain the pressure drop and its perturbation.

MOMENTUM BALANCE AND THE CHARACTERISTIC EQUATION

The test section pressure drop can be obtained by integrating the momentum Equation 10. Integrated over the entire test section it is

$$\Delta p = \int_0^1 \left[\rho \frac{\partial u}{\partial t} + \rho u \frac{\partial u}{\partial z} + g\rho + \varphi\rho u^2\right] dz \tag{50}$$

The steady-state and perturbation expressions Equations 21 to 23, 32, 34, 30, 36, 43, 44, and 49 may be introduced into Equation 50, the terms linearized, and the steady-state and perturbation pressure drops evaluated.

The heavy-region portion Δp_h of the total pressure drop Equation 50 becomes

$$\Delta p_h = \int_0^{\tau_{12}} \left[s\,\delta\lambda\, \delta u_1 + g + \varphi_{12}\,(1 + 2\,\delta u_1)\right] dz \tag{51}$$

In writing Equation 51, the steady-state and perturbation expressions for both ρ and u have already been used, and the time derivative of the perturbation δu_1 has been replaced by s. Integrating Equation 51 and omitting second-order perturbations gives

$$\Delta\bar{p}_h + \delta\,\Delta p_h = (g+\varphi_{12})\,\tau_{12} + (g+\varphi_{12})\,\delta\lambda + (s+2\varphi_{12})\,\tau_{12}\,\delta u_1 \tag{52}$$

The light-region pressure drop Δp_ℓ may be written in linearized form as

$$\Delta\bar{p}_\ell + \delta\Delta p_\ell = \int_{\tau_{12}+\delta\lambda}^{1}\left[\left(\frac{s}{\bar{u}}\,\delta u\right) + \left(\frac{d\bar{u}}{dz} + \frac{d\,\delta u}{dz} + \frac{1}{\bar{u}}\frac{d\bar{u}}{dz}\,\delta u + \bar{u}\,\frac{d\bar{u}}{dz}\,\delta\rho\right) + g\left(\frac{1}{\bar{u}} + \delta\rho\right) + \varphi_{23}\,(\bar{u} + 2\,\delta u + \bar{u}^2\,\delta\rho)\right]\,dz \tag{53}$$

The steady-state relation $\bar{\rho}\bar{u} = 1$ has been used to eliminate $\bar{\rho}$ in Equation 53. Consider Equation 53 term by term. The linearized inertia term is written as the following in terms of the new distance coordinate ζ, defined by Equation 41,

$$\delta\Delta p_I = \int_{\tau_{12}}^{1} s\,\frac{\delta u}{\bar{u}}\,dz = \int_0^{\tau_{23}} s\,\delta u\;d\zeta \tag{54}$$

where at the upper limit $\zeta = \ln(\bar{u}_3)/\Omega \equiv \tau_{23}$. Substituting the expression for δu, Equation 44, and integrating yields

$$\delta\Delta p_I = s\tau_{12}\left[\frac{m_2}{m_1}\,A\,(e^{m_1\tau_{23}} - 1) + \frac{m_1}{m_2}\,B\,(e^{m_2\tau_{23}} - 1)\right] \tag{55}$$

The acceleration term is

$$\Delta\bar{p}_a + \delta\Delta p_a = \int_{\delta\lambda}^{\tau_{23}}\left[\frac{d\bar{u}}{d\zeta} + \frac{d\,\delta u}{d\zeta} + \Omega\delta u + \bar{u}^2\,\Omega\delta\rho\right]d\zeta \tag{56}$$

After integration of Equation 56 with the expressions for δu and $\delta\rho$ the acceleration pressure drop is

$$\Delta\bar{p}_a + \delta\Delta p_a = (\bar{u}_3 - 1) - \Omega\delta\lambda + \tau_{12}\left[m_2 A\,(e^{m_1\tau_{23}} - 1) + m_1 B\,(e^{m_2\tau_{23}} - 1)\right]$$
$$+ \Omega\tau_{12}\left[\frac{m_2}{m_1}\,A\,(e^{m_1\tau_{23}} - 1) + \frac{m_1}{m_2}\,B\,(e^{m_2\tau_{23}} - 1)\right]$$
$$-\Omega^2\tau_{12}\left[\frac{A}{m_1}\,(e^{m_1\tau_{23}} - 1) + \frac{B}{m_2}\,(e^{m_2\tau_{23}} - 1)\right]$$

This may be simplified to

$$\Delta\bar{p}_a + \delta\Delta p_a = (\bar{u}_3 - 1) - \Omega\delta\lambda + \Omega\tau_{12}\left[\left(\frac{m_2}{\Omega} + \frac{m_2}{m_1} - \frac{\Omega}{m_1}\right) A\,(e^{m_1\tau_{23}} - 1)\right.$$

$$\left. + \left(\frac{m_1}{\Omega} + \frac{m_1}{m_2} - \frac{\Omega}{m_2}\right) B\,(e^{m_2\tau_{23}} - 1)\right] \qquad (57)$$

The body force pressure drop is

$$\Delta\bar{p}_{bg} + \delta\Delta p_{bg} = g\int_{\delta\lambda}^{\tau_{23}} (1 + e^{\Omega\zeta}\,\delta\rho)\,d\zeta$$

$$= g\left\{\tau_{23} - \delta\lambda - \Omega\tau_{12}\left[\frac{A}{m_1 - \Omega}\left(\frac{e^{m_1\tau_{23}}}{\bar{u}_3} - 1\right) + \frac{B}{m_2 - \Omega}\left(\frac{e^{m_2\tau_{23}}}{\bar{u}_3} - 1\right)\right]\right\} \qquad (58)$$

Here the definition of ζ, Equation 41, has been used to replace $\bar{u}$ by $e^{\Omega\zeta}$. Finally, the friction pressure drop term becomes

$$\Delta\bar{p}_{23} + \delta\Delta p_{23} = \varphi_{23}\int_{\delta\lambda}^{\tau_{23}} \left[e^{2\Omega\zeta} + 2e^{\Omega\zeta}\,\delta u + e^{3\Omega\zeta}\,\delta\rho\right] d\zeta$$

$$= \varphi_{23}\left\{\frac{\bar{u}_3^2 - 1}{2\Omega} - \delta\lambda + 2\tau_{12}\left[\frac{m_2}{m_1 + \Omega} A\,(\bar{u}_3\, e^{m_1\tau_{23}} - 1)\right.\right.$$

$$\left. + \frac{m_1}{m_2 + \Omega} B\,(\bar{u}_3\, e^{m_2\tau_{23}} - 1)\right] - \Omega\tau_{12}\left[\frac{A}{m_1 + \Omega}\,(\bar{u}_3\, e^{m_1\tau_{23}} - 1)\right.$$

$$\left.\left. + \frac{B}{m_2 + \Omega}\,(\bar{u}_3\, e^{m_2\tau_{23}} - 1)\right]\right\}$$

This may be simplified to

$$\Delta\bar{p}_{23} + \delta\Delta p_{23} = \varphi_{23}\left\{\frac{\bar{u}_3^2 - 1}{2\Omega} - \delta\lambda + \tau_{12}\left[\left(\frac{2m_2 - \Omega}{m_1 + \Omega}\right) A\,(\bar{u}_3\, e^{m_1\tau_{23}} - 1)\right.\right.$$

$$\left.\left. + \left(\frac{2m_1 - \Omega}{m_2 + \Omega}\right) B\,(\bar{u}_3\, e^{m_2\tau_{23}} - 1)\right]\right\} \qquad (59)$$

The light-region pressure drop is then the sum of the inertia, acceleration, body force, and friction pressure drops.

$$\Delta\bar{p}_\ell + \delta\Delta p_\ell = \Delta\bar{p}_I + \delta\Delta p_I + \Delta\bar{p}_a + \delta\Delta p_a + \Delta\bar{p}_{bg} + \delta\Delta p_{bg} + \Delta\bar{p}_{23} + \delta\Delta p_{23} \qquad (60)$$

This completes the analysis for the test section. It may be verified that if there is no wall heat transfer effect, $W = 0$, the result agrees identically with

that obtained by Zuber.[1] The momentum balance for the remainder of the system shown in Figure 1 will be taken in order.

Upstream Constriction

The pressure drop across an orifice can be written

$$\Delta p_{o1} = k_i \rho_o u_o^2 = k_i \rho_1 u_1^2 \tag{61}$$

for the incompressible heavy fluid. Introducing the perturbation variables in Equation 61 yields

$$\Delta \bar{p}_{o1} + \delta \Delta p_{o1} = k_i (1 + 2\delta u_1) \tag{62}$$

where the fact that the dimensionless steady-state density and velocity are unity has been used.

Outlet Plenum

The analysis of the dynamics of a plenum into and from which an ideal gas is flowing has been considered in detail many times before. This derivation will be adapted from those presented by Bird, Stewart, and Lightfoot.[16]

Consider a tank of dimensionless volume, V. Assume that there is flow of an ideal gas into and from the tank. Also assume that the contents of the plenum are homogeneous so that the properties ρ_p, T_p are the same throughout, as well as in the exit flow stream before the orifice is reached. It will be assumed that the only significant pressure drop will be across the orifice so the inlet pressure p_3 will equal the plenum pressure p_p. With these assumptions the mass balance on the plenum is

$$V \frac{d\rho_p}{dt} = A_c (u_3 \rho_3 - u_p \rho_p) \tag{63}$$

The velocity u_p is the exit velocity based on a cross section A_c. It is immaterial whether the actual exit cross section is A_c or the velocity is equal to u_p. The energy balance is

$$\frac{V}{\gamma} \frac{d(\rho_p T_p)}{dt} = A_c (u_3 \rho_3 T_3 - u_p \rho_p T_p)$$

For an ideal gas $p = \rho RT$ and T may be eliminated from this equation to give

$$\frac{V}{A_c \gamma} \frac{dp_p}{dt} = \frac{V}{A_c \gamma} \frac{dp_3}{dt} = p_3 (u_3 - u_p) \tag{64}$$

Perturbing Equations 63 and 64, linearizing and replacing the time derivative by s, the following equations are obtained for the perturbations in pressure, velocity, and density.

$$\frac{V}{A_c}\, s\,\delta\rho_p = \bar{\rho}_3\,\delta u_3 + \bar{u}_3\,\delta\rho_3 - \bar{\rho}_3\,\delta u_p - \bar{u}_3\,\delta\rho_p \tag{65}$$

$$\frac{V}{A_c}\,\frac{s}{\gamma}\,\delta p_3 = \bar{p}_3\,(\delta u_3 - \delta u_p) \tag{66}$$

In writing Equations 65 and 66 the steady-state equalities $\bar{u}_p = \bar{u}_3$ and $\bar{\rho}_p = \bar{\rho}_3$ have already been employed.

Outlet Constriction

The flow characteristics through a sonic orifice* may be written

$$p_3 = k_e \rho_p u_p^2 \tag{67}$$

Introducing the perturbation variables into Equation 67 gives

$$\bar{p}_3 + \delta p_3 = k_e\,[\bar{u}_3 + \bar{u}_3^2\,\delta\rho_p + 2\,\delta u_p] \tag{68}$$

Again the steady-state solutions for $\bar{u}_p$, $\bar{\rho}_p$, and $\bar{u}\bar{\rho}$ have already been used. Eliminating $\delta\rho_p$ and δu_p from the perturbed part of Equation 68, using Equations 65 and 66 and the steady-state part of Equation 68, and solving for δp_3 yields

$$\delta p_3 = \frac{k_e\left[\dfrac{\bar{u}_3^2\,\delta\rho_3}{1+c_3 s} + 2\,\delta u_3\right]}{1 + \dfrac{c_3 s}{\gamma}\,\dfrac{1+2c_3 s}{1+c_3 s}} \tag{69}$$

where $c_3 = V/A_c\bar{u}_3$ is the volumetric capacitance of the plenum.

Equation 69 may be compared with the result without the plenum by letting c_3 equal zero. This result is identical with that used by Zuber[1] provided the back pressure p_4 is considered unperturbed.

*Zuber[1] considered a subsonic orifice but the experimental data considered below require use of the sonic orifice equation. In terms of the perturbations, though, there is no difference at all between the results, provided there is no plenum.

Overall System Momentum Balance

The pressure drops for the entire system of Figure 1 have now been formulated both in the steady state and in the perturbed state. The total system pressure drop must, of course, balance the external pressure rise for the system

$$- \Delta p_{ex} = \Delta p_{o1} + \Delta p_h + \Delta p_\ell + p_3 \tag{70}$$

The overall momentum balance may now be divided into steady-state and perturbation terms giving the two equations

$$- \Delta \bar{p}_{ex} = \Delta \bar{p}_{o1} + \Delta \bar{p}_h + \Delta \bar{p}_\ell + \bar{p}_3$$

and

$$- \delta \Delta p_{ex} = \delta \Delta p_{o1} + \delta \Delta p_h + \delta \Delta p_\ell + \delta p_3 \tag{71}$$

Recall that in formulating the perturbed problem for the test section above it was assumed that the only disturbance entering the system was in the inlet velocity δu_1. Therefore, all of the linear perturbations on the right side of Equation 71 are proportional to the initially assumed disturbance δu_1. It is convenient then to rewrite Equation 71 as

$$\frac{\delta u_1}{\delta \Delta p_{ex}} = \frac{-1}{\frac{\delta \Delta p_{o1}}{\delta u_1} + \frac{\delta \Delta p_h}{\delta u_1} + \frac{\delta \Delta p_\ell}{\delta u_1} + \frac{\delta p_3}{\delta u_1}} \tag{72}$$

Equation 72 expresses the response of the inlet velocity to an external pressure disturbance. If that response to any disturbance grows with time the system is said to be unstable. Whether the response is stable or not depends uniquely on the denominator of Equation 72.[17] Setting the denominator of Equation 72 equal to zero gives the characteristic equation for the system.*

$$\frac{\delta \Delta p_{o1}}{\delta u_1} + \frac{\delta \Delta p_h}{\delta u_1} + \frac{\delta \Delta p_\ell}{\delta u_1} + \frac{\delta p_3}{\delta u_1} = 0 \tag{73}$$

The characteristic equation is a function of the parameter s introduced to replace the time derivatives in the system equations. If Equation 73 has any

*Although Equation 72 implies that the response is being determined only for an external pressure disturbance, it may be readily shown that the denominator, and therefore the characteristic equation, will be the same for any disturbance to the system. Consequently, the question of stability is independent of the particular disturbance assumed.

roots in s with positive real parts the system will be unstable. The purpose of the mathematical formulation, then, has been to derive this characteristic equation. The characteristic equation can be considered alone to determine the stability. The characteristic equation and the relationships required to evaluate it are all collected together in the Appendix.

SIGNAL FLOW DIAGRAM

It does not appear to be instructive to substitute here for the various pressure drop terms in Equation 73. These are given by Equations 62, 52, 60, and 69. For reference in later sections the full characteristic equation and all terms needed to calculate it are listed in the Appendix; there it is compared with the equation obtained by Zuber.[1]

At this point it might be well to review the physical significance of what has been done thus far in the perturbation analysis. This can perhaps be done most clearly by considering the schematic signal flow diagram of Figure 3. In this diagram the vertical dotted lines divide the system of Figure 1 into five parts. Start with the velocity signal at the top as it enters the test section. It has been initially assumed that there is a disturbance of unspecified cause in the inlet velocity. This signal enters the test section and influences the velocity, enthalpy, and density first in the heavy region. This is indicated by the block at the top in the heavy region. How the inlet velocity disturbance affected the system variables was determined by solving the continuity, energy, and state equations as indicated by the labels on the block. The output from the heavy region which serves as input disturbances to the light region is the velocity perturbation δu_2 (which happens to equal δu_1 for this problem) and the perturbation in the location of the transition point, $\delta\lambda$. The continuity, energy, and state equations were then solved again in the light region subject to the inlet disturbances δu_2 and $\delta\lambda$. The signals of importance coming out of the test section at the right are the velocity and density perturbations, δu_3 and $\delta\rho_3$. The test section equations presented under the heading Solution Procedure (page 14) were solved approximately to obtain the relations which belong in the two top blocks for the heavy and light regions.

This is not the complete problem, however; on page 26 the system momentum balance is considered. This forms the bottom line of the diagram and constitutes the feedback in the system. Without some sort of feedback, either internal or external, no system can be unstable. First, the momentum equation for the heavy region is considered; as indicated by the vertical lines dropping from the top block in the heavy region. The signals of density and velocity as a function of distance in the heavy region are used in the integration of the momentum equation to obtain the heavy-region pressure-drop perturbation $\delta\Delta p_h$. Similarly in the light region.

Moving on to the right, the output signals from the test section are acted on by the plenum and then by the orifice to yield the perturbation in downstream

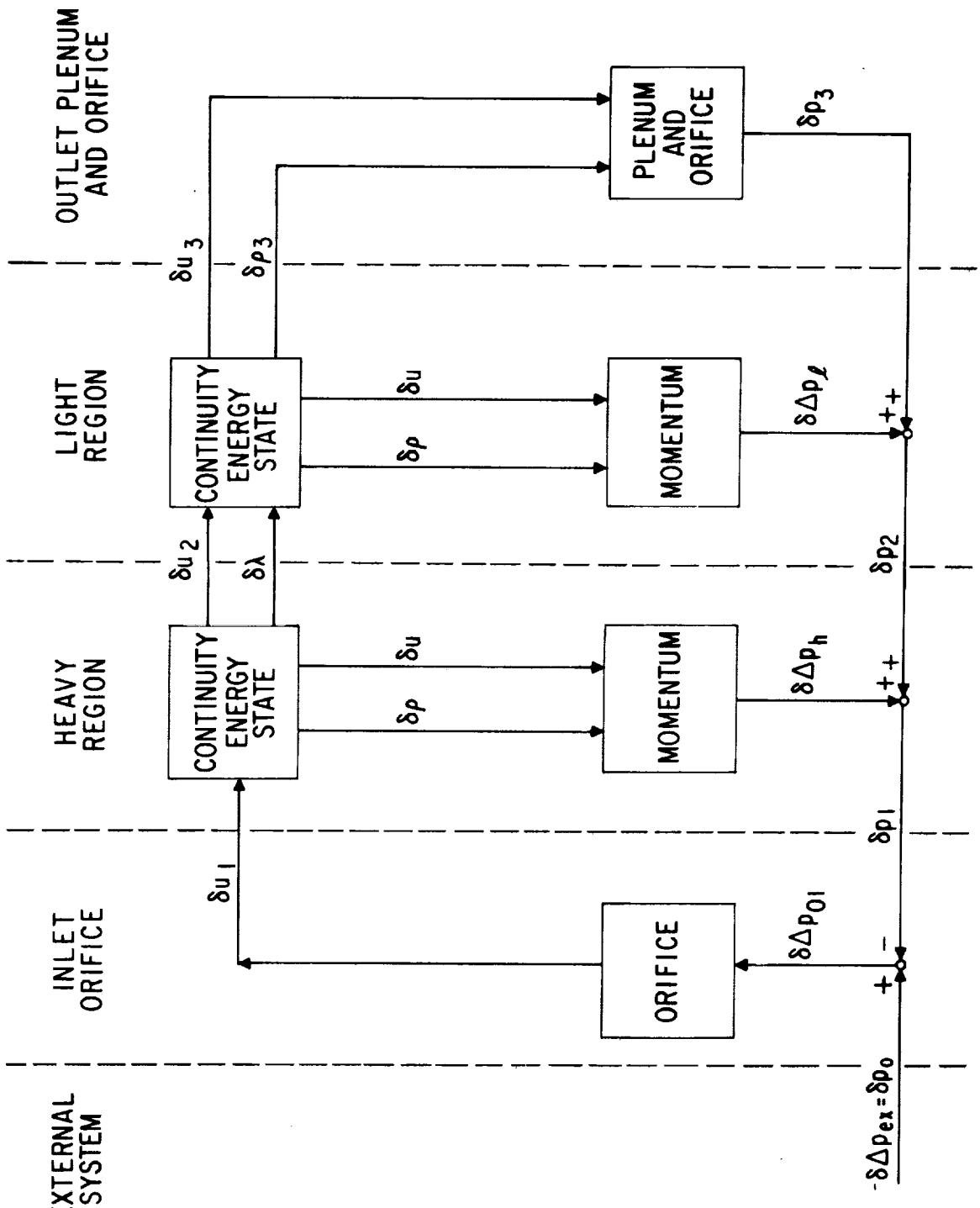

Figure 3. Schematic Signal Flow Diagram for System of Figure 1

pressure δp_3. Proceeding from right to left along the bottom line then, the downstream pressure is added to the light region pressure drop and then to the heavy region pressure drop to obtain the perturbation in pressure at the inlet to the test section. That signal is then subtracted from any upstream or external pressure perturbation to obtain the perturbation in pressure drop across the inlet orifice. The orifice acts on this signal to yield δu_1, feeding it back into the test section and closing the loop.

Two comments are in order here before the significance of this diagram is discussed in terms of the instability phenomenon. First, it has been assumed here that any external pressure disturbance is completely independent of the velocity disturbance δu_1. This may not always be true, of course. For example, there may be a pump upstream with a pressure head depending on the discharge rate. This can be added to Figure 3 simply by adding another section upstream of the inlet orifice and reversing the sense of the signal flow through the orifice. Second, the discussion above was in qualitative terms for the sake of simplicity. The exact functional forms which belong in the blocks of the diagram are in general much too complex to warrant their inclusion in Figure 3. However, they can be illustrated by the blocks for the inlet and outlet orifices. The inlet orifice relation is given by Equation 62, which can be rewritten as

$$\delta u_1 = \frac{1}{2k_i} \delta \Delta p_{01} \tag{74}$$

Therefore, the block for the inlet orifice should contain just $1/2k_i$. The outlet plenum and constriction is governed by Equation 69, which gives δp_3 as a function of both $\delta \rho_3$ and δu_3. The transfer functions implied by that block are the factors of $\delta \rho_3$ and δu_3. This and the preceding comment are illustrated in more detail for Zuber's original model in Reference 18.

Figure 3 itself can be used to help understand the instability phenomenon qualitatively. First, recall from Equation 36 that $\delta \lambda$ has in it the delay $e^{-s\tau_{12}}$. Also recall that the exponential $e^{m_1 \tau_{23}}$ in the expression for $\delta \rho_3$ or δu_3, Equations 49 or 44, represents an additional delay of τ_{23}. Therefore, the blocks for the test section in Figure 3 have buried in them delays up to $\tau_{13} \equiv \tau_{12} + \tau_{23}$, the total residence time of the fluid. The pressure drops downstream from these delays feed back delayed signals to the upstream pressure drops. It is well known in the field of process control that the feedback of delayed signals can be a source of instability;[19] the effect of this delay on the signals was clearly discussed by Zuber.[1]

It is generally true that the larger the magnitude of the feedback the less stable the system. Therefore, one would expect qualitatively that the larger the downstream pressure drops the more feedback and the less stable the system. (This should include any pressure drop downstream from the delay, both the light region and the outlet orifice pressure drops.) Conversely, the upstream system pressure drops should be stabilizing; this can be seen for the

inlet orifice from Equation 74. The larger the pressure drop (k_i larger) the more the feedback is cut down. The strength of the destabilizing effect of the downstream pressure drops can be traced to two sources, either tighter choking (k_e large) or greater expansion of the fluid ($\bar{v}_3$ large). The same holds true for the light-region friction pressure drop as well. Then for a given orifice or friction factor the feedback is greater for larger heat inputs relative to the fluid velocity and for greater expansion of the fluid as would occur at lower pressures for a gas-like fluid. Therefore, the signal flow diagram would indicate qualitatively that higher energy input and lower flow rate and pressure should make the system less stable.

All of these qualitative effects have been observed experimentally and are reviewed by Zuber.[1] It is significant that they can all be explained by consideration of the signal flow diagram with very little detailed information about the relations entering the blocks. It should not be surprising that many models having this same general framework would prove useful for correlating the instability data. It is believed that the more nearly correct physical models on which these blocks are based would permit the correct qualitative prediction of the instability phenomenon. The model formulated under headings Assumptions and Equations of Change (page 9) is an attempt in this direction.

STABILITY ANALYSIS

The stability of the system is determined by the characteristic equation, Equation 73. If the characteristic equation has any roots in s which have positive real parts, the system is unstable. For a characteristic equation as complicated as Equation 73, it appears that the Nyquist criterion is the most convenient to determine if any roots lie in the right half plane.

A detailed review of the theory of the Nyquist diagram may be found in Reference 20. For a brief explanation of its significance, suppose it is desired to determine if the equation $K + G(s) = 0$ has any roots in the right half plane. It is a property of functions of a complex variable that if s is allowed to follow a contour encircling the entire right half plane, G (s) will be mapped into a curve which encircles the point -K the number of times equal to the total number of zeros in the right half plane minus the number of poles of $K + G(s)$ which lie in the right half plane. The Nyquist diagram is simply a mapping of a semicircle of infinite radius circling the right half of the plane. By counting the net number of encirclements of the operating point -K the stability of the system can be determined.

A sketch of a typical Nyquist diagram for this system is given in Figure 4. The point -K is marked with the cross and it will be called the operating point. The spiraling curve is mapped by G (s) as s travels from the origin up the positive imaginary axis. The curve starts at G (0) (marked with the circle) on real axis. This will be called the starting point. As s grows very large the spiral becomes smaller and smaller and moves away from the origin. As s traverses the semicircle around the right half plane, the map of G (s) does also,

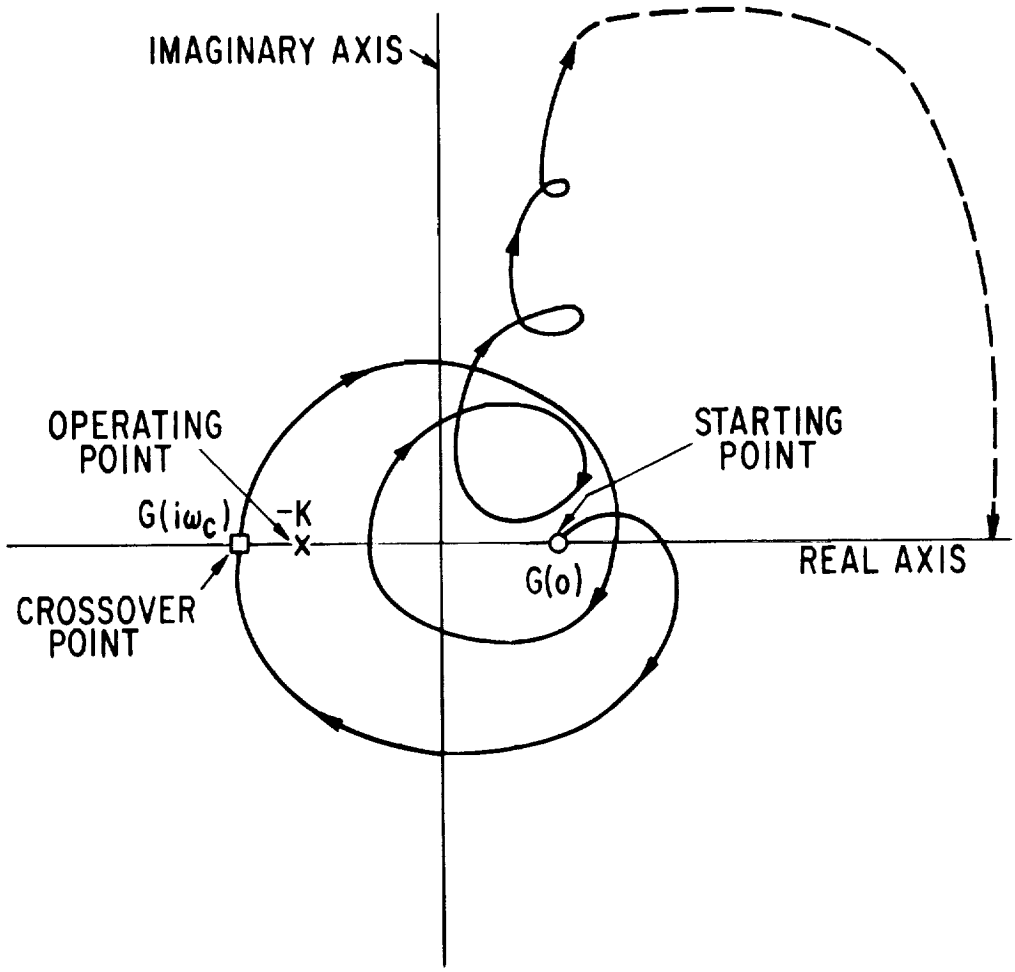

Figure 4. Typical Nyquist Diagram for the Heat Exchanger System

as is shown by the dotted portion of the curve. The mapping will be symmetric with respect to the real axis so that the portion of the map drawn will be repeated as reflected below the axis. Consequently, the total number of times the map will encircle -K, the operating point, will be twice the number indicated by this half of the mapping. In Figure 4, there is one encirclement shown, so there will be two roots in the right half plane. One is sufficient for instability. An additional term to be frequently used is the crossover point G ($i\omega_c$) marked with the square. This is the point at which the phase angle of G (s) first crosses -180°. The frequency, or value of ω in $s = i\omega$, at which this occurs will be called the crossover frequency ω_c. If the crossover point is more negative than the operating point this system will be unstable. Therefore the negative operating point plus the crossover point will be called the stability number N_s of the system

$$N_s = K + G\ (i\omega_c) \tag{75}$$

A stability number greater than zero is sufficient for stability.

In the application of the Nyquist criterion below, it will be adopted as a convention that the negative operating point K will be the upstream pressure drop perturbation plus the s independent part of the heavy-region pressure-drop term in Equation 73. Using Equations 62 and 52, the negative crossover point will be $K = 2\,(k_i + \varphi_{12}\,\tau_{12})$. This leaves G (s) to include everything else.

$$G\ (s) \equiv (g + \varphi_{12})\frac{\delta\lambda}{\delta u_1} + s\ \tau_{12} + \frac{\delta \Delta p_\ell}{\delta u_1} + \frac{\delta p_3}{\delta u_1} \tag{76}$$

With this convention the upstream pressure drop k_i appears only in the expression for the operating point. The operating point, then, is proportional to the upstream and heavy region pressure drops. The larger these are the farther to the left the operating point is, and the more stable the system will be.

Another point can be noted concerning the general form of the Nyquist diagram shown in Figure.4. It is not difficult to convince oneself that if the starting point falls to the left of the operating point there will always be at least one encirclement. Therefore,

$$K + G\ (0) > 0 \tag{77}$$

is a necessary condition for stability. This zero frequency, or steady-state, stability criterion is well known as the Ledinegg criterion.[21] It was designated the excursive criterion by Zuber.[1]

Section 6

APPLICATION OF ANALYSIS TO EXPERIMENTAL DATA

NASA OXYGEN DATA

Data for eight experimental runs using oxygen as the test fluid are recorded by Fleming and Staub.[22] Little detail is known about the source of these data except that they were submitted to Fleming by the Marshall Space Flight Center for analysis. Since the experimental facilities were apparently similar to Figure 1 except that there was no outlet plenum, the present analysis was first applied to these data. Table 1 is a duplicate of Fleming and Staub's[22] Table I, containing all the available data. The nomenclature has been modified slightly to agree with that used here.

In calculating the dimensionless parameters from the data the following assumptions were made. Both $\Delta i'_{12}$ and $1/\rho'_1$ given in Table 1 were used. Ω was calculated by using the steady-state two-region approximation Equation 14 and the correct outlet density based on the enthalpy rise from the fluid. The outlet orifice coefficient was calculated from the pressure, density, and flow rate, assuming a sonic orifice. Inlet coefficients were used as estimated by Fleming. The friction factor was assumed constant throughout the test section, $\varphi_{12} = \varphi_{23}$. It was assumed to be constant for all calculations, as suggested by Fleming. The plenum volume was taken to be zero. The wall capacitance C_w and conduction time τ_w were calculated assuming that the tube was a standard 5/8 inch O.D. stainless steel pipe; the recorded inside diameter agrees with that assumption. Properties of the wall were taken near room temperature. The film heat transfer coefficient was calculated from the Dittus-Boelter correlation[23] based on inlet bulk fluid properties. A heat transfer coefficient of 1000 Btu per square foot °F was obtained for Run 5. As discussed in Section 5 under Solution Procedure, the approximate solution to the system equations was obtained only by assuming an appropriate average density in the reaction frequency $\mathcal{R}$, Equation 38. This was taken to be the arithmetic average density. This and the other more important assumptions made above are discussed in more detail in Section 7.

Table 2 lists the calculated dimensionless parameters required in the characteristic equation. The first four columns under Results give the results of plotting Nyquist diagrams for each run. The results are also plotted on Figure 5 as the negative operating point plus the crossover point or stability number, N_s, against the overall fluid expansion $\overline{u}_3$. On Figure 5 the solid points are the experimentally stable ones.

Note first the starting points of the Nyquist diagrams listed in Table 2. Those for Runs 1 and 2 both lie to the left of the operating point. This would indicate that the system is unstable in the steady-state, or Ledinegg, sense; therefore, the steady state could not have been experimentally attainable.

Table 1

TABLE OF DATA FROM NASA, 1 APRIL 1965
Copied from Fleming & Staub [22]

Case No.	1	2	3	4	5	6	7	8
p_o' (bars)	60.2**	60.2**	60.2**	60.2**	68.2	68.2	57.0	57.0
p_1' (psia)	843	847	860	864	960	942	788	820
p_3' (psia)	813	839	844	848	923	903	748	770
$p'_{average}$ (bars)	57.1	58.1	58.9	59.1	65.0	63.7	53.0	54.9
T_1' (° F)	-293	-293	-293	-295	-306	-308	-267	-267
$\Delta i_{13}'$ (joules/kg)	149(3)	149(3)	149(3)	153(3)	157(3)	157(3)	123(3)	123(3)
v_1' (m^3/kg)	1.0(-3)	1.0(-3)	1.0(-3)	1.0(-3)	1.0(-3)	1.0(-3)	1.0(-3)	1.0(-3)
$A_C'\rho_1'u_1'$ (kg/sec)	0.676	0.572	0.460	0.426	0.423	0.660	0.633	0.433
$q'\xi'\ell'$ (watts)	1.60(5)	1.42(5)	1.28(5)	1.25(5)	1.61(5)	1.70(5)	1.40(5)	1.00(5)
k_1' ($m^{-1}kg^{-1}$)***	4.37(5)	4.37(5)	4.37(5)	4.37(5)	9.6(5)	9.6(5)	4.1(5)	4.1(5)
Stable ?	Yes	Yes	No	No	No	Yes	Yes	No

In all tests, ℓ'=3.56 meters, D'=0.0141 meters, $A_C'=\pi D'^2/4$.
f varied from case to case, but generally assumed = 0.050 for calculations.

Note 1. Numbers in parentheses refer to powers of 10 (e.g., 5(3)=5 x 10^3).
Note 2. There were 3 tubes in parallel. $A_C'\rho_1'u_1'$ and q' are each 1/3 of the total $A_C'\rho_1'u_1'$ and q'.

** Calculated from assumption to constant k_1 for Cases 1, 2, 3, and 4.
*** Averages for the cases in a single test.

Table 2

DIMENSIONLESS PARAMETERS AND RESULTS FOR NASA OXYGEN DATA

	Dimensionless Parameters									Results						
Run*	Ω	τ_{12}	k_e	k_i	φ	c_3	C_w	$\mathcal{J}$	$\mathcal{J}_w$	Starting Point $G(0)$	Crossover Frequency x_c	Crossover Point $G(i\omega_c)$	Negative Operating Point K	Stability Number N_s	Pressure Drop Ratio Ψ	Nyquist Loop Size Σ
1	11.8	0.63	55.6	10.5	6.31	0	0.553	0.492	0.233	-70	12.7	-16	30	14	1.27	0.90
2	12.2	0.60	73.3	10.5	6.31	0	0.553	0.476	0.198	-42	13.3	-40	29	-11	1.20	0.97
-3	13.6	0.53	94.3	10.5	6.31	0	0.553	0.456	0.159	105	3.8	-108	28	-80	1.16	1.26
-4	14.2	0.52	100.9	10.5	6.31	0	0.553	0.448	0.148	132	3.9	-135	28	-107	1.15	1.33
-5	16.8	0.41	80.0	23.4	6.31	0	0.553	0.448	0.147	400	5.7	-327	52	-275	1.34	2.12
6	11.5	0.61	63.3	23.4	6.31	0	0.553	0.489	0.229	-43	13.0	-23	55	32	1.43	0.91
7	11.9	0.56	59.3	10.0	6.31	0	0.553	0.485	0.220	33	3.3	-41	27	-14	1.24	1.07
-8	12.0	0.53	104.4	10.0	6.31	0	0.553	0.450	0.150	121	3.7	-70	27	-43	1.14	1.07

* A negative sign on the run number is used to indicate that the run is experimentally unstable.

** In all cases $g = 0$ and $\varphi_{12} = \varphi_{23} = \varphi$ were used.

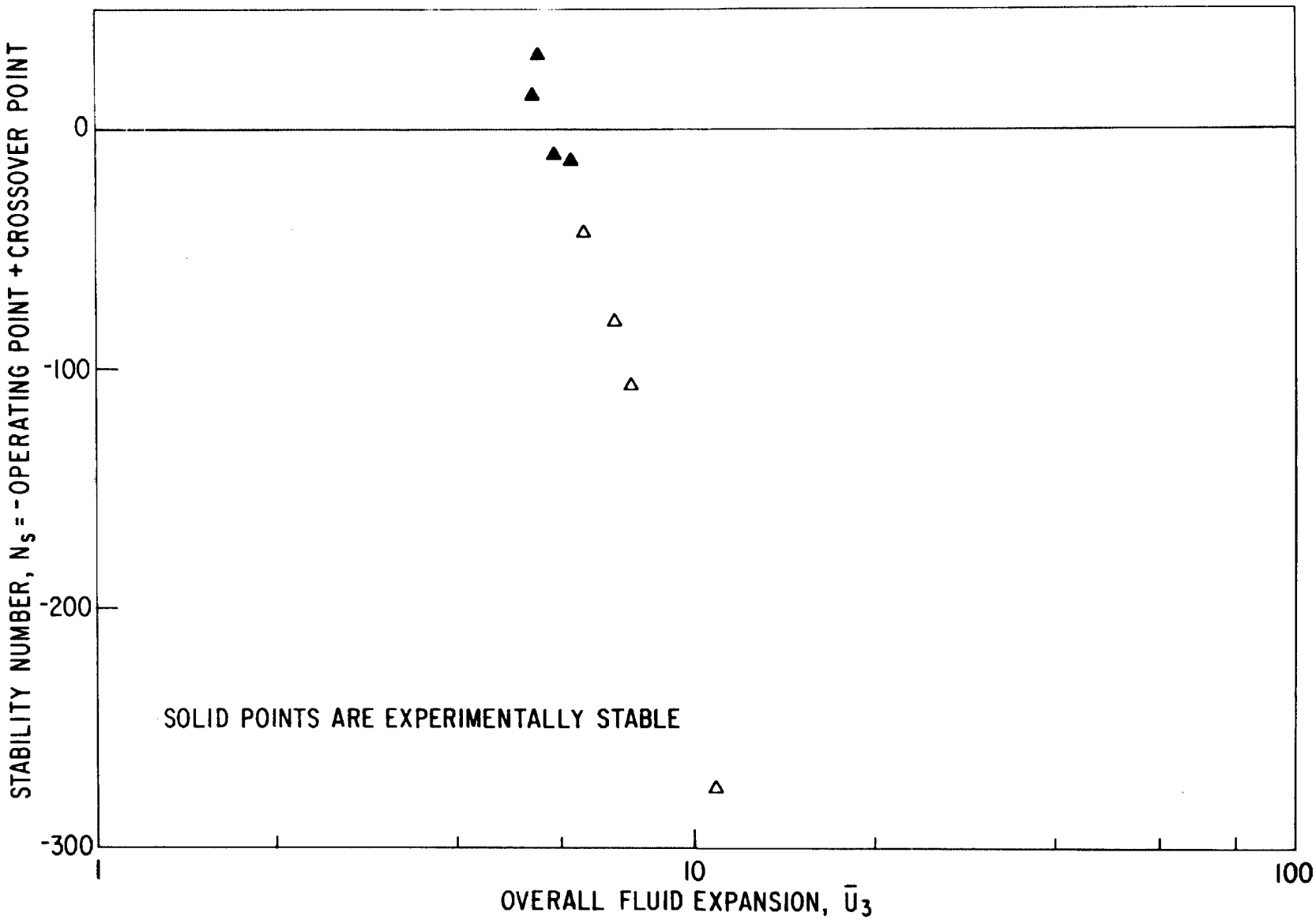

Figure 5. Stability Number for NASA Data

But it was. It will have to be assumed, then, that this results from inaccuracies in applying the model to the data or the set of data itself. This perhaps indicates the precision with which the model can be applied. The fact that the unstable runs have starting points lying much farther to the right than the stable runs indicates that these runs are more stable in the Ledinegg sense but less stable in the oscillatory sense that we are interested in here. This was also observed by Fleming in analyzing these data.[22]

The more important aspect of the stability analysis is the prediction of the oscillatory behavior. This is indicated by the stability number N_s in Table 2 and on Figure 5. A positive stability number indicates that the runs should be stable. All four unstable runs lie below $N_s = -43$. Therefore, the model and the Nyquist diagram predict a clear demarcation between the stable and the unstable runs. It is very close on the actual numerical value of $N_s > 0$ for stability. An error of - 14 could easily be accounted for in the inaccuracies of applying the model; it is less than that suggested by the error in the Ledinegg criterion discussed above for Run 1. The prediction then will be considered successful for all eight of these runs.

It can be noted also from Figure 5 that the unstable runs all have the higher outlet velocities or greater overall fluid expansion. This was the way that Stenning and Veiroglu were able to correlate their data[8] on boiling Freon. It will be seen from the data considered in this section that this is commonly observed for a given apparatus.

THURSTON PARAHYDROGEN DATA

The most extensive set of data available on instabilities occurring in the forced convection heating of a supercritical fluid is that by Thurston.[2] The apparatus used was of the same configuration shown in Figure 1 except that no upstream orifice was used. The test section was heated electrically. Thurston presented a total of 140 test runs made with his apparatus. Series of runs were made with different sized outlet orifices and outlet plena; some runs were also made with different heated lengths of the test section.

Only 47 of Thurston's runs were analyzed using the model described in Section 5 on page 9 . These runs were selected in the following manner. Thurston obtained far fewer stable than unstable runs, and about half of the stable runs had a very small temperature rise, and therefore expansion along the test section. All stable runs but these were analyzed. After analysis of one of the low-expansion runs (Run 66), it was felt that these would always give correct stability prediction because of their limited expansion; in order to give a stiffer test to the model, the remainder of these runs were omitted from analysis. The experimentally unstable runs analyzed were those immediately before and after a stable one; it was felt that this would allow a more direct comparison of the behavior of the predictions. In addition, the entire series of Runs 43 to 51, 52 to 68, and 69 to 72 were analyzed, except for the very low expansion runs.

Table 3 contains the data taken from Thurston's report[2] which were used to calculate the dimensionless system parameters. Parahydrogen physical property data were taken from Reference 24. The following assumptions were made in calculating the dimensionless variables from these data. The subcooling τ_{12} was estimated in such a way that the total fluid residence time τ_{13} was approximated as nearly as possible. The reason for this is discussed in more detail in Section 7. For a few of the runs that were considered in detail, the total residence time was adequately approximated if the enthalpy at the transition point followed the relation

$$i_2' = (2/3)(i_1' + 35)$$

where the enthalpies are expressed in British thermal units per pound. This relation was assumed to be adequate for the entire range of inlet conditions encountered. Once the subcooling τ_{12} was known Ω was calculated from Equation 14, using the correct outlet density. The fact that the pressure varied considerably in some runs was otherwise ignored. The friction factor was assumed constant throughout the test section and was back-calculated from the recorded pressure drop using the expressions for $\Delta\bar{p}$ in Section 5. This approach was used in all cases even though the $\Delta\bar{p}$ for some runs was quite low and of very limited accuracy. For these runs the flow was choked strongly downstream, and it was felt that less accuracy was needed for the friction pressure drop. The heat transfer coefficient was calculated from wall temperature measurements which Thurston reported for Run 57. For this run the coefficient obtained was about 1500 Btu/hr.ft.^{2} $^\circ$F. The coefficients for other runs were calculated from this figure, assuming that the Nusselt number varied as

$$N_u \propto (R_e)^{0.8} (P_r)^{0.4}$$

Bulk inlet physical properties were used in this relation except in a few cases. In those the Prandtl number was abnormally high because the temperature neared the transposed critical temperature. For those runs P_r was adjusted to a somewhat lower value.

Table 4 lists the calculated dimensionless parameters required in the characteristic equation. The stability results are tabulated in the last columns. Figure 6 has the stability number N_S plotted against the overall fluid expansion $\bar{u}_3$. Again the solid points were experimentally stable.

The results on Figure 6 indicate that the stability number gives a reasonable prediction for the system stability. As before, there appears to be a region down to about $N_S = -15$ for which the system is experimentally stable. If the predicted stability line were drawn at that point instead of at zero, only six data points would violate the criterion. Of these, three would differ only about ± 10 from the line. It is not believed that the data or the application of the analysis are more accurate than about ± 20 in the stability number. For example, in Run 30, which is incorrectly predicted to be unstable with

Table 3

EXPERIMENTAL DATA SELECTED FROM THURSTON[1]

Run*	T_1' (°R)	T_2' (°R)	p_1' (psia)	p_2' (psia)	Current (amps)	Voltage (volts)	V' (in.^{3})	ℓ' (in.)	Orifice Diameter (in.)
-6	59	322	206	204	567	8.8	22	120	0.052
-7	59	201	206	204	476	6.8	22	120	0.052
9	56	100	258	256	444	6.0	22	120	0.052
10	57	183	258	256	525	7.4	22	120	0.052
-11	62	311	259	257	617	9.5	22	120	0.052
-17	56	204	184	179	424	6.1	22	120	0.052
18	57	128	172	166	372	5.0	22	120	0.052
-28	52	364	262	250	1000	16.6	22	120	0.0995
29	52	276	262	249	930	14.7	22	120	0.0995
30	48	109	217	206	692	9.7	22	120	0.0995
-31	51	236	211	200	813	12.2	22	120	0.0995
-43	56	413	158	117	1334	24.0	22	120	0.201
-44	57	517	158	113	1390	26.4	22	120	0.201
-45	57	551	158	115	1388	26.5	22	120	0.201
-46	56	285	162	117	1216	20.4	22	120	0.201
47	52	126	162	117	1116	17.3	22	120	0.201
-48	57	507	242	180	1704	33.1	22	120	0.201
-49	57	368	236	177	1540	28.0	22	120	0.201
50	58	246	237	177	1380	23.0	22	120	0.201
51	61	231	238	173	1164	18.2	22	120	0.201
-52	58	444	248	184	1624	31.0	58	120	0.201
-53	57	383	248	185	1586	29.2	58	120	0.201
-54	58	309	247	187	1504	26.5	58	120	0.201
-55	56	182	246	186	1352	21.4	58	120	0.201
-56	58	478	205	148	1526	28.8	58	120	0.201
-57	57	424	207	158	1480	27.3	58	120	0.201
-58	57	340	207	153	1420	24.9	58	120	0.201
59	58	258	206	154	1326	22.0	58	120	0.201
-60	57	504	166	124	1678	26.1	58	120	0.201
-61	57	448	166	124	1366	75.1	58	120	0.201
-62	58	381	167	125	1320	23.4	58	120	0.201
-63	58	315	173	128	1276	22.0	58	120	0.201
-64	58	248	170	129	1200	19.8	58	120	0.201
-65	52	179	170	131	1136	17.8	58	120	0.201
66	49	56	170	133	996	14.1	58	120	0.201
67	53	574	117	85	1188	22.6	58	120	0.201
-68	52	291	112	85	994	16.3	58	120	0.201
-69	61	396	223	212	888	14.8	58	120	0.0995
70	61	319	223	211	842	13.5	58	120	0.0995
-71	60	342	202	185	808	13.0	58	120	0.0995
72	58	269	173	159	690	10.7	58	120	0.0995
-97	56	382	220	198	1090	18.7	58	120	0.130
98	50	119	218	203	838	12.0	58	120	0.130
-99	61	543	267	247	1280	24.0	58	120	0.130
-138	47	263	260	246	1284	15.3	58	83	0.130
-139	46	206	262	249	1212	13.8	58	83	0.130
140	45	140	264	251	1130	12.3	58	83	0.130

* A negative sign on the run number indicates that the run was experimentally unstable. For all runs: D' = 0.25 inch; ℓ_w' = 0.155 inch. The tube was stainless steel.

ble 4

.TS FOR THURSTON'S PARAHYDROGEN DATA

Results						
Starting Point $G(0)$	Crossover Frequency ω_c	Crossover Point $G(i\omega_c)$	Operating Point K	Stability Number N_s	Pressure Drop Ratio Ψ	Nyquist Loop Size Σ
13,900	18	-1150	0	-1150	4.33	1.85
9,700	18	-350	1	-349	4.28	0.73
5,000	14***	15***	3	18***	4.32	0.31
8,900	12	-450	1	-449	4.39	1.17
7,100	25***	-53***	0	-53***	4.10	0.62
18,400	12	-2100	6	-2094	4.05	2.47
7,300	19***	15***	7	22***	3.65	0.79
3,200	12	-700	1	-699	3.78	5.85
2,400	11	-350	1	-349	3.69	3.87
1,100	8	-58	3	-55	3.69	1.26
2,500	10	-550	1	-549	3.76	4.37
558	46	-74	0	-74	2.95	16.22
450	56	-56	0	-56	2.84	10.96
515	58	-61	0	-61	2.85	11.66
391	34	-55	0	-55	2.83	9.67
112	15	-13	0	-13	2.74	4.16
448	47	-54	0	-54	2.89	12.24
364	37	-41	0	-41	2.83	8.20
232	27	-22	0	-22	2.74	4.20
255	27	-3	0	-3	2.66	1.44
414	42	-55	0	-55	2.67	9.50
367	38	-47	0	-47	2.66	8.22
281	32	-30	0	-30	2.64	5.63
152	20	-16	0	-16	2.55	3.25
504	48	-81	0	-81	2.68	13.50
492	43	-65	0	-65	2.73	11.17
384	36	-55	0	-55	2.65	8.77
264	30	-31	0	-31	2.61	5.37
347	53	-43	0	-43	2.86	12.90
435	48	-54	0	-54	2.71	10.99
236	38	-14	0	-14	2.69	4.40
218	35	-14	0	-14	2.65	4.10
143	29	-5	0	-5	2.67	2.41
231	21	-30	0	-30	2.70	5.86
10	2	1	0	1	1.34	0.076
914	71	-161	0	-161	2.78	23.51
760	37	-128	0	-128	2.93	18.02
2,400	33	-18	0	-18	3.34	2.58
1,900	30	-5	0	-5	3.22	1.80
3,000	34	-65	1	-64	3.00	2.95
2,100	29	-24	1	-23	2.96	2.69
1,700	36	-87	0	-87	3.12	7.29
554	13	-10	1	-9	3.28	1.54
1,300	38	-26	0	-26	3.17	4.69
1,100	24	-29	0	-29	3.49	4.87
896	19	-18	0	-18	3.52	3.12
562	14	-8	1	-7	3.33	1.65

DIMENSIONLESS PARAMETERS AND RESU

	Dimensionless Parameters**								
Run*	Ω	τ	k_e	k_i	φ	c_3	C_w		
- 6	22.5	0.027	592	0	9.1	0.163	12.7	2.77	1.77
- 7	14.0	0.050	660	0	10.1	0.261	12.7	2.97	2.12
9	6.4	0.146	760	0	8.8	0.578	12.7	4.95	2.88
10	12.7	0.070	683	0	7.9	0.292	12.7	4.83	2.22
-11	10.6	0.009	570	0	6.2	0.324	12.7	3.73	3.53
-17	20.4	0.062	906	0	46.2	0.186	12.7	4.34	1.30
18	9.9	0.079	686	0	43.1	0.370	12.7	5.13	2.31
-28	30.0	0.035	103	0	7.6	0.125	12.7	5.75	3.47
29	22.7	0.049	103	0	8.3	0.165	12.7	5.92	3.99
30	11.3	0.150	107	0	9.8	0.353	12.7	6.76	5.08
-31	24.4	0.061	103	0	8.9	0.156	12.7	6.03	3.47
-43	61.0	0.026	6.96	0	2.80	0.062	12.7	5.58	7.00
-44	53.1	0.011	6.04	0	2.73	0.070	12.7	3.79	9.52
-45	55.4	0.010	6.72	0	2.94	0.067	12.7	3.79	8.88
-46	42.5	0.040	6.98	0	3.25	0.089	12.7	5.48	8.40
47	22.3	0.119	4.43	0	1.39	0.181	12.7	7.45	14.1
-48	50.2	0.020	6.70	0	2.52	0.074	12.7	5.59	10.5
-49	37.0	0.029	7.52	0	2.88	0.101	12.7	6.04	10.5
50	23.7	0.045	7.55	0	2.91	0.158	12.7	6.07	13.3
51	13.6	0.024	12.5	0	6.81	0.260	12.7	5.05	16.4
-52	41.1	0.022	7.54	0	3.12	0.239	12.7	6.03	10.4
-53	37.0	0.028	7.50	0	2.98	0.266	12.7	6.05	10.5
-54	23.4	0.034	7.59	0	2.71	0.347	12.7	6.25	12.4
-55	18.3	0.073	6.69	0	2.09	0.547	12.7	7.70	15.9
-56	53.3	0.020	6.95	0	3.26	0.185	12.7	5.80	8.50
-57	46.4	0.024	8.20	0	2.98	0.213	12.7	5.80	8.50
-58	38.8	0.032	7.50	0	3.16	0.255	12.7	5.95	9.62
59	27.9	0.042	7.29	0	2.75	0.355	12.7	5.99	11.8
-60	51.7	0.013	5.00	0	1.32	0.189	12.7	6.00	10.6
-61	45.4	0.015	7.15	0	2.74	0.215	12.7	6.00	9.48
-62	25.0	0.008	6.75	0	2.36	0.382	12.7	6.00	15.5
-63	23.7	0.014	6.55	0	2.43	0.404	12.7	6.00	15.5
-64	17.0	0.017	6.03	0	1.63	0.558	12.7	6.00	20.1
-65	28.1	0.083	7.20	0	2.13	0.368	12.7	6.98	10.2
66	1.76	0.579	5.98	0	0.13	5.67	12.7	9.65	43.1
-67	91.7	0.013	7.35	0	3.47	0.108	12.7	3.45	5.32
-68	67.2	0.046	9.34	0	3.84	0.151	12.7	5.15	4.69
-69	18.4	0.010	115	0	9.32	0.514	12.7	5.54	5.35
70	14.6	0.014	110	0	9.77	0.638	12.7	5.68	6.09
-71	22.3	0.020	116	0	18.5	0.430	12.7	4.30	4.13
72	16.0	0.017	112	0	16.6	0.589	12.7	8.34	5.07
-97	35.3	0.029	44.6	0	7.64	0.279	12.7	5.45	4.58
98	12.2	0.133	47.4	0	5.01	0.846	12.7	7.06	7.51
-99	26.0	0.010	43.3	0	4.76	0.369	12.7	6.00	7.32
-138	23.9	0.058	47.3	0	3.16	0.606	12.7	7.68	7.98
-139	18.8	0.079	48.1	0	2.76	0.777	12.7	6.82	8.96
140	12.6	0.122	46.6	0	2.71	1.173	12.7	7.09	11.1

* A negative sign on the run number indicates that it was experimentally unstable.

** In all cases g = 0 and $\varphi_{12} = \varphi_{23} = \varphi$ were used.

*** Estimated, see discussion.

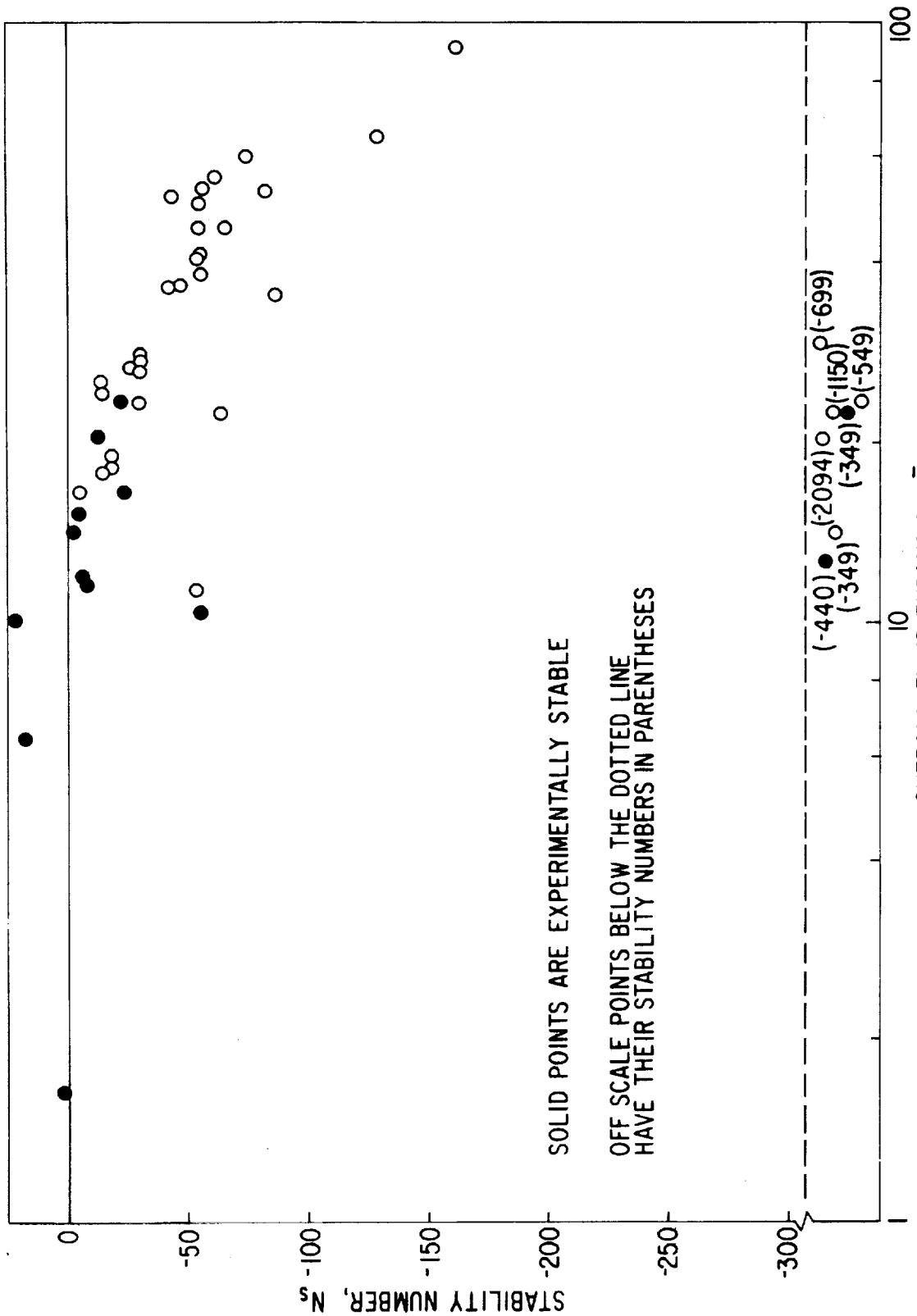

Figure 6. Stability Number for Thurston Data

a stability number of - 55, an upstream pressure drop of only 1 psia would increase the stability number by 10.

All Nyquist diagrams encountered for these data were of the form of Figure 4, except three--for Runs 9, 11, and 18 of Table 4. These were only slightly different, as shown by the solid curves in Figures 7, 8, and 9. The failure, shown here, of the first loop of the diagram to cross the real axis appears to be a peculiarity of this particular series of runs. The dotted curves are exact numerical solutions which will be discussed in Section 7. For these diagrams the crossover point and frequency was estimated from the maximum in the first loop. This would be where the loop would cross over the real axis if it were shifted up slightly until it was tangent. However, it should be clear that great caution should be used before drawing any firm conclusions from these Nyquist diagrams.

CLEVELAND OXYGEN DATA

A development study of the J-2 Four-coil Heat Exchanger for the Apollo spacecraft was conducted by J.R. Cleveland[25] at the Rocketdyne Division of North American Aviation, Inc. These tests were aimed primarily at obtaining heat transfer data for operation with liquid oxygen. The limit of stable performance was also determined, by reducing the oxygen flow rate until oscillations occurred.

The following discussion applies the results of the asymptotic analysis to the data of Cleveland.

System

The system was a helically wound four-coil, three-pass heat exchanger, 61.2 feet in length and 5/8 inch in outside diameter. The liquid oxygen was heated by hot gas in the shell side of the exchanger. The system is essentially represented by Figure 1 if the plenum is disregarded and the downstream constriction is assumed to be a valve.

Table 5 is a summary of the pertinent information for the Cleveland tests. The orifice sizes considered were: 0.0, 0.108, and 0.1 inch diameter. The flow rate was controlled by a downstream valve. Temperature and pressure measurements were taken upstream of the orifice and upstream of the valve. Table 6 outlines the range of temperature, pressure, and flow rate conditions.

A more extensive tabulation of the inlet and exit conditions of the nine runs considered in detail is presented in Table 7 along with the flow rate at which oscillations first occur and the engine conditions for a given run.

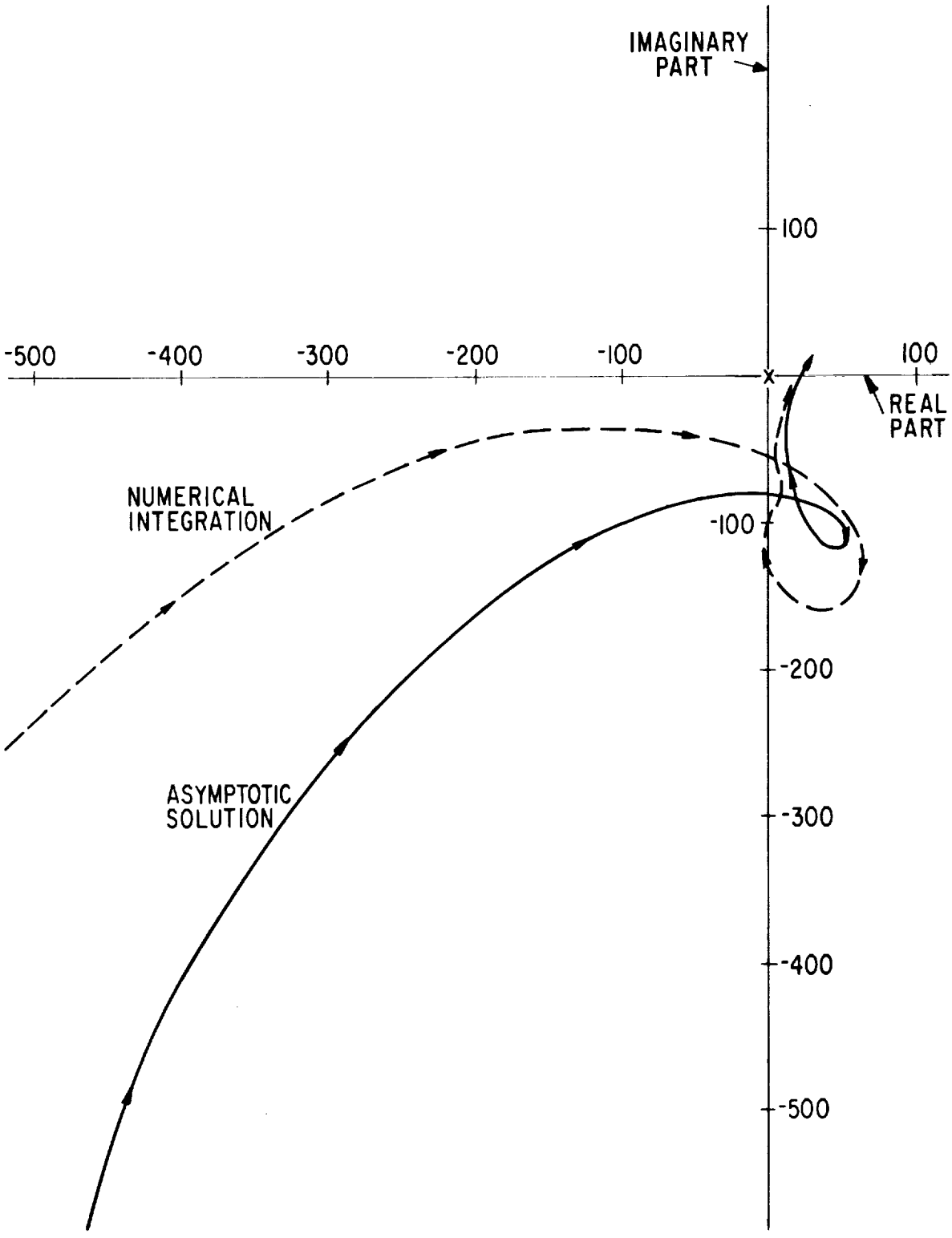

Figure 7. Nyquist Diagram for Thurston Run 9

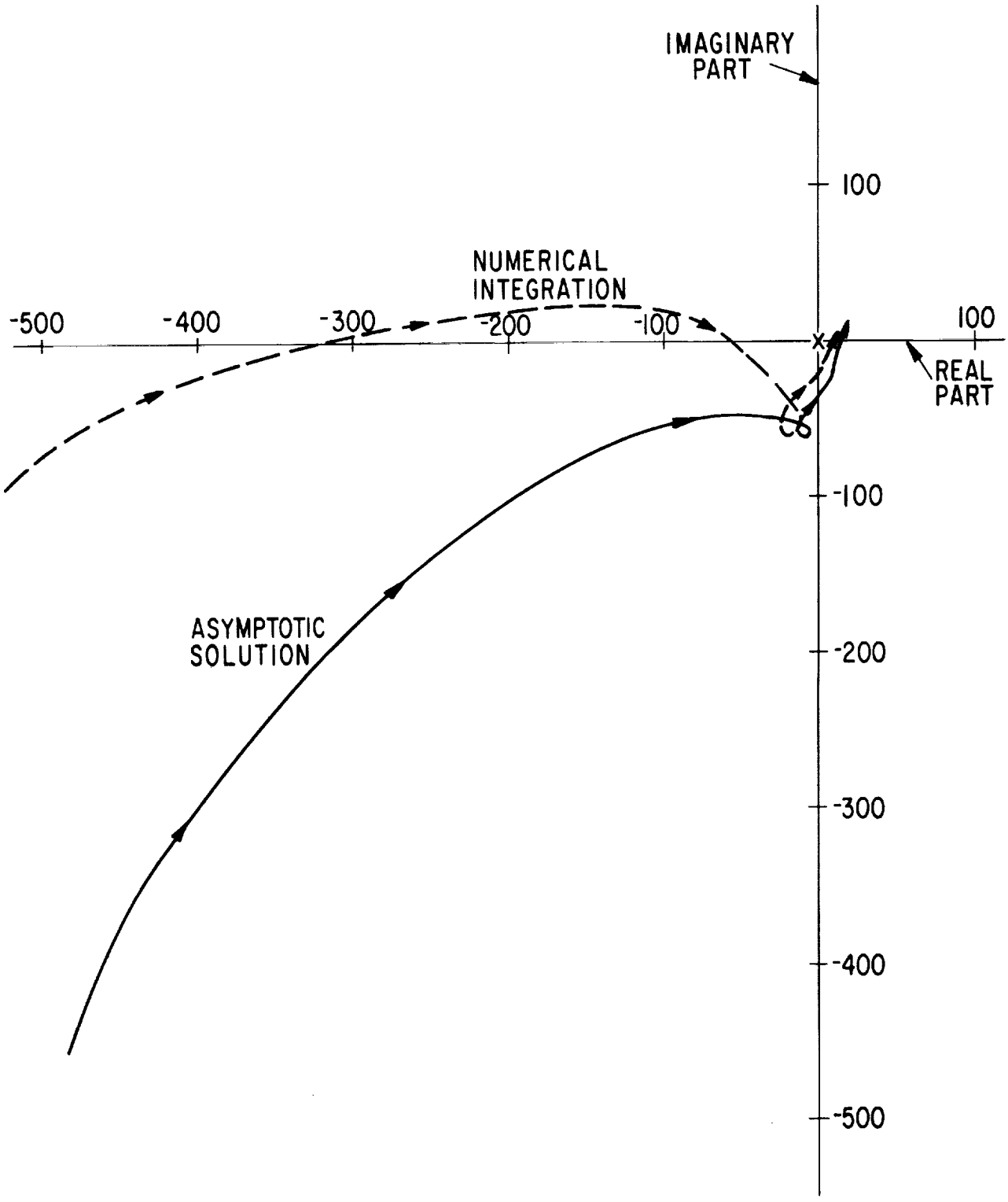

Figure 8. Nyquist Diagram for Thurston Run 11

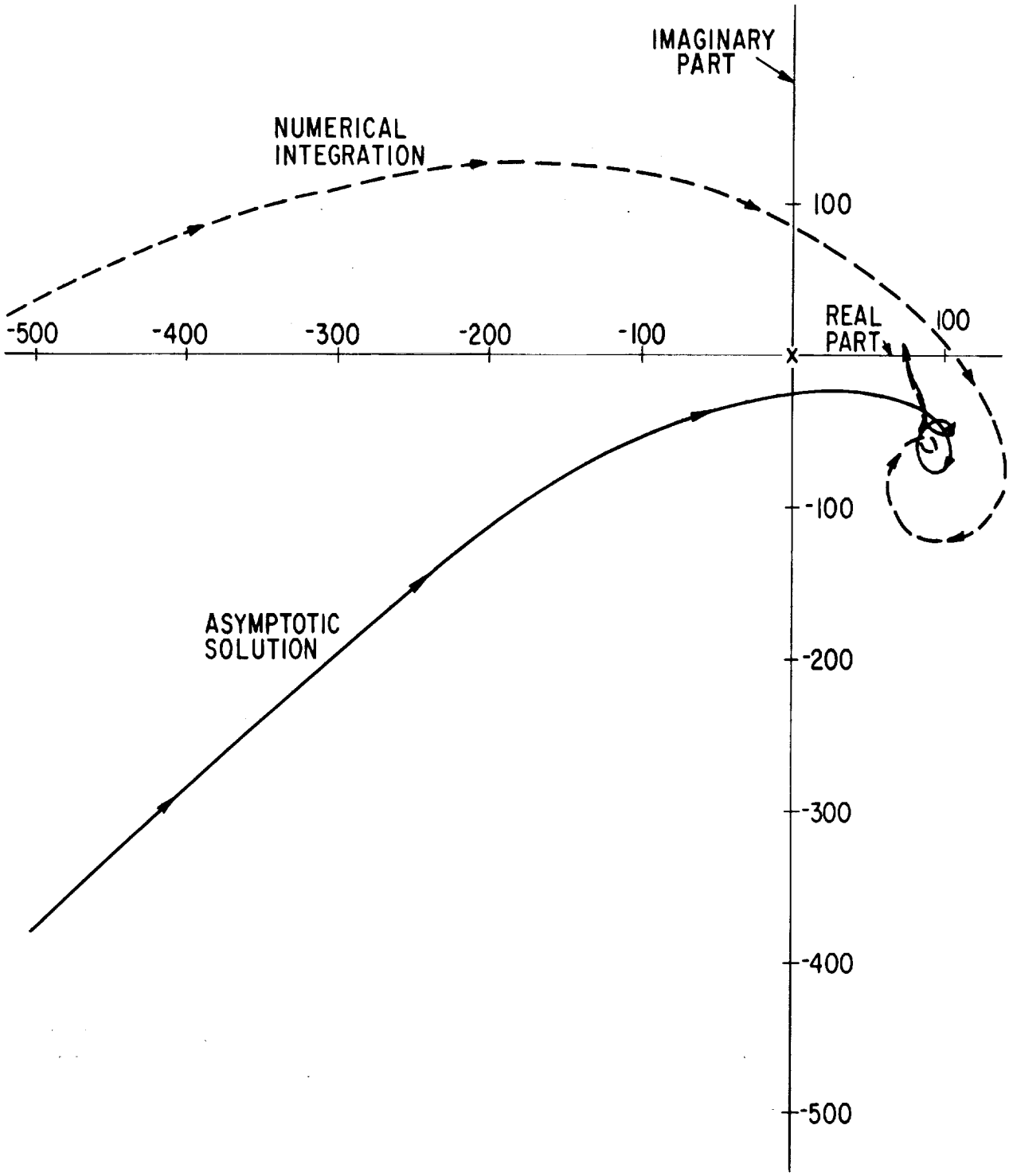

Figure 9. Nyquist Diagram for Thurston Run 18

Table 5

HEAT EXCHANGER DATA FOR CLEVELAND TESTS

Outside Diameter = 5/8 in.

Wall Thickness = 0.035 in.

Cross-sectional Area of Tube = 1.679×10^{-3} ft^2

Cross-sectional Area of Wall = 4.34×10^{4} ft^2

No. of Passes = 3

Length per Pass = 20.4 ft

Total Length = 61.2 ft

Table 6

TEMPERATURE, PRESSURE, AND FLOW RATE RANGES

	T_o (°C)	p_o (atm)	T_3 (°C)	p_3 atm	w (lb/sec coil)
Maximum	-154	70.8	314	67.6	5.29
Minimum	-177	44.8	-73.9	31.6	0.395

Engine conditions refer to the temperature and, to a lesser extent, the flow rate of the hot gas entering the shell side of the heat exchanger. The engine conditions and corresponding approximate temperatures are listed below.

Engine Conditions	Inlet Hot Gas Temperature
minimum	550° F
nominal	700° F
maximum	820° F

The hot gas flow rate varied between 4.32 and 7.29 pounds per second.

Table 7

INLET AND OUTLET CONDITIONS

Run	Slice	w (lb/sec)	T_1 (°C)	p_o (atm)	T_3 (°C)	p_3 (atm)	Minimum Stable Flow Rate (lb/sec)	Engine Conditions
17	24	1.4	-169	60.7	108.9	54.7	0.73	Nominal
17	44	1.13	-120	62.3	149.0	58.1		
17	64	0.96	-170	62.6	182.0	59.5		
17	5	0.733	-169	64.0	230.0	61.5		
19	20	2.08	-166	59.6	37.8	51.5	0.95	Nominal
19	36	1.71	-167	61.7	79.4	55.1		
19	52	1.31	-167	62.6	136.6	58.0		
19	68	1.1	-167	63.2	173.9	59.8		
19	100	0.95	-166	63.4	204.4	60.9		
20	59	1.40	-170	51.6	37.7	47.0	0.95	Minimum
20	70	1.14	-168.8	52.3	65.5	48.6		
20	100	0.95	-168.9	52.2	100.5	49.8		
27	64	1.04	-166	44.8	176.1	41.1	0.35	Nominal
27	109	0.845	-165	53.0	231.0	50.7		
27	122	0.445	-162	61.5	298.3	60.9		
27	95	0.395	-161	62.1	302.0	61.5		
30	64	0.985	-170	36.3	51.0	33.6	0.7	Minimum
30	125	0.74	-167	44.7	148.0	43.2		
30	88	0.72	-168	44.0	142.0	42.5		
31	138	0.835	-167	53.6	222.0	51.3	0.4	Nominal
31	69	0.76	-169	55.3	239.0	53.4		
31	90	0.455	-167	60.9	299.0	60.2		
31	116	0.437	-165	62.9	314.4	62.2		
33	52	4.02	-170	50.7	-73.9	31.6	0.91	Minimum
33	76	3.00	-169	52.7	-27.8	31.8		
33	99	1.95	-167	54.1	37.0	47.3		
33	121	1.48	-165	54.1	85.6	50.0		
33	157	0.91	-154	54.7	186.0	52.7		
34	23	5.29	-172	59.5	-71.7	32.3	0.9	Nominal
34	43	5.01	-127	60.2	-67.2	35.0		
34	60	3.99	-173	62.2	-37.8	45.9		
34	78	2.14	-172	64.9	55.5	52.7		
34	94	1.92	-170	64.9	82.8	58.1		
34	106	1.05	-168	65.6	194.0	63.6		
34	132	1.05	-167	66.3	197.0	63.6		
35	36	4.5	-174	64.9	-17.7	36.3	0.9	Maximum
35	54	4.03	-175	65.6	-1.11	42.5		
35	74	3.04	-174	67.6	52.7	53.1		
35	90	2.05	-174	68.7	138.0	60.0		
35	100	1.37	-176	68.7	221.0	67.6		

From Table 7 it is seen that with the one exception of Run 27, slice 64, all the tests were conducted for oxygen above its critical pressure* at the exchanger inlet. The majority of exit pressures are also supercritical. Subcritical pressure occurred at the exit for large valve openings and/or small inlet orifices.

The variables of greatest importance in determining the minimum flow for stable performance are: inlet orifice diameter, pressure, and engine conditions.

Calculation for Dimensionless Parameters

τ_{12} and Ω. The dimensionless parameters τ_{12} and Ω represent the fraction of the exchanger tube which contains fluid in the dense phase and the volumetric expansion, respectively. These parameters are evaluated from a knowledge of the inlet and exit temperatures and pressures. The inlet and exit points were connected by a straight line on a pressure-enthalpy diagram for oxygen. The specific volume-enthalpy curves were computed from this line. As will be discussed in Section 7, τ_{12} was computed by finding that line for the light fluid on the specific volume-enthalpy curve which will generate a curve of the same area for the density versus enthalpy curve. The quantity Ω is then computed from the slope of the specific volume-enthalpy curve at the exit. Inlet and exit conditions are forced to agree with those actually measured. The inlet pressure is that pressure calculated downstream of the orifice.

k_e, k_i, and φ. The dimensionless coefficient k_e which describes the constriction of the exit valve was computed from Equation 67, which is written in dimensioned terms to become, after rearrangement,

$$k_e = \frac{4610\ p_3'}{G'\bar{u}_3'} \tag{78}$$

where the units of p_3', G', and $\bar{u}_3'$ are psia, pound per square foot per second, and foot per second, respectively. The exit velocity $\bar{u}_3'$ was computed via the ideal gas law, thus

$$\bar{v}_3' = \frac{G'}{\bar{\rho}_3'} \tag{79}$$

and the exit density for gaseous oxygen is given by

$$\rho_3' = \frac{2.98\ p_3'}{T_3'} \tag{80}$$

---

*Critical constants for oxygen are:

$T_c' = 154\ ^\circ K \qquad p_c' = 49.7$ atm $\qquad v_c' = 2.33$ cc/g

where the units for ρ_3' and T_3' and pounds per cubic foot and degrees Rankine, respectively.

The dimensionless inlet orifice coefficient was obtained from the following relation:

$$\Delta\bar{p}_{o1} = k_i \tag{81}$$

This is recast into dimensioned quantities and put in terms of the mass velocity, G', to yield

$$k_i = \frac{3.1 \times 10^5 \, \Delta\bar{p}_{o1}'}{G'} \tag{82}$$

where $\Delta p_{o1}'$ has units of psi. The pressure drop across the inlet orifice is computed from the following relation:

$$\Delta\bar{p}_{o1} = (\Delta\bar{p}_{o3})_{meas} - (\Delta\bar{p}_{13})_{calc} \tag{83}$$

where $(\Delta p_{o3})_{meas}$ is the measured pressure drop across the exchanger and $(\Delta p_{13})_{calc}$ is the calculated pressure drop. The pressure drop Δp_{13} is the sum of the friction and acceleration pressure drops.

The friction pressure drop was obtained from the formula

$$\Delta\bar{p}_{12} + \Delta\bar{p}_{23} = \varphi_{12} = \varphi_{23} = \varphi \tag{84}$$

where

$$\varphi = \frac{f\ell'}{2D'} \tag{85}$$

and

$$f = \frac{0.316}{R_e^{1/4}} \tag{86}$$

Conversion of Equation 84 to dimensioned quantities produces

$$\Delta\bar{p}_{12} + \Delta\bar{p}_{23} = 2.02 \times 10^3 \, f \, w'^2 \tag{87}$$

where w' has units of pounds per second. Greater consistency of analysis would be achieved by calculating the friction pressure drop from both the light and heavy region friction losses (Equations 52 and 59). However, the approach adopted gave more nearly constant values for the orifice coefficient during a given run.

The acceleration pressure drop results from the increased velocity of the light region and is given by

$$\Delta\bar{p}'_a = \frac{G'(\bar{u}'_3 - \bar{u}'_1)}{4610} \tag{88}$$

where the units are as already given. Therefore,

$$(\Delta\bar{p}_{13})_{calc} = \Delta\bar{p}_{12} + \Delta\bar{p}_{23} + \Delta\bar{p}_a \tag{89}$$

Equation 89 was used in conjunction with Equation 83 to obtain the pressure drop across the orifice, $\Delta\bar{p}_{o1}$. This was then inserted into Equation 82 to yield the inlet orifice coefficient.

Table 8 is a tabulation of the calculated friction and acceleration pressure drops compared to the measure drop $(\Delta p'_{o3})_{meas}$. The first section of the table is based on the usual friction factor of Equation 86. However, allowance might be made for the curves in the heat exchanger tube by multiplying the friction factor by a factor up to 1.5, as was done in the second part of Table 8. It is seen that the measured and calculated pressure losses are in fair agreement for runs with no inlet orifices.

Estimation of the inlet orifice coefficient was based on the unmodified friction factor given by Equation 86.

The quantity φ is directly computed from

$$\varphi = \frac{f\ell'}{2D'} \tag{90}$$

which for the dimensions of this system becomes

$$\varphi = 662\ f \tag{91}$$

C_w, $\mathfrak{I}$, and $\mathfrak{I}_w$. These parameters are defined by the relations

$$C_w = \frac{A'_w\ \rho'_w\ c'_w}{A'_c\ \rho'_1\ c'_p} \tag{92}$$

$$\mathfrak{I} = \frac{A'_w\ \rho'_w\ c'_w\ \bar{u}'_1}{h'\ \xi'\ \ell'} \tag{93}$$

and

$$\mathfrak{I}_w = \frac{\rho'_w\ c'_w\ \ell'\bar{u}'^2}{h'_w} \qquad \frac{\bar{u}'_1}{\ell'} \tag{94}$$

Table 6

COMPUTED AND MEASURED PRESSURE DROPS

1. $f = \frac{0.316}{R_e^{1/4}}$, Normal friction factor

Run Number	Orifice (in.)	Friction Δp (psia)	Acceleration Δp (psia)	Total Calculated Δp_{ca} (psia)	Meas. Δp_{ca} (psia)
1724	None	21.6047	41.2257	62.8304	90.00
1744		14.9546	28.1569	43.1115	60.00
1764		11.144	21.2088	32.3528	50.00
17135		7.0184	13.3549	20.3733	40.00
1920	None	43.0478	78.4756	121.5235	136.00
1936		30.5241	56.1377	86.6618	97.00
1952		19.2424	36.4734	55.7158	72.00
1968		14.2132	27.3702	41.5834	58.00
19100		11.0207	21.4704	32.4911	44.00
2059	None	21.6801	39.1967	60.8767	67.00
2070		15.0789	27.2855	42.3645	54.00
20100		10.9989	20.50	31.499	37.00
2727	0.1	20.4595	91.0318	111.4913	600.00
2764		12.6375	34.9176	47.5552	350.00
2795		2.3897	4.4608	6.8505	50.00
27109		9.0624	21.7425	30.8042	210.00
27122		2.9443	5.6815	8.6257	60.00
3036	0.108	19.7776	64.9577	84.7352	540.00
3064		11.8379	28.6018	40.4397	300.00
3088		6.8441	15.509	22.3531	170.00
30125		7.1796	16.3384	23.5179	160.00
3128	0.108	21.3478	84.6099	105.9577	560.00
3168		7.5182	16.9443	24.4625	150.00
3190		3.0624	6.0156	9.078	70.00
31116		2.8586	5.5241	8.3827	40.00
31138		8.8657	20.5555	29.4212	200.00
3335	None	164.9126	396.4786	561.3912	340.00
3352		136.1268	305.3465	441.4733	280.00
3376		81.2386	157.5621	238.8007	160.00
3399		38.4621	74.9595	113.4216	100.00
33121		23.8437	47.4524	71.2961	60.00
33138		10.2458	20.8748	31.1206	30.00
33157		10.2661	21.9564	32.2225	30.00
3423	None	257.6282	626.6031	884.2317	400.00
3443		199.3323	440.5701	639.9023	370.00
3460		132.7043	241.2803	373.9846	240.00
3478		73.3421	126.3341	199.6763	180.00
3494		37.2921	67.4948	104.787	100.00
34106		13.0917	24.5009	37.5925	30.00
34132		13.0953	24.6539	37.7492	40.00
3536	None	166.7547	428.7238	595.4779	420.00
3554		136.8319	311.8545	448.6864	340.00
3574		83.3548	169.6658	253.0206	214.00
3590		42.0744	86.7866	128.8611	129.00
35100		20.8962	43.7203	64.6165	75.00

Table 8 (Cont'd)

2. $f = 1.5 \left(\frac{0.316}{R_e^{1/4}}\right)$, Friction factor increased by 50%

Run Number	Orifice (in.)	Friction Δp (psia)	Acceleration Δp (psia)	Total Calculated Δp_{ta} (psia)	Meas. Δp_{ob} (psia)
1724	None	32.3908	41.2257	73.6166	90.00
1744		22.4206	28.1569	50.5775	60.00
1764		16.7076	21.2088	37.9164	50.00
1784		16.7076	21.2088	37.9164	50.00
17135		10.5224	13.3549	23.8773	40.00
1920	None	64.5395	78.4756	143.0151	136.00
1936		45.7632	56.1377	101.9009	97.00
1952		28.8492	36.4734	65.3225	72.00
1968		21.3091	27.3702	48.6793	58.00
19100		16.5228	21.4704	37.9932	44.00
2059	None	32.5038	39.1967	71.7005	67.00
2070		22.6071	27.2855	49.8926	54.00
20100		16.4901	20.50	36.9902	37.00
2727	0.1	30.674	91.0318	121.7057	600.00
2764		18.9468	34.9176	53.8645	350.00
2795		3.5827	4.4608	8.0435	50.00
27109		13.5868	21.7425	35.3293	210.00
27122		4.4142	5.6815	10.0957	60.00
3036	0.108	29.6515	64.9577	94.6092	540.00
3064		17.748	28.6018	46.3498	300.00
3088		10.261	15.509	25.77	170.00
30125		10.764	16.3384	27.1023	160.00
3128	0.108	32.0057	84.6099	116.6156	560.00
3168		11.2716	16.9443	28.2159	150.00
3190		4.5913	6.0156	10.6069	70.00
31116		4.2857	5.5241	9.8098	40.00
31138		13.2919	20.5555	33.8474	200.00
3335	None	247.2453	396.4786	643.7239	340.00
3352		204.0882	305.3465	509.4347	280.00
3376		121.797	157.5621	279.3591	160.00
3399		57.6644	74.9595	132.6239	100.00
33121		35.7476	47.4524	83.2001	60.00
33138		15.361	20.8748	36.2359	30.00
33157		15.3914	21.9564	37.3478	30.00
3423	None	386.2497	626.6031	1012.8528	400.00
3443		298.849	440.5701	739.4191	370.00
3460		198.9569	241.2803	440.2373	240.00
3478		109.9582	126.3341	236.2923	180.00
3494		55.9102	67.4948	123.4051	100.00
34106		19.6277	24.5009	44.1286	30.00
34132		19.6331	24.6539	44.287	40.00
3536	None	250.0071	428.7232	678.7302	420.00
3554		205.1452	311.8545	516.9997	340.00
3574		124.9697	169.6658	294.6355	214.00
3590		63.0801	86.7866	149.8668	129.00
35100		31.3286	43.7203	75.0489	75.00

The parameter C_w, which is the ratio of wall to fluid heat content, remains substantially constant from run to run. Inserting the following values for density and heat capacity

$$\rho'_w = 488 \text{ lb/ft}^3$$

$$\rho'_l = 67.3 \text{ lb/ft}^3$$

$$c'_w = 0.11 \text{ Btu/lb } ^\circ\text{F}$$

$$c'_p = 0.4 \text{ Btu/lb } ^\circ\text{F}$$

there results

$$C_w = 0.528$$

This value was used throughout the series of tests.

Calculation of the heat transfer coefficient h' used for $\mathcal{J}$ is based on the equation

$$N_u = 0.023 \, R_e^{0.8} \, P_r^{0.4} \left(\frac{T_w}{T}\right)^{-0.765} \tag{95}$$

recommended by Thurston[26, 27] and Williamson[28] for hydrogen flowing through tubes.

For purposes of illustration, the heat transfer coefficient is calculated for Run 20 slice 70. The property values are taken to be[29]

$$\mu' = 9.6 \times 10^{-5} \text{ poise} = 6.45 \times 10^{-6} \text{ lb}_m/\text{ft sec}$$

$$k' = 0.02 \text{ Btu/hr ft } ^\circ\text{F}$$

$$c'_p = 0.4 \text{ Btu/lb}_m \, ^\circ\text{F}$$

The temperature of the wall and bulk fluid are taken to be 1110° R and 580° R, respectively. The flow rate for Run 20 slice 70 is 1.14 pounds per second; hence the mass velocity is

$$G' = 6.8 \times 10^2 \text{ lb}_m/\text{ft}^2 \text{ sec}$$

With the introduction of these values into Equation 95 there results a heat transfer coefficient for the run of

$$h' = 1000 \text{ Btu/hr ft}^2 \,^\circ\text{F}$$

The transfer time $\mathcal{T}_w$ is now written in terms of mass flow rate:

$$\mathcal{T} = 0.0931\, w'^{0.2} \tag{96}$$

The conduction time $\mathcal{T}_w$ is directly related to the flow rate by

$$\mathcal{T}_w = 0.02775\, w' \tag{97}$$

where the thermal conductivity of the wall was taken as 8.5 Btu/ft $^\circ$F hr.

Table 9 is a summary of the dimensionless parameters for Cleveland's runs. Also included are results derived from the Nyquist plot, i.e., the starting point G(o): the crossover frequency, ω_c; the crossover point $G(i\omega_c)$; the negative of the operating point K; the stability number $K + G(i\omega_c)$; the stabilizing-to-destabilizing pressure drop ratio Ψ; and the Nyquist loop size $\leq$. As the oxygen flow rate is reduced, τ_{12} is decreased while Ω tends to be increased. Naturally the exit orifice coefficient tends to be increased as the valve is closed. The inlet orifice coefficient used was an average of the several values found for a particular run.

Results

The sum of the crossover point and the negative of the operating point is an indication of the stability of a particular run. This sum, defined as the stability number N_s, is plotted versus the mass flow rate in Figures 10 to 18. The curves are plotted for an average inlet orifice coefficient as well as the maximum and minimum values found for the run.

It should be kept in mind that several variables are simultaneously varying with flow rate at a fixed inlet coefficient, namely, τ_{12}, Ω, and k_e. Hence, the curves should be expected to exhibit nonlinear behavior. This seems to be the case generally. In the neighborhood of minimum stable flow rate there is usually found a rapid decline in the stability number.

Assuming other parameters such as Ω and τ_{12} are unchanged, the stabilizing effect of a large inlet orifice coefficient is readily apparent from the figures. The stability number, maintaining the other variables constant, will vary linearly with inlet orifice coefficient.

The agreement of the analysis with the data is generally good for runs where no inlet orifice was present. However, in those runs where an inlet orifice was used (see Figures 16, 17, and 18) it was found that the predictions tended to be far on the stable side.

DIMENSIONLESS PARAMETE

Run/Slice	Inlet Orifice Diameter (in.)	w (lb/sec)	Dimensionless Parameters Ω	τ_{12}	k_e	k_i	φ	c_3
17/24	none	1.4	22.3	0.198	18.5	17.5	5.07	0
17/44		1.13	24.5	0.178	28.8	17.5	5.34	0
17/64		0.96	26.7	0.177	39.3	17.5	5.57	0
17/135		0.733	28.0	0.161	64.7	17.5	8.90	0
19/20	none	2.08	21.4	0.242	9.0	7.56	4.59	0
19/36		1.71	22.8	0.22	13.6	7.56	4.82	0
19/52		1.31	23.5	0.18	22.2	7.56	5.15	0
19/68		1.10	25.1	0.17	30.5	7.56	5.38	0
19/100		0.95	27.1	0.17	39.0	7.56	5.58	0
20/59	none	1.4	23.5	0.24	16.7	5.26	5.06	0
20/70		1.14	22.6	0.21	24.8	5.26	5.33	0
20/100		0.95	26.7	0.208	34.0	5.26	5.58	0
27/64	0.1	1.04	36.9	0.167	16.7	235.0	5.48	0
27/109		0.845	35.3	0.163	33.0	235.0	5.75	0
27/122		0.445	31.5	0.141	151.0	235.0	6.75	0
27/95		0.395	31.2	0.139	195.0	235.0	6.95	0
30/64	0.108	0.985	30.5	0.197	16.6	231.0	5.5	0
30/125		0.74	33.7	0.176	37.4	231.0	5.9	0
30/88		0.72	34.3	0.179	38.8	231.0	6.0	0
31/138	0.108	0.835	35.0	0.167	35.3	202.0	5.77	0
31/68		0.76	33.1	0.158	44.6	202.0	5.90	0
31/90		0.455	31.8	0.141	141.0	202.0	6.71	0
31/116		0.437	32.2	0.139	159.0	202.0	6.78	0
33/52	none	4.02	18.7	0.303	1.43	-5.3	3.9	0
33/76		3.00	17.8	0.264	3.70	-5.3	4.2	0
33/99		1.95	23.5	0.244	8.8	-5.3	4.7	0
33/121		1.48	24.9	0.213	14.7	-5.3	5.0	0
33/157		0.91	31.0	0.176	33.8	-5.3	5.6	0
34/33	none	5.29	18.5	0.310	0.70	-5.2	3.6	0
34/43		5.01	20.9	0.334	1.10	-5.2	3.7	0
34/60		3.99	16.8	0.293	2.60	-5.2	2.6	0
34/78		2.84	17.5	0.257	5.70	-5.2	4.2	0
34/94		1.92	21.3	0.217	11.9	-5.2	4.7	0
34/106		1.05	24.8	0.169	36.3	-5.2	5.4	0
34/132		1.05	24.8	0.168	36.1	-5.2	5.4	0
35/36	none	4.5	24.8	0.301	1.10	-2.4	3.78	0
35/54		4.03	22.8	0.283	1.90	-2.4	3.89	0
35/74		3.04	20.5	0.234	4.30	-2.4	4.18	0
35/90		2.05	22.7	0.191	9.6	-2.4	4.61	0
35/100		1.37	25.7	0.166	20.6	-2.4	5.09	0

* In all runs $\varphi_{12} = \varphi_{23} = \varphi$ and $g = 0$

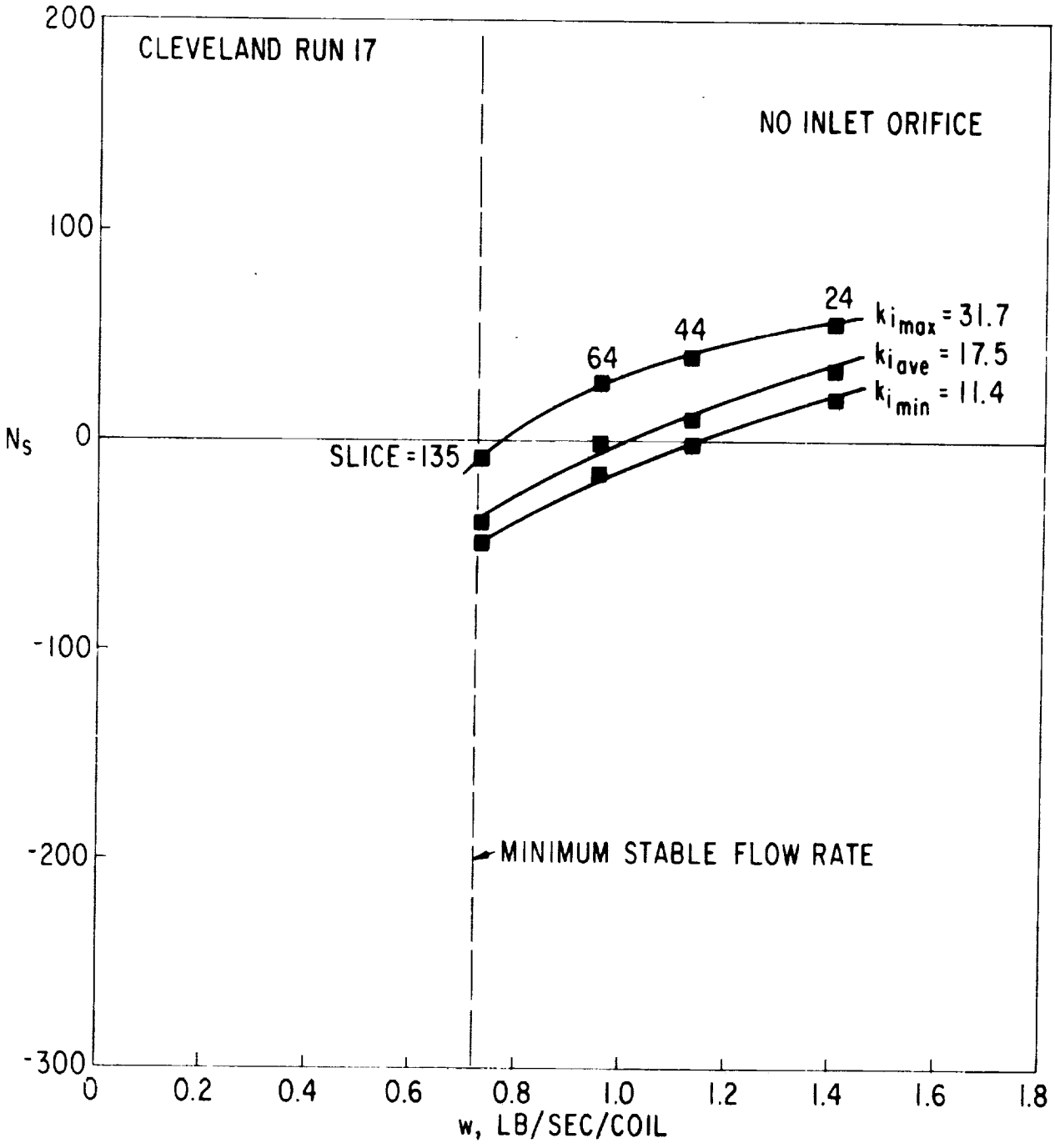

Figure 10. Stability Number Versus Flow Rate for Cleveland Run 17

le 9

RS FOR CLEVELAND'S DATA

			Results						
C_w	γ	γ_w	G(o)	w_c	G(iw_c)	K	N_s	ψ	Σ
0.528	0.0994	0.0397	326	11.8	-4.1	37.0	32.9	1.99	0.73
0.528	0.0952	0.031	562	13.2	-26.0	37.0	11.0	1.67	0.89
0.528	0.0924	0.027	832	13.4	-40.2	38.0	-2.2	1.51	0.91
0.528	0.088	0.020	1446	14.7	-75.8	37.9	-37.9	1.34	0.40
0.528	0.1078	0.058	146	9.5	0.42	17.3	17.7	1.94	0.66
0.528	0.104	0.048	236	10.7	-4.0	17.2	13.2	1.68	0.76
0.528	0.098	0.036	425	13.0	-22.7	17.0	-5.7	1.45	0.86
0.528	0.095	0.031	619	13.9	-41.0	17.0	-24.0	1.34	0.97
0.528	0.092	0.026	833	13.9	54.0	17.0	-177.0	1.27	1.26
0.528	0.099	0.039	270	9.6	10.2	12.9	23.1	1.46	0.65
0.528	0.094	0.032	414	11.1	17.5	12.7	30.5	1.33	0.63
0.528	0.092	0.026	645	11.4	6.04	12.8	18.8	1.25	0.83
0.528	0.094	0.029	520	14.7	-91.2	471.0	380.0	13.2	2.00
0.528	0.090	0.024	928	15.0	-131.0	472.0	341.0	2.21	1.11
0.528	0.079	0.012	3804	17.0	-207.0	472.0	265.0	7.56	1.75
0.528	0.077	0.011	4872	17.3	-173.0	472.0	299.0	2.55	1.20
0.528	0.093	0.0047	363	9.4	2.8	465.0	468.0	12.96	1.05
0.528	0.088	0.020	929	12.4	-39.0	464.0	425.0	6.59	1.32
0.528	0.088	0.020	968	12.1	-37.4	464.0	427.0	6.78	1.30
0.528	0.087	0.023	968	14.6	-120.0	406.0	286.0	6.34	1.65
0.528	0.088	0.021	1175	15.2	-139.0	406.0	267.0	5.30	1.52
0.528	0.080	0.013	3588	17.0	-231.0	406.0	175.0	2.43	1.24
0.528	0.079	0.012	4104	17.3	-273.0	406.0	133.0	2.27	1.27
0.528	0.123	0.112	28.5	6.7	0.7	-8.2	-7.5	0.36	0.54
0.528	0.116	0.083	58.8	8.3	2.0	-8.4	-6.4	0.64	0.51
0.528	0.106	0.054	154.0	9.5	-2.0	-8.3	-10.3	0.84	0.76
0.528	0.101	0.041	279.0	11.1	-8.9	-8.5	-17.4	0.91	0.87
0.528	0.092	0.025	810.0	14.0	-72.0	-8.6	-80.6	0.97	1.31
0.528	0.130	0.147	19.9	6.5	-0.6	-8.2	-8.8	0.14	0.58
0.528	0.129	0.139	21.6	5.8	-0.6	-7.9	-8.5	0.29	0.63
0.528	0.123	0.111	35.8	7.2	0.9	-8.9	-9.8	0.29	0.46
0.528	0.115	0.079	80.9	8.7	3.0	-8.2	-5.2	0.74	0.49
0.528	0.106	0.053	200.0	10.8	-4.6	-8.3	-12.9	0.88	0.72
0.528	0.094	0.029	721.0	13.9	-37.6	-8.6	-46.2	0.97	0.92
0.528	0.094	0.029	720.0	14.1	-38.7	-8.5	-47.2	0.97	0.93
0.528	0.126	0.125	31.4	7.2	-4.8	-2.5	-7.3	1.17	0.93
0.528	0.123	0.112	42.9	7.8	-4.7	-2.6	-7.3	1.14	0.83
0.528	0.116	0.084	82.6	9.8	-6.3	-2.8	-9.1	1.10	0.96
0.528	0.107	0.057	193.0	12.2	-20.0	-3.0	-23.0	1.08	0.93
0.528	0.099	0.038	448.0	14.2	-54.0	-3.1	-57.1	1.05	1.14

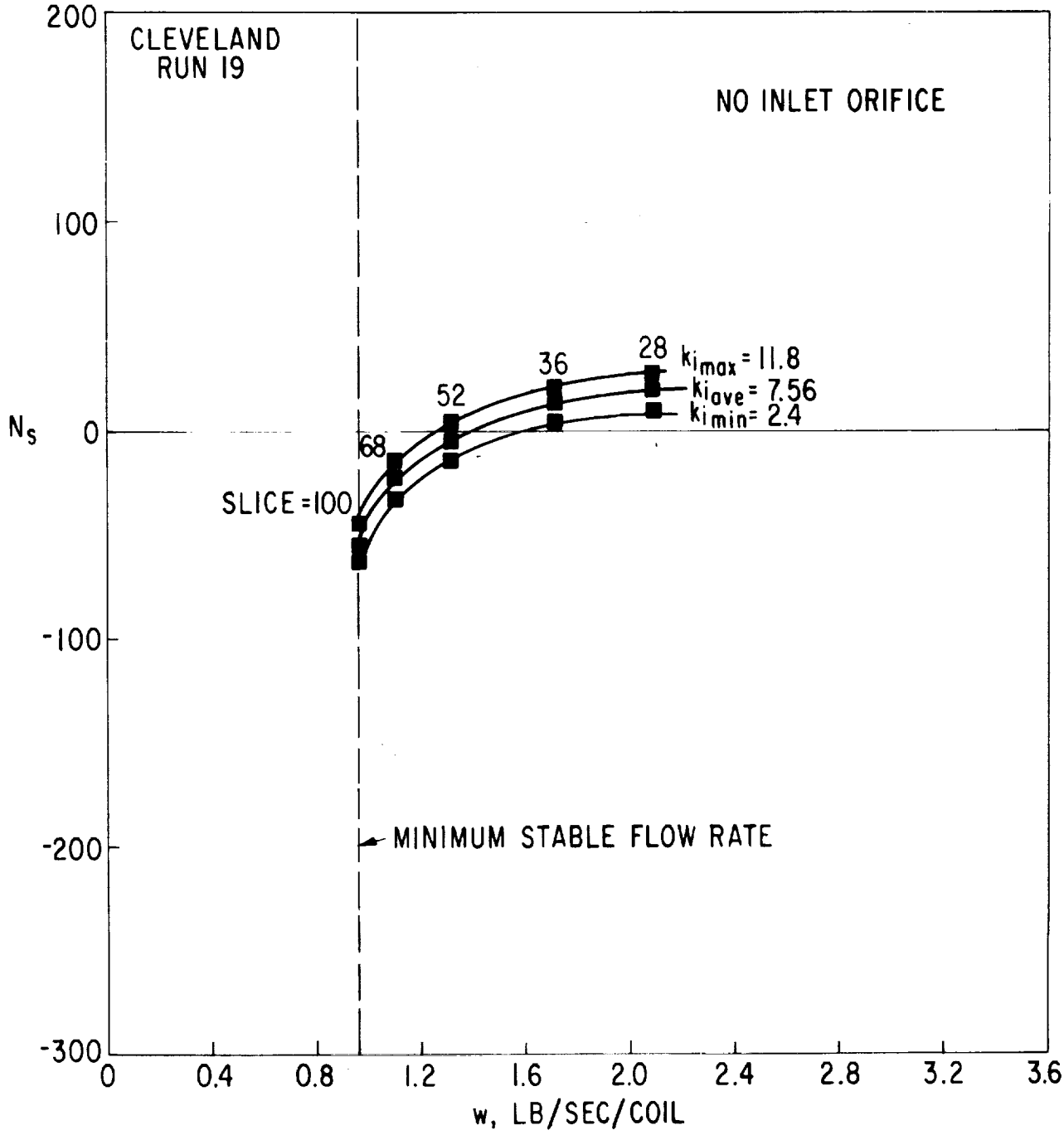

Figure 11. Stability Number Versus Flow Rate for Cleveland Run 19

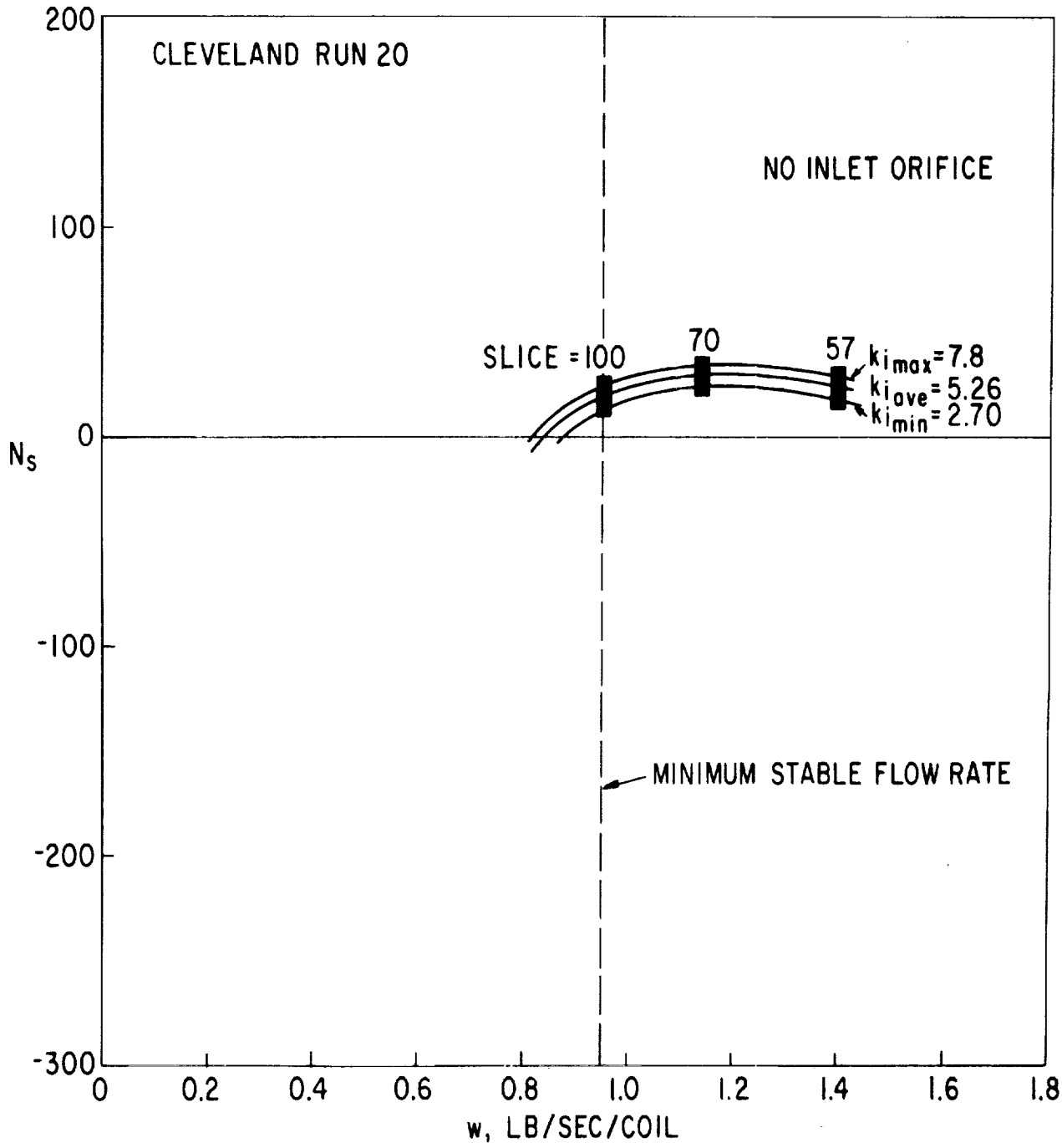

Figure 12. Stability Number Versus Flow Rate for Cleveland Run 20

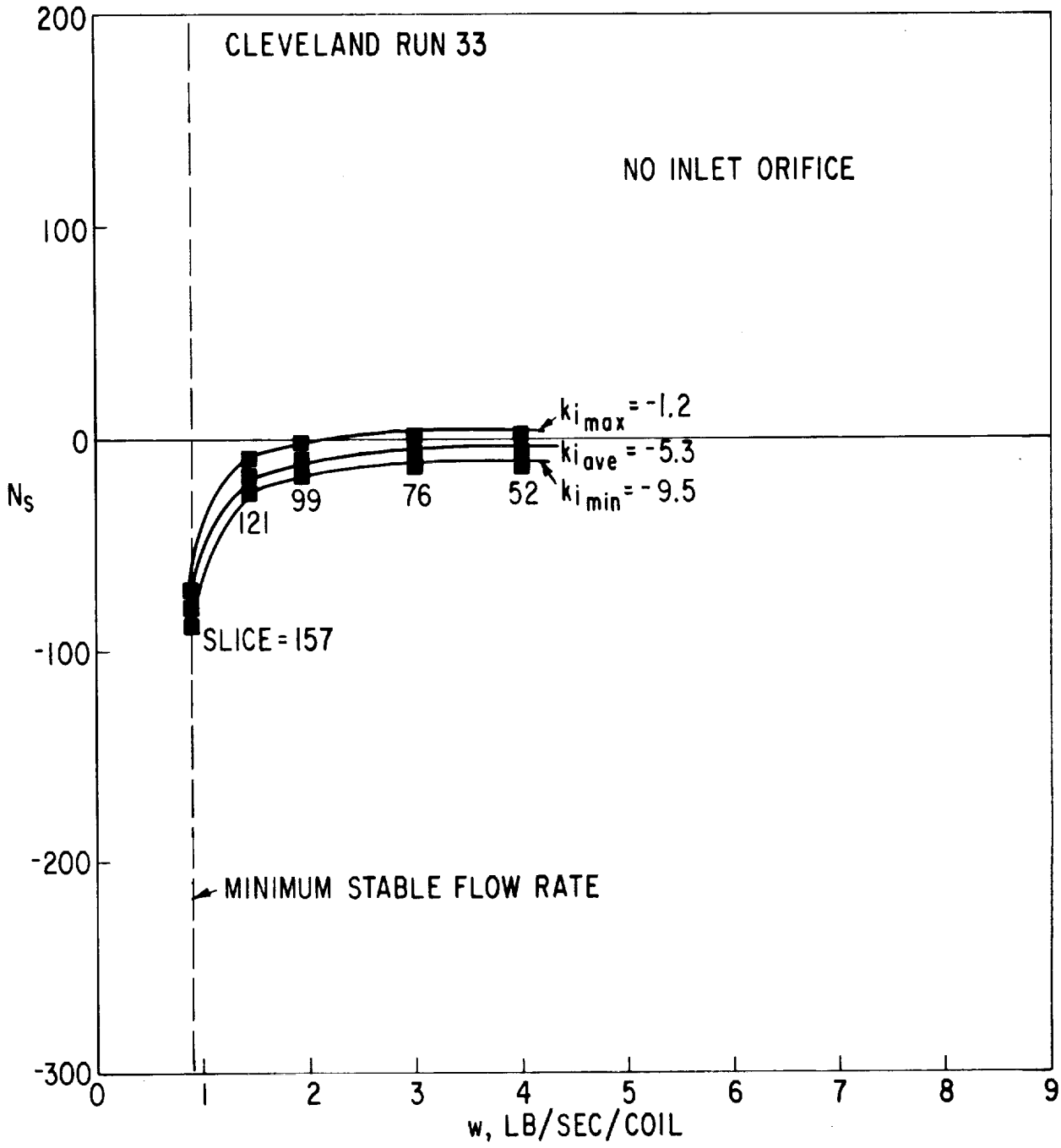

Figure 13. Stability Number Versus Flow Rate for Cleveland Run 33

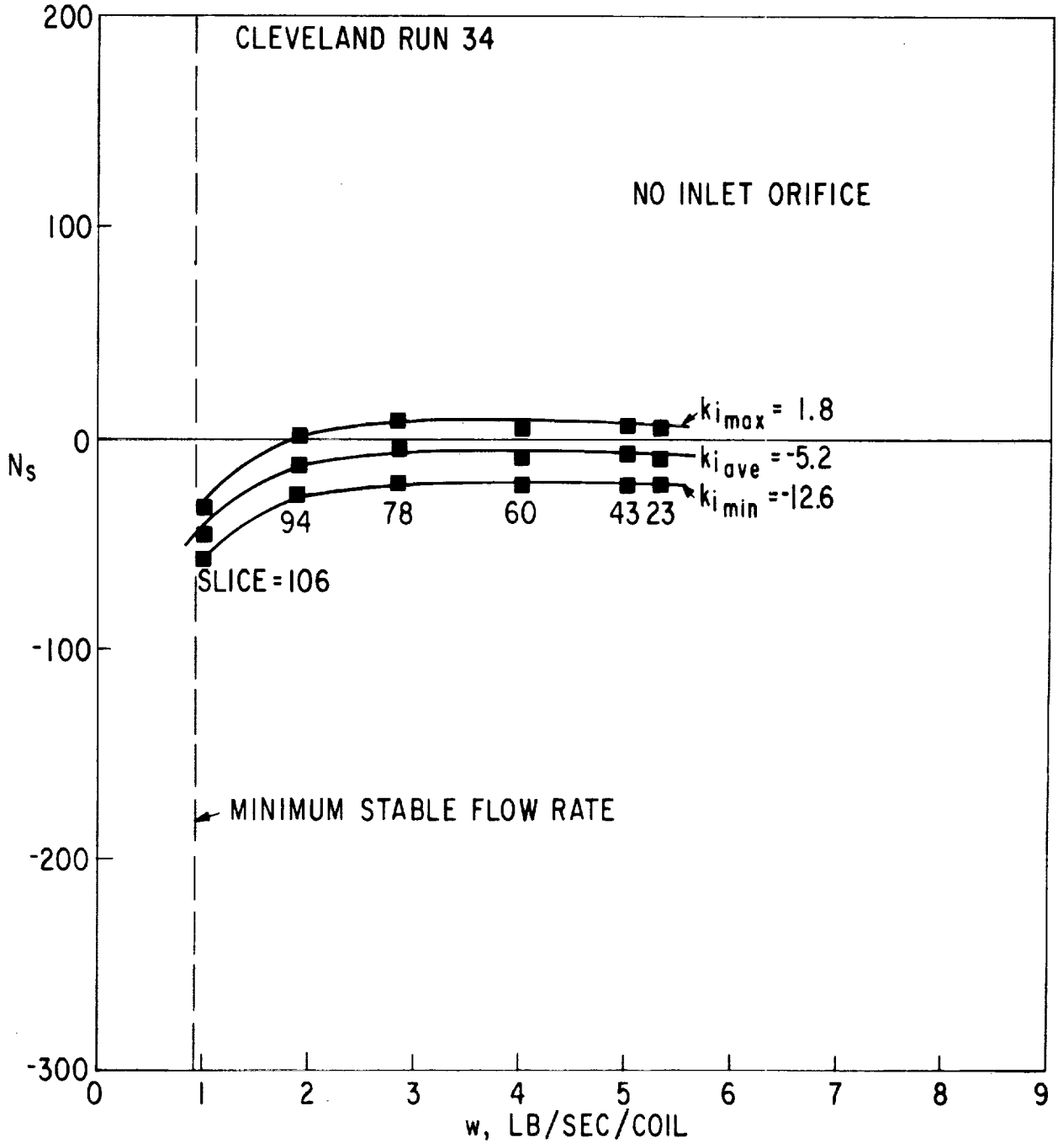

Figure 14. Stability Number Versus Flow Rate
Cleveland Run 34

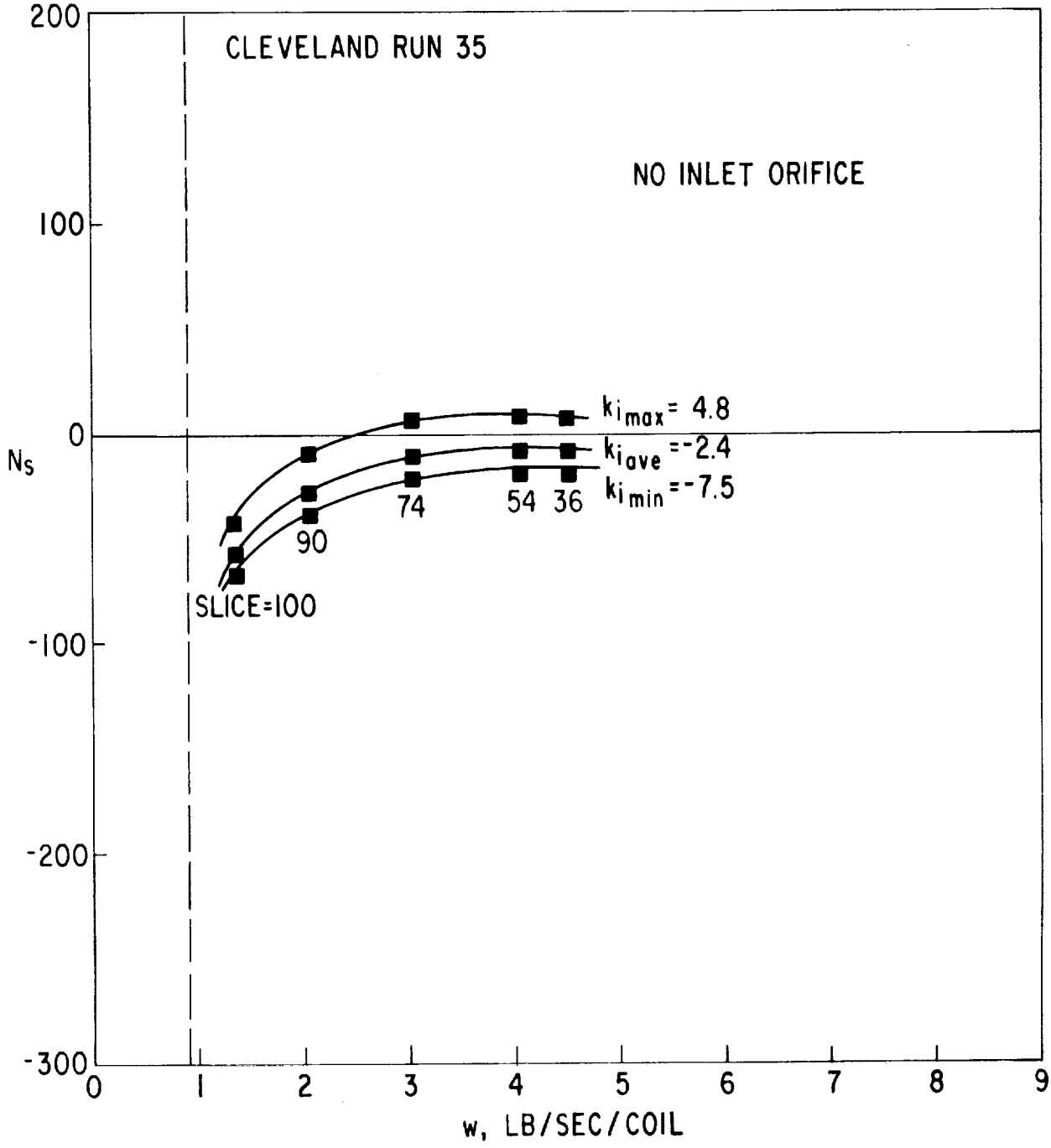

Figure 15. Stability Number Versus Flow Rate for Cleveland Run 35

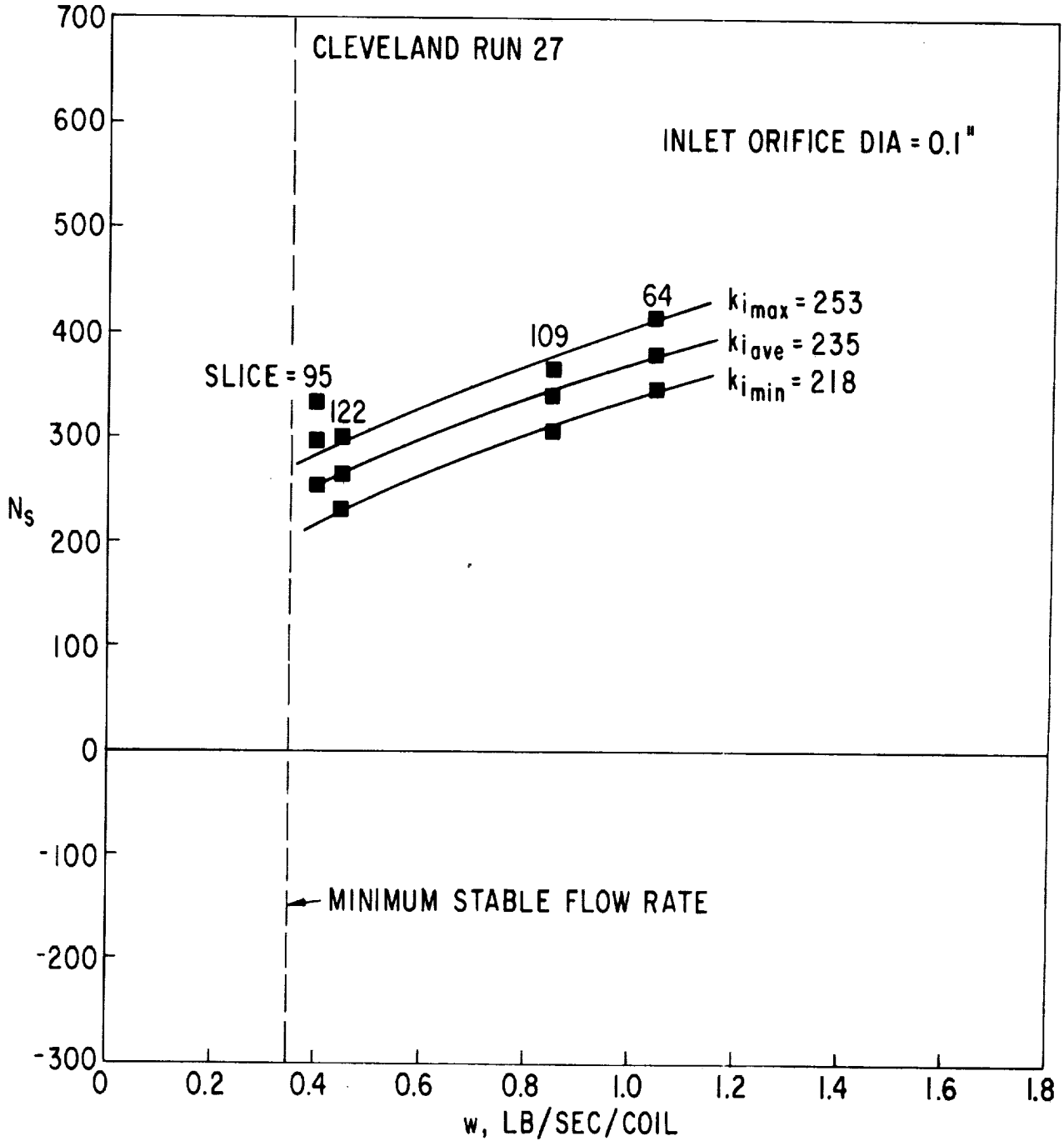

Figure 16. Stability Number Versus Flow Rate for Cleveland Run 27

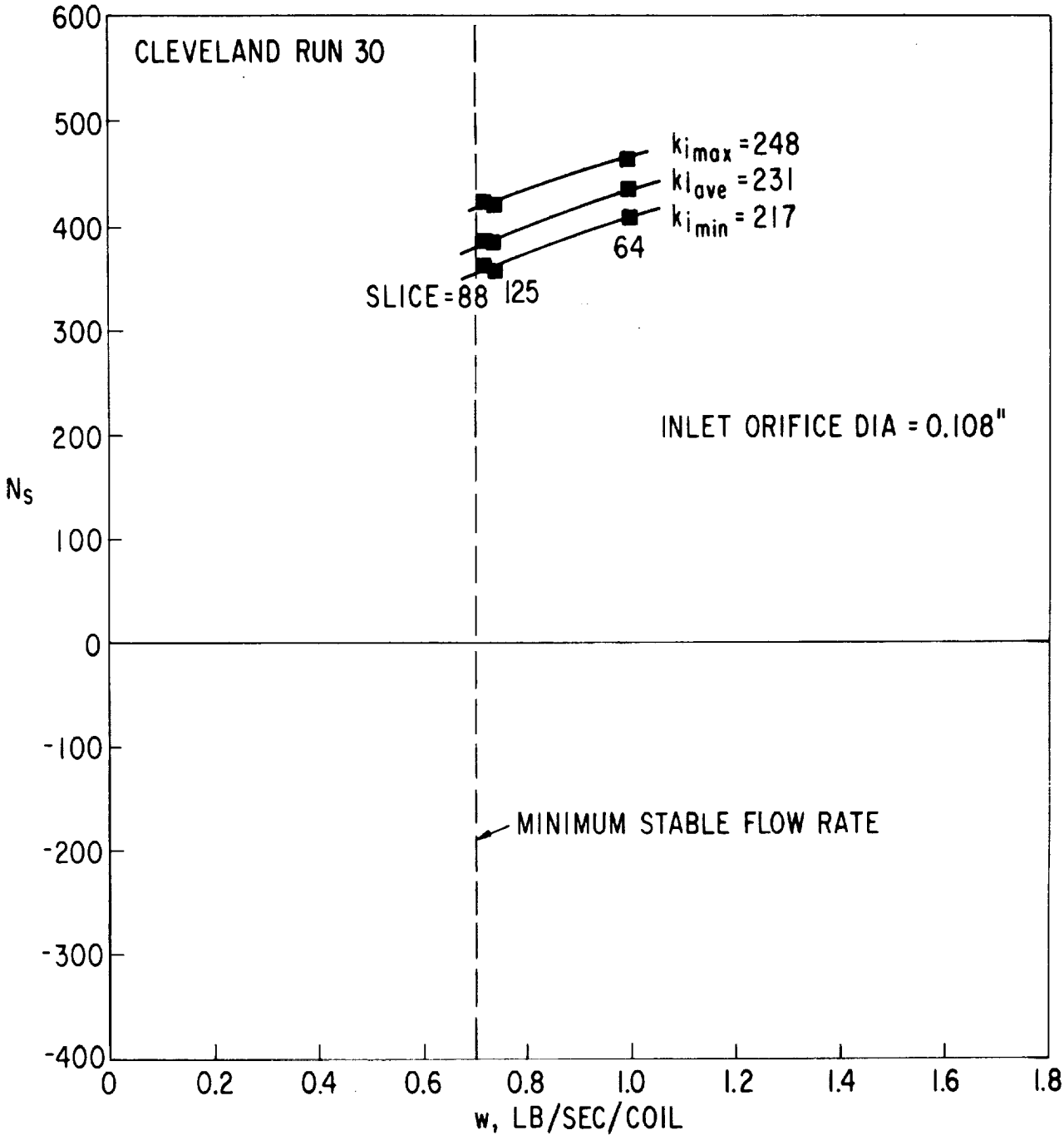

Figure 17. Stability Number Versus Flow Rate for Cleveland Run 30

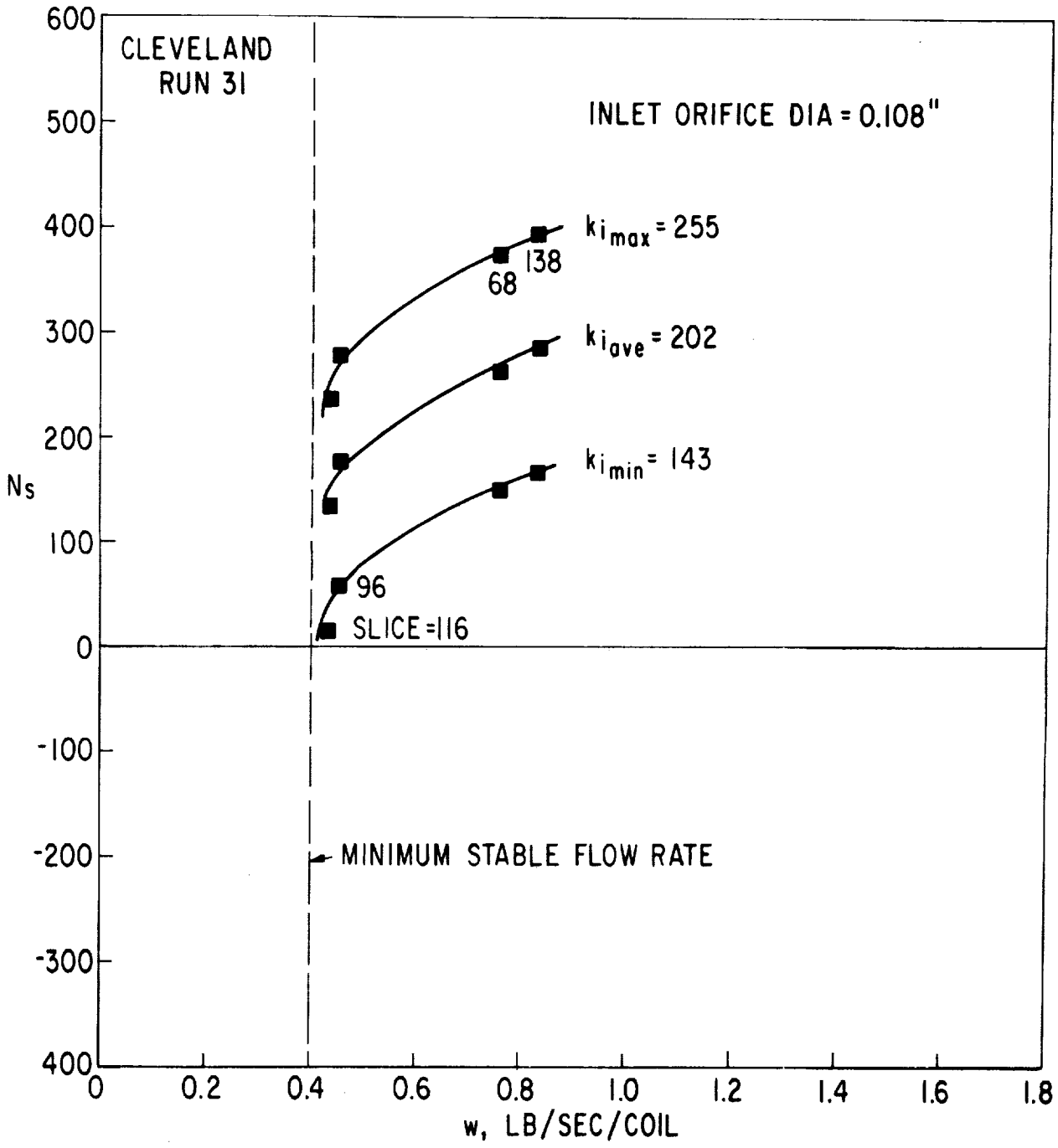

Figure 18. Stability Number Versus Flow Rate for Cleveland Run 31

ADDITIONAL DATA

The analysis was unsuccessfully applied to three other sets of data. Two of these were subcritical two-phase systems and one was supercritical.

Shitsman[30] encountered instabilities while measuring heat transfer to supercritical water. He reports limited data for four experimental runs near the stability limit, two of which were unstable.* In applying this analysis to these data points it became apparent that the points were far different from those considered before. Shitsman observed the instabilities in spite of very limited expansion of the water along the test section. The expansion ranged from $\bar{u}_3$ of 1.2 to 2.2. Primarily because of this the analysis predicted that the system would be very stable. No assumptions could be made which would indicate that instability could be encountered. It appears, then, that the kind of instability observed by Shitsman was not the kind being considered in this analysis.†

In contrast the analysis failed to predict any stability at all for the two low-pressure boiling systems considered. This appears to have an adequate explanation, however.

Zuber's original formulation of the mathematical model[1] was intended to apply only near or above the critical pressure of the fluid. He observed that the equations of change would apply equally well for the bulk state of two-phase mixtures if there is no velocity difference between the phases. A reduced pressure of 0.85 was estimated as the lower limit for which the analysis should apply. Zuber since then has extended the analysis to apply at lower pressures.[4]

Because the oscillations observed in two-phase systems appear to be quite similar in nature to those considered above, the analysis was applied to data reported by Fleming[22] for subcritical nitrogen and by Stenning[8] for Freon. It was hoped that the presence of any slip velocity would be of little consequence to the stability predictions.

The analysis, including the wall heat transfer effect, developed in Section 5 had to be modified slightly to apply to two-phase systems. It was implicitly assumed in writing Equation 27 that the fluid temperature fluctuation would result when the bulk enthalpy changes. In a two-phase

---

*There is an apparent discrepancy as to which runs are stable and which unstable as reported by Shitsman. In the presentation of the data, one set of two was implied to be unstable, but in the conclusions a different set was named.

†In a very recent paper Rogers (9) also observed instabilities with apparently very little bulk expansion of subcritical hydrogen.

mixture this is not true; the bulk enthalpy changes because the quality changes, but the temperature should remain constant at the saturation temperature. The stability analysis must be performed, then, taking the wall effect W equal to zero in the two-phase region.

Additional details on the application to Fleming's and Stenning's data may be found in Reference 31. The analysis consistently predicted that the system would be extremely unstable, even when the data were taken at the stability limit. No reasonable assumptions concerning possible experimental error could make the predictions stable. Even lowering the expansion $\bar{u}_3$ by a factor of 3 to 5 was not sufficient.

To determine whether the slip velocity might indeed be important in these systems, an estimate was made of the actual bulk density of the fluid as a function of the position in the test section.* Slip velocity and change in boiling regimes were taken into account using the methods of Reference 32. Figures 19 and 20 compare the specific volumes predicted with and without slip. The dotted portion of the curves with slip are uncertain, owing to the large void fraction of the two-phase mixture. Clearly, slip is a major factor which must be considered. There is no reason to expect, then, that the present analysis should apply to these data.

*These estimates were performed for the authors by F.W. Staub.

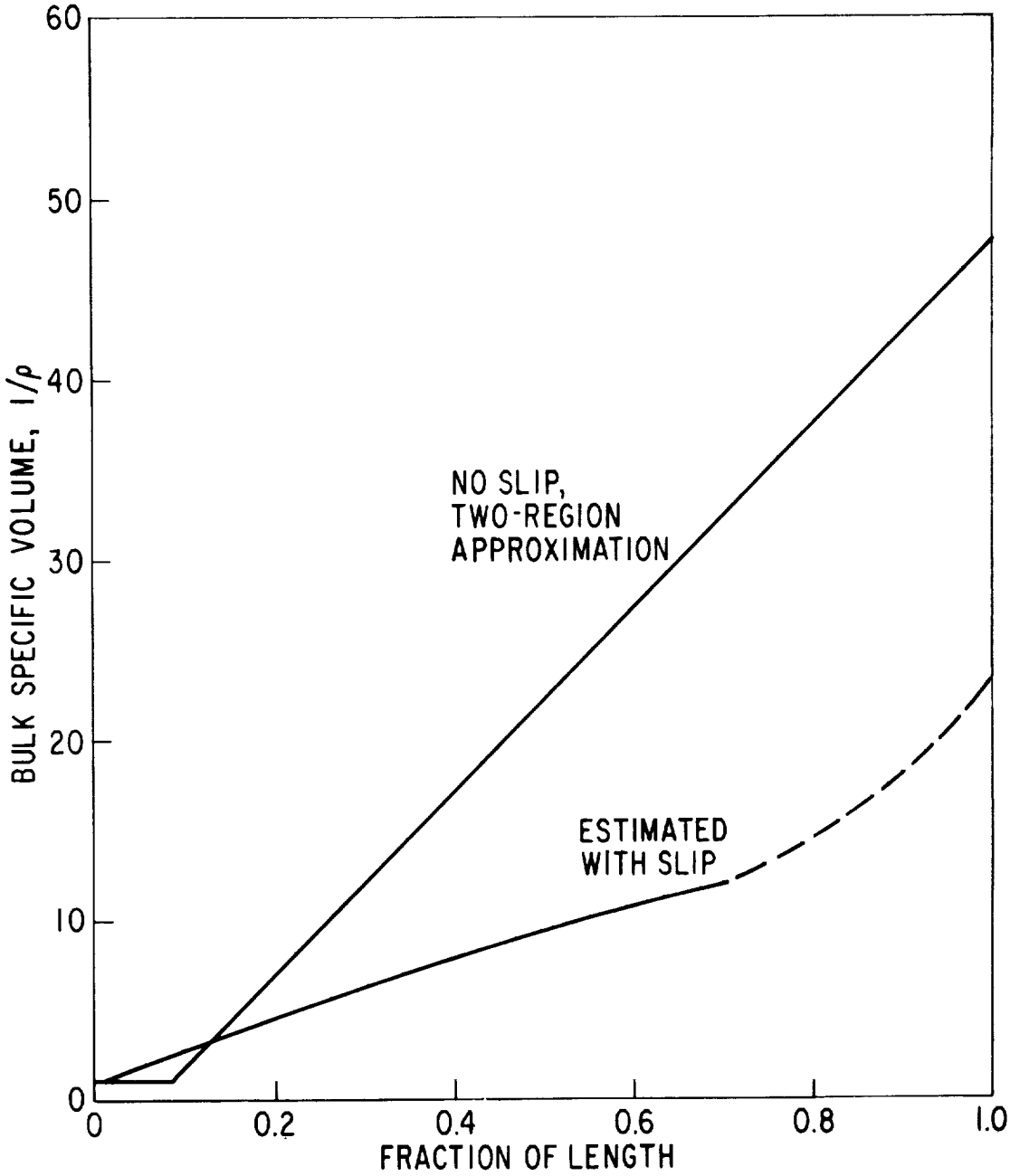

Figure 19. Effect of Slip Velocity on Specific Volume of Nitrogen (Run 7-13-1A [22])

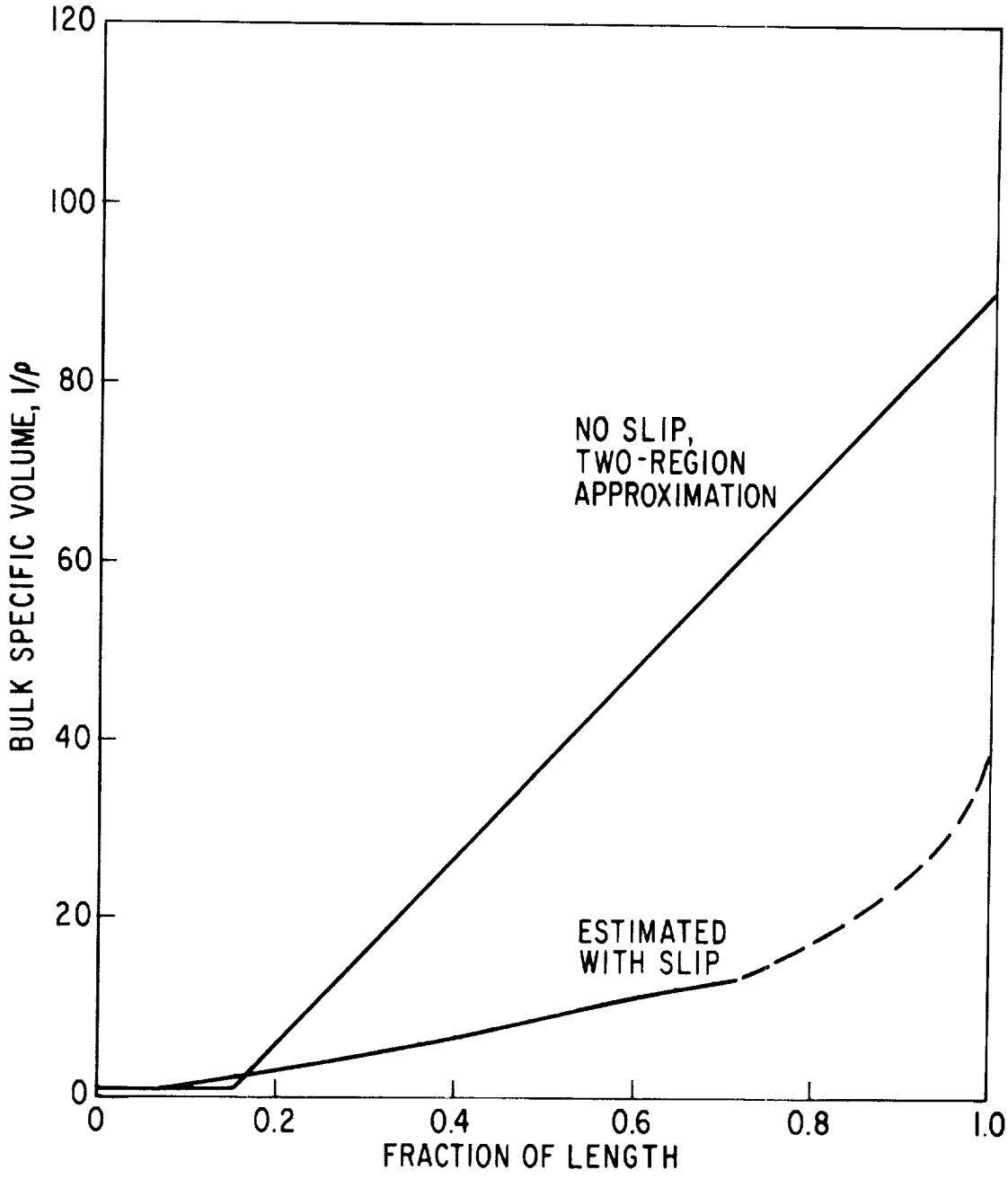

Figure 20. Effect of Slip Velocity on Specific Volume of Freon (Run A001(8))

Section 7

DISCUSSION OF APPLICATIONS AND ASSUMPTIONS

TWO-REGION APPROXIMATION

A great deal of experience has been gained in applying the two-region approximation to these data. The approximation is considered a useful tool for such systems; however, the results can be particularly sensitive to the way the approximation is applied. It is therefore recommended that the following rules of thumb be applied in future applications.

- The two-region approximation should be applied between the correct inlet and exit densities.
- The transition point should be selected so that the total residence time of the fluid is approximated as closely as possible. This is accomplished if the area under the density-enthalpy curve is closely approximated.
- If the total residence time is not particularly sensitive to the two-region approximation, the slope in the light region Ω should closely approximate the actual slope at the outlet. This is especially true when the system is strongly choked downstream.

In general these suggestions are not consistent with taking the transition point to be the transposed critical temperature, as suggested by Zuber[1] and used by Thurston.[2]

The sensitivity of the results to the total fluid residence time can be illustrated by Figure 21 and the Nyquist diagram of Figure 22. Figure 21 has the specific volume-enthalpy relationship for pure hydrogen corresponding to Run 57 of Thurston's data. Here the transposed critical temperature is used as the transition point. Figure 22 compares the Nyquist diagrams resulting when the two region approximation shown in Figure 21 is used and when the heavy region is neglected; i.e., $\tau_{12} = 0$. Both curves are plotted for $C_w \equiv 0$. There is a 40 percent difference in the predicted stability numbers. In view of the $1/\rho - i$ curve in Figure 21, it seems unlikely that the curve could be fitted with two straight lines with much more accuracy than has been achieved. The difference between the two-region approximation used in Figure 21 to obtain the correct outlet density and one with a zero length of the heavy region is probably within the engineering accuracy which can be demanded. However, the crossover points of Figure 22 show a 40 percent difference between these two cases.

The difference can be traced to the total residence time of the fluid. As discussed in Section 5, the instability is caused by the feedback of a signal delayed by as much as τ_{13}. The Nyquist diagrams reflect the importance of the delay time. For example, a complete loop in the diagram of

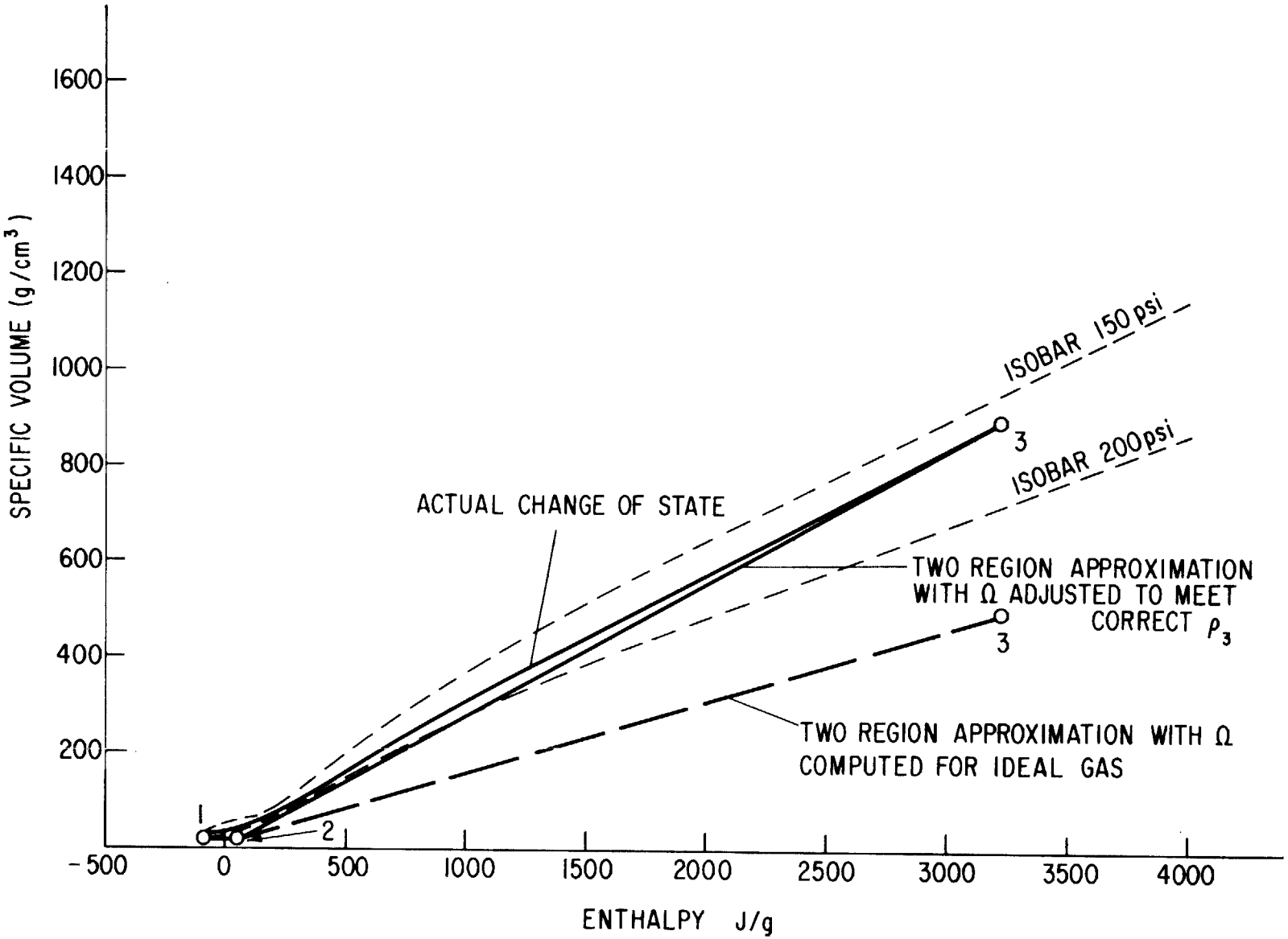

Figure 21. Specific Volume Versus Enthalpy for Thurston Run 57

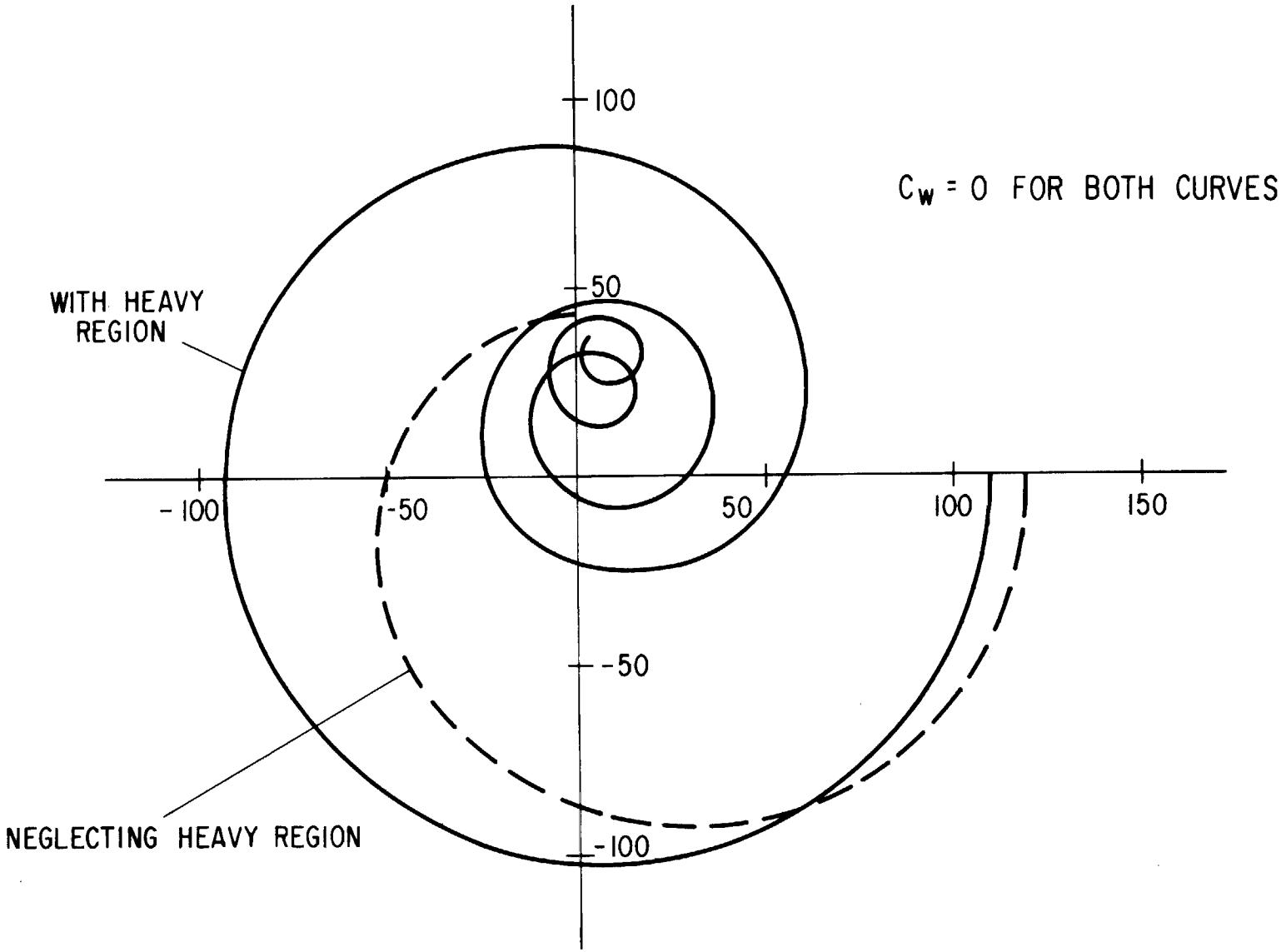

Figure 22. Nyquist Diagram for Thurston Run 57 Comparing Different Subcoolings

Figure 22 occurs at the frequency of about $2\pi/\tau_{13}$. The first crossover point occurs when $s \approx i\,(3\pi/2\tau_{13})$ and successive crossover points (or the leftmost point of the successive loops) occur when $s \approx i(\pi/\tau_{13})(1/2 + 2n)$, $n = 2, 3, \ldots$ These loops of the Nyquist diagram correspond to the "resonance" peaks which have been observed in the dynamics of distributed parameter systems for a number of years. (See, for example, Reference 33.) It is very important in describing these systems to correctly take into account the delay times associated with the passage of disturbance waves through the system. Reference 12 contains several examples of this.

The delay time τ_{13} is the total time required for the fluid to travel from one end of the test section to another. Therefore the correct value of τ_{13}, independent of any two-region approximation, will be given by

$$\tau_{13} = \int_0^1 \frac{dz}{\bar{u}(z)} \tag{98}$$

Since the steady-state velocity is related to the density in any system by the continuity equation, $\bar{\rho}\,\bar{u}$ = constant = 1 for a steady-state, one-dimensional flow. Furthermore, the steady-state enthalpy (Equation 21) of this system is proportional to the distance. This also is independent of the two-region approximation. Therefore the integral in Equation 98 is

$$\tau_{13} \propto \int_{i_1}^{i_3} \bar{\rho}(i)\, di \tag{99}$$

This is simply the area under the ρ-i curve.

Figure 23 has the ρ-i curve for Thurston's Run No. 57; it is replotted from Figure 21. The cross-hatched area under the curve is proportional to the correct value of τ_{13}. On Figure 23, the two dotted lines represent the two different two-region approximations used on this run. When subcooling is used, the area under the curves is about 20 percent higher than the correct area, but the area is 20 percent lower when subcooling is neglected. This constitutes a difference of about 40 percent. This difference in the values of τ_{13}, predicted by the two-region approximation, corresponds to the 40 percent change in the crossover point observed in Figure 22. Judging from the agreement with the ρ-i curve of Figure 23, the correct crossover point should lie midway between the two. The relation used to obtain i_2' for Thurston's and Cleveland's data was estimated in this manner.

The NASA data were taken with a much larger degree of subcooling than Thurston's. Consequently, the residence time τ_{13} is much less sensitive to the two-region approximation. Figure 24 shows the density–enthalpy curve plotted for Run 6 of the NASA data. For curve 2 the transition point is the transposed critical temperature. Curves 2 and 3 give τ_{13}'s which differ by only about ten percent from the correct one. This can be com-

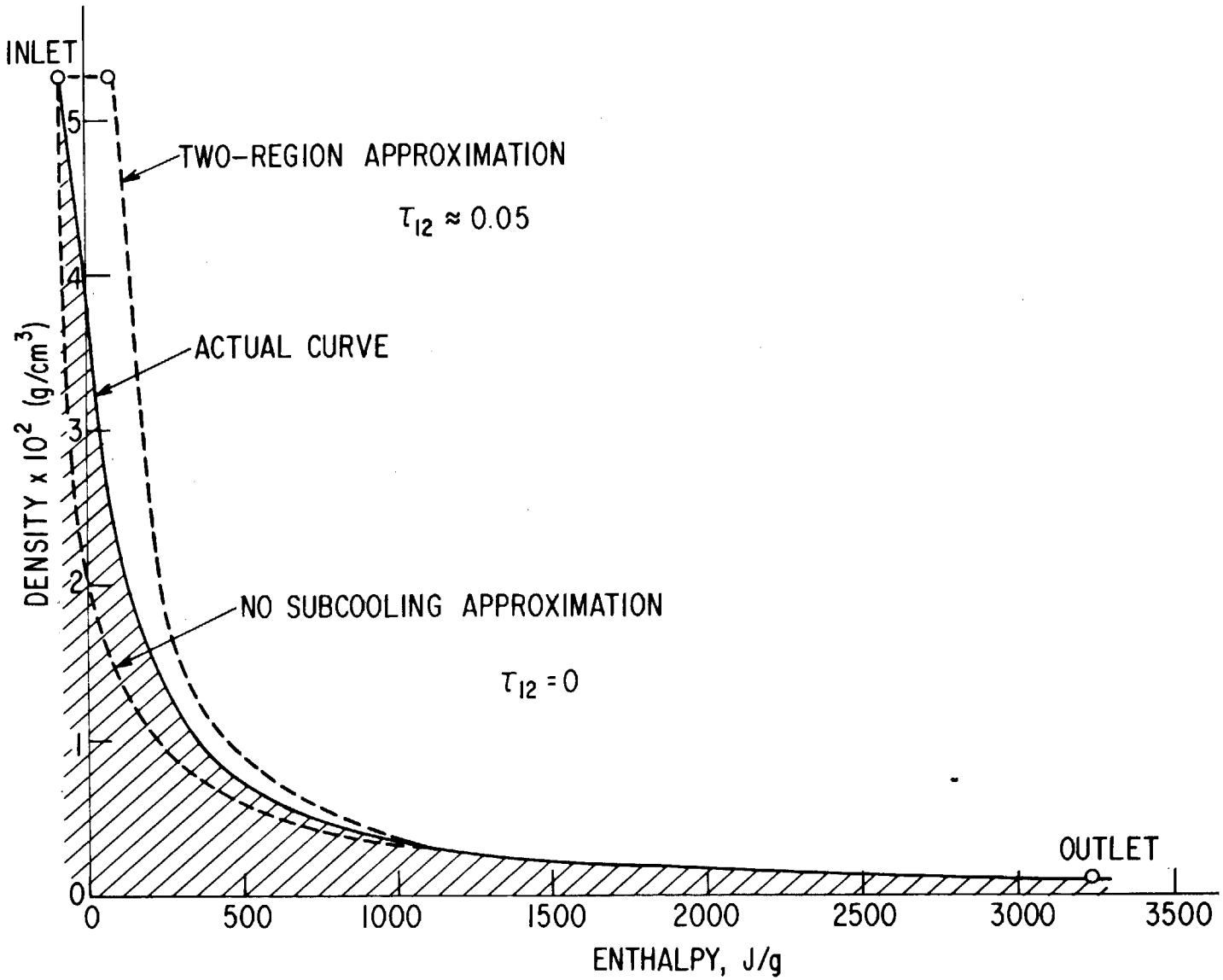

Figure 23. Density-enthalpy Diagram for NASA Run 57

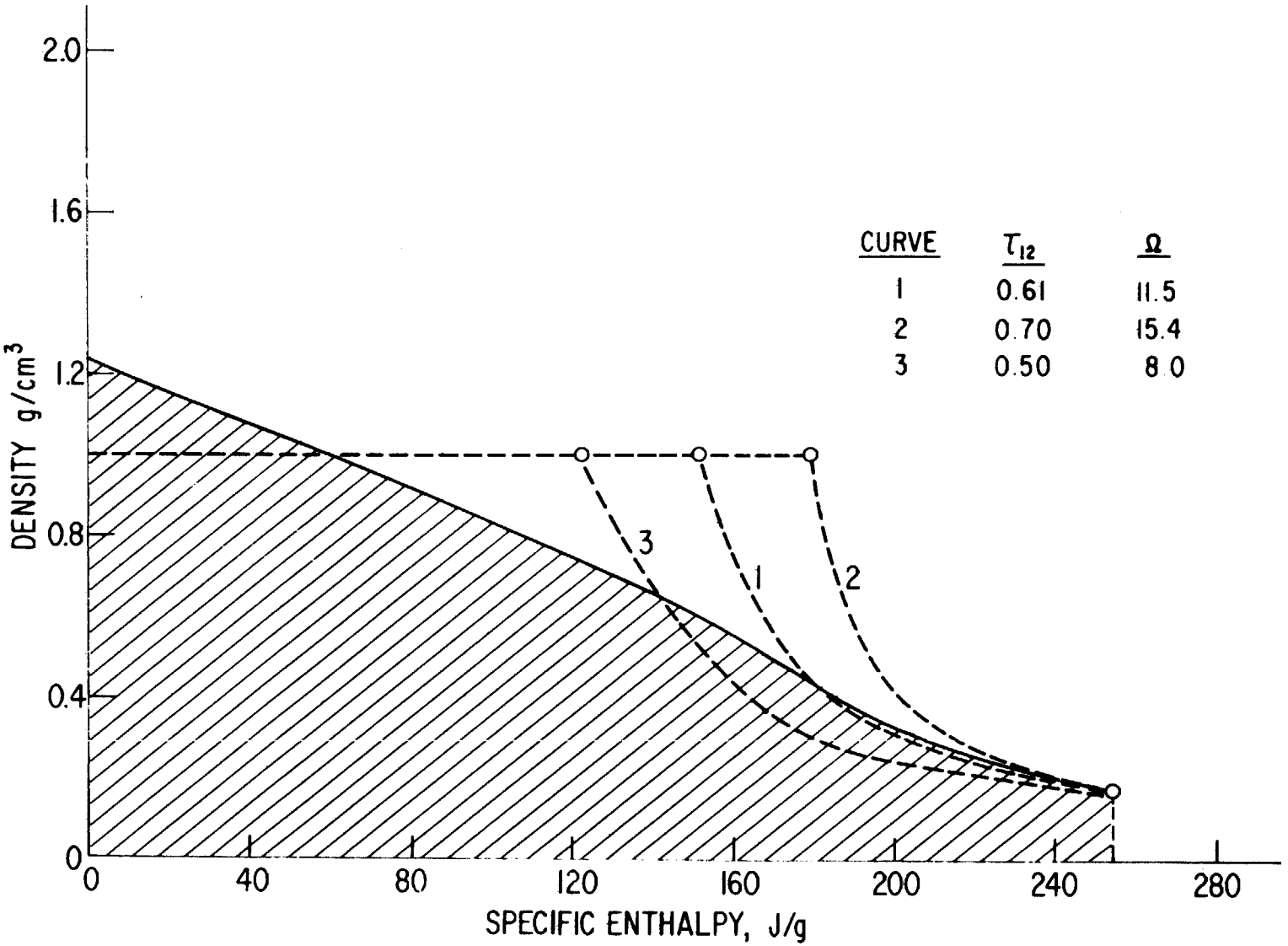

Figure 24. Density-enthalpy Diagram for NASA Run 6

pared with the difference in crossover points shown on the Nyquist diagrams shown in Figure 25, calculated with $C_w = 0$.

Figure 25 does illustrate the sensitivity of the starting point to the two-region approximation. The entire character of the Nyquist diagram is altered in curve 2. Curve 1 is the more nearly correct result. This was determined by extending the analysis to permit approximating the specific volume-enthalpy curve by an arbitrary number of straight lines. Figure 26 shows the curve for Run 6 of the NASA data approximated by three straight dotted lines. It can be shown from this analysis that the approximation should closely match the correct slope of the $1/\rho$ - i curve at the outlet when the system is strongly choked downstream.

Based on the sensitivities discussed above, limits on the accuracy of the results can be estimated. The two-region approximation probably cannot be consistently applied with less than about 10 to 15 percent maximum error. In terms of the Nyquist diagrams it is believed that a stability number of about 15 is the limit of accuracy when $N_s \lesssim 100$. For larger stability numbers, 15 percent of N_s is the estimated accuracy.

ASYMPTOTIC APPROXIMATION TO THE SOLUTION

The sensitivities to the two-region approximation presented above were obtained for $C_w = 0$. These were exact solutions to the problem; however, when there is an effect of heat transfer to the wall the solutions are only asymptotically correct -- another source of possible error in the analysis. The error was minimized by selecting an appropriate average for the density in the expression for the modified reaction frequency $\mathcal{R}$, Equation 38. The arithmetic average was always used for the results in Section 6.

To determine how good the asymptotic approximation is for this sytem, some Nyquist diagrams were calculated numerically for comparison. This was accomplished by selecting a frequency in $s = i\omega$ and integrating the perturbed continuity and energy equations, Equations 24 and 25, along with the wall heat transfer equation, Equation 29, and the equation of state, Equation 30. Of course, the steady-state relations, Equations 19 to 23, were also used. A Runge-Kutta integration procedure with a step size of 0.01 gave sufficient accuracy. The complex values of $\delta\rho$ and δu obtained as a function of distance were used in Equation 50 as the momentum equation was integrated simultaneously. The outlet values were used in Equation 69 for the downstream pressure perturbations. This was sufficient to evaluate $G(i\omega)$ in Equation 76 and the Nyquist curve at a given frequency. The procedure was repeated for different frequencies to complete the diagram.

Table 10 compares stability numbers for the exact solution, or the numerical integration solution, with those obtained with different average desnities in the reaction frequency $\mathcal{R}$. The average densities considered were the arithmetic, the log mean, and the averaged based on the log mean

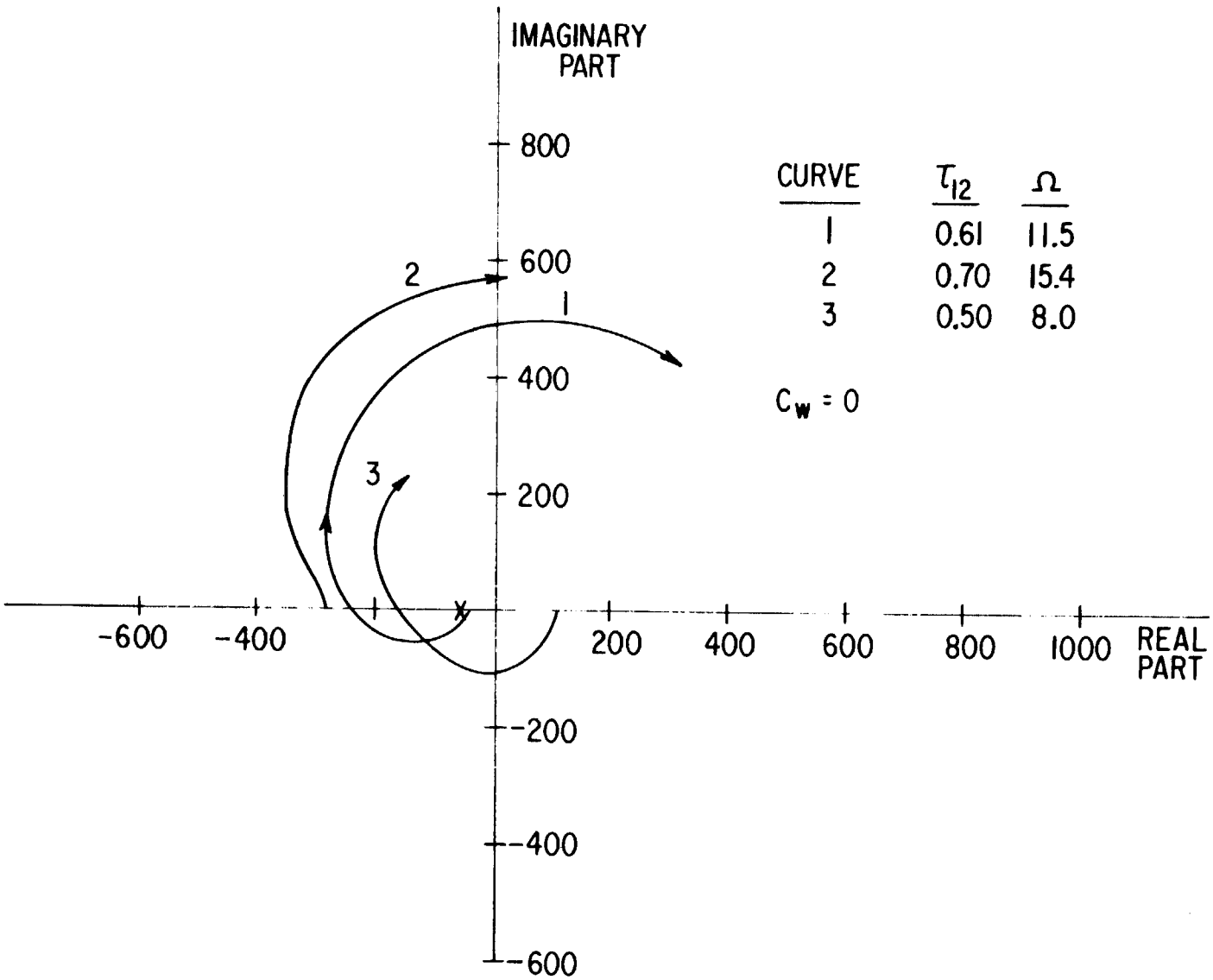

Figure 25. Nyquist Diagrams for NASA Run 6

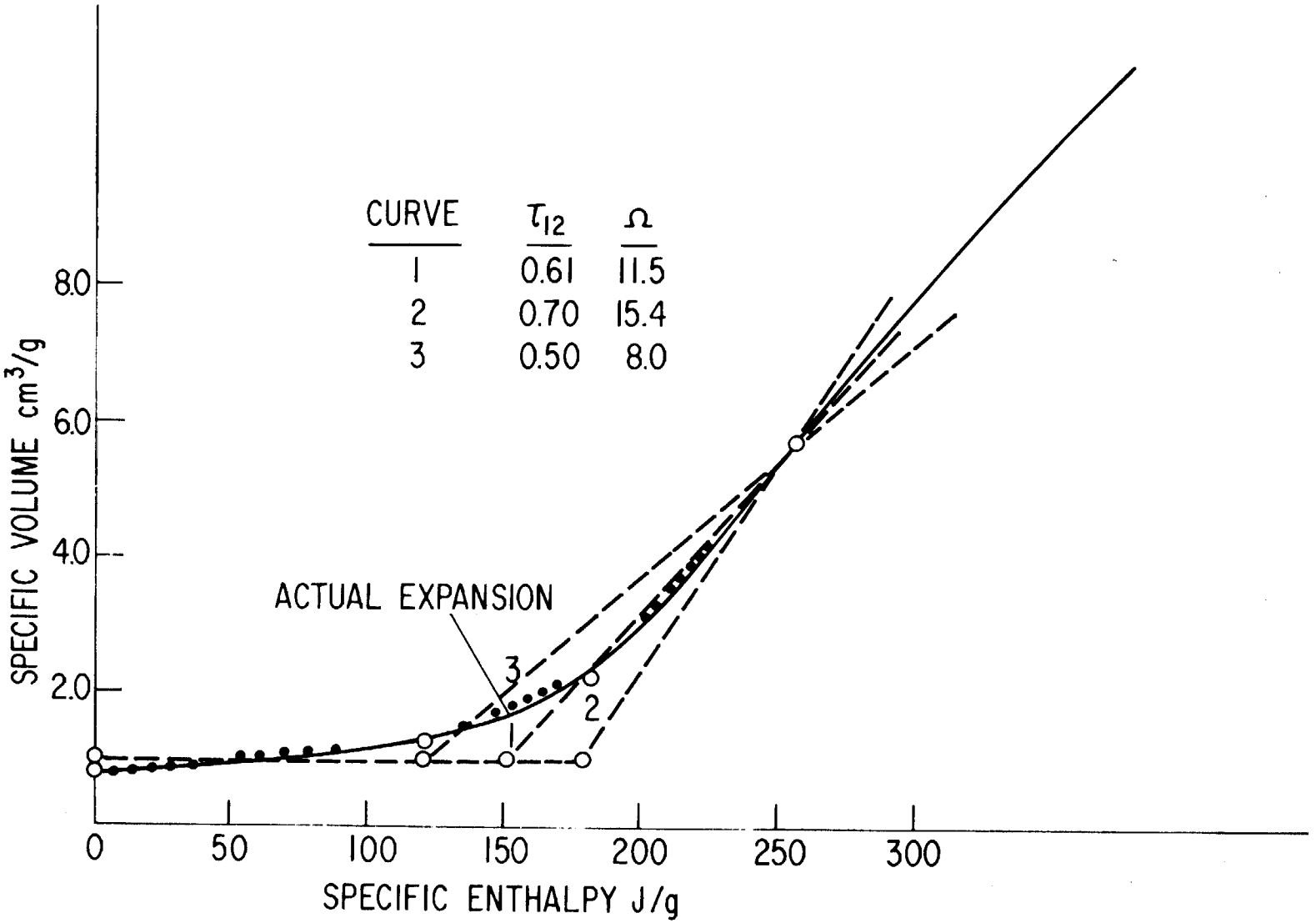

Figure 26. Specific Volume-enthalpy Curve for NASA Run 6

velocity. The arithmetic average gives the best fit to the exact solution. The results are basically good but there can be significant differences.

Table 10

STABILITY NUMBERS FOR NASA DATA WITH VARIOUS AVERAGE DENSITIES IN $\bar{\rho}$

Run	N_s by: Exact Numerical Integration	Approximate Solution		
		$\bar{\rho}_{ave} = \frac{1+\bar{\rho}_3}{2}$	$\bar{\rho}_{ave} = \frac{1-\bar{\rho}_3}{\ln(1/\bar{\rho}_3)}$	$\bar{\rho}_{ave} = \frac{\bar{\rho}_3 \ln(1/\bar{\rho}_3)}{1-\bar{\rho}_3}$
1	53	14	43	51
2	0	-11	18	36
-3	-112	-80	-71	-20
-4	-116	-107	-92	-34
-5	-259	-275	-205	-110
6	44	32	57	72
7	12	-14	-3	19
-8	-68	-43	-35	9

Figure 27 compares the exact and asymptotic stability numbers for a few selected runs from the three sets of data. Again the results are reasonably good but there are significant differences. No general statement can be made as to whether the approximation will be conservative or not, but the trend is toward smaller stability numbers from the approximate solution. In general, the larger the stability numbers the larger the deviations will be. Discrepancies between the exact and approximate solutions do not appear to alter the stability results too significantly. Runs 11 and 18 of Thurston's data are an exception. As discussed in Section 6, the crossover points were estimated differently for Runs 9, 11, and 18, which had Nyquist diagrams, Figures 7 to 9, differing from the usual ones. On these figures the exact numerically integrated solutions are presented as the dashed curves, and the deviation is fairly large for the large loops of the diagram. Figure 8 shows that Run 11 fails to circle the operating point even in the exact solution, although it is very close. The reverse is true for Run 18. Therefore, the exact solution does not confirm the estimated predictions recorded in Table 4.

The asymptotic approximation used in solving the system equations appears to be adequate for the purposes of rough stability predictions. Deviations from it can be of the order of 10 to 20 stability number units for N_s near zero, but it can be much greater when the Nyquist loops are

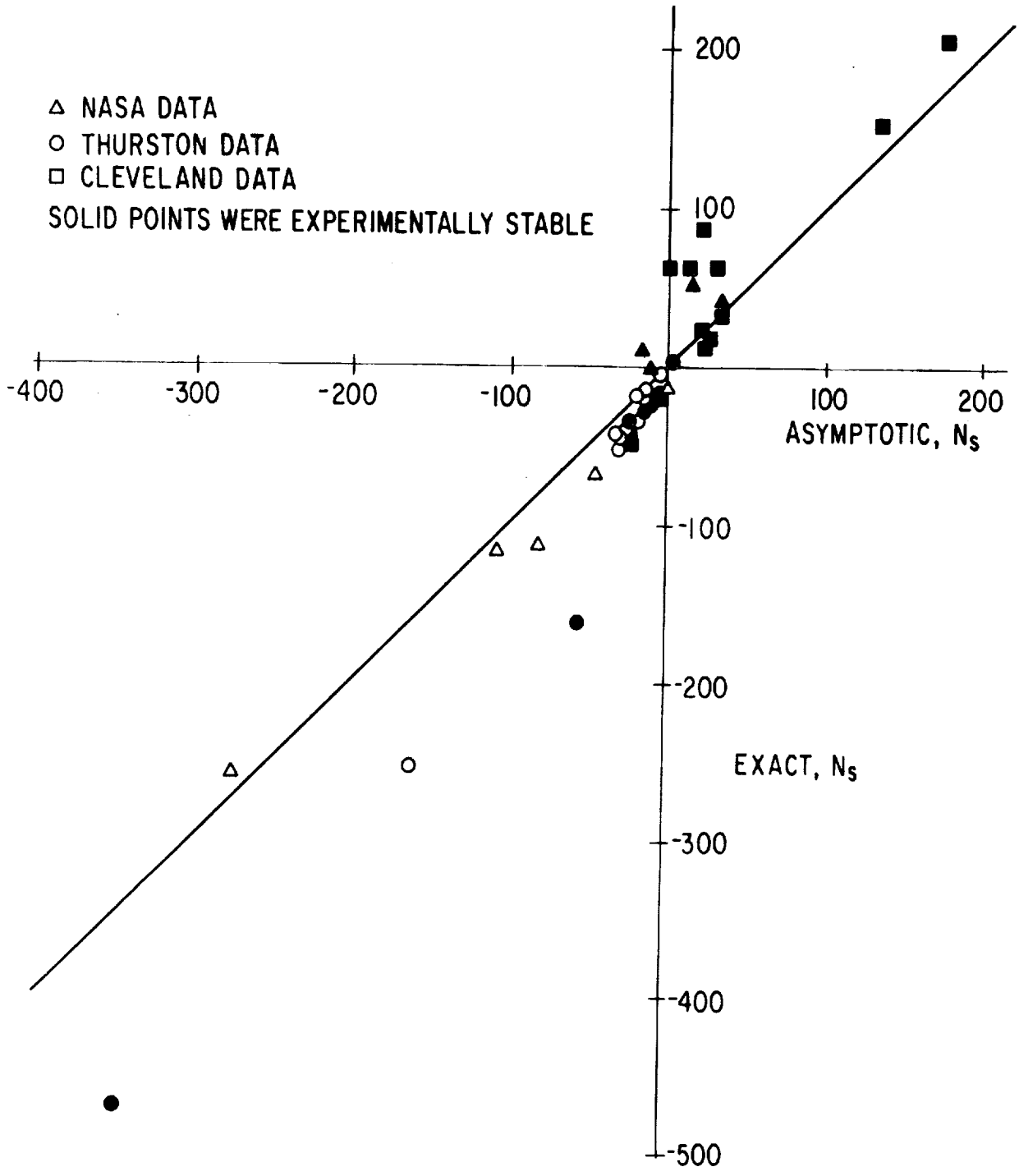

Figure 27. Comparison of Exact and Asymptotic Stability Numbers for Selected Runs

very large. No general statement can be made that the approximation gives conservative results.

HEAT TRANSFER AT SUPERCRITICAL PRESSURES

The estimates of the heat transfer coefficient can be of major importance. Introduction of the heat transfer coefficient in the analysis is a consequence of accounting for the tube wall heat capacity. This tends to have a stabilizing effect on predictions.

Some of the literature on heat transfer to a fluid near its critical pressure will be surveyed briefly here; and the influence of heat transfer coefficient on the predictions based on the present method will be discussed.

Literature Review

Empirical or semi-empirical correlations for heat transfer to a fluid flowing in a pipe have been applied and thoroughly tested.[34] The conditions for which the correlations are usually applied are those of moderate pressures and wall to bulk temperature ratios. Large differences in the wall and bulk temperatures can cause considerable variation in physical properties. Furthermore, when the fluid is near its critical pressure and temperature, its physical properties become a sensitive function of temperature. In many cryogenic heat transfer applications it is just this combination of large temperature differences and pressures near the critical which is encountered.

A literature review of heat transfer to cryogenic fluids has been made by Richards and co-workers.[35]

Strong property variations in the fluid can cause estimation of the heat transfer coefficient by means of the classical correlations to be in error. Dickinson and Welch[36] and Miropolskii and Shitsman[37] have investigated heat transfer to water at supercritical and near-critical pressures.

Dickinson and Welch[36] suggest the use of the standard pipe flow correlation,

$$N_u = 0.023\, P_r^{0.4}\, R_e^{0.8} \qquad (100)$$

for wall temperatures below 660°F. Wall temperatures between 800 and 1100°F indicated the use of a constant Stanton number of 0.00189. These results were obtained for pressures of 3500 and 4500 psi and heat fluxes of less than 600,000 Btu/hr ft^2.

Miropolskii and Shitsman correlated heat transfer data based on a modified pipe flow equation:

$$N_u = 0.023\, P_{r_m}^{0.4}\, R_e^{0.8} \qquad (101)$$

where

$$P_{r_m} = \begin{cases} P_{r_b}, & \text{if } P_{r_b} < P_{r_f} \\ P_{r_f} & \text{if } P_{r_f} < P_{r_b} \end{cases}$$

That is, the Prandtl number based on bulk conditions is to be used when it is less than the Prandtl number calculated from film properties, and conversely.

Correlation of data for heat transfer to supercritical water was obtained by Bringer and Smith[38] by means of the relation

$$N_{u_x} = 0.0266 (P_{r_w})^{0.55} (R_{e_x})^{0.77} \quad (102)$$

where the reference temperature T'_x was computed from the following table:

$(T'_m - T')/(T_o - T)$	Reference Temperature T'_x
<0	T'
0 to 1.0	T'_m
>1.0	T'_w

Where T'_m is the transposed critical temperature (that is, that temperature at which the specific heat achieves a maximum value). Equation 102 was found to yield good agreement for heat transfer to water at 5000 psi, but to be 30 percent too low for carbon dioxide data.

Monroe et al.[39] have presented data for heat transfer with oxygen flowing through tubes.

Correlation of hydrogen heat transfer data was discussed by Hendricks et al.[40,41] In the region of near-critical or supercritical pressure when the reduced temperature was much larger than unity, a relation such as Equation 100 gives satisfactory results. McCarthy and Wolfe[42] found good agreement of experimental data with a modified Dittus-Boelter equation for heat transfer with gaseous hydrogen. They suggested the use of

$$N_u = 0.023 P_r^{0.4} R_e^{0.8} \left(\frac{T_w}{T}\right)^{-0.3} \quad (103)$$

Thurston[26,27] quotes a recent study of Williamson[28] regarding data for heat transfer to gaseous hydrogen obtained from several different sources. The correlation suggested was

$$N_u = 0.023 C_1 P_r^{0.4} R_e^{0.8} \left(\frac{T_w}{T}\right)^{-C_2} \quad (104)$$

where,

$$\text{for } T_w/T \leq 1.8: \quad C_1 = 1 \text{ and } C_2 = 0.765$$

$$\text{for } T_w/T > 1.8: \quad C_1 = 0.7 \text{ and } C_2 = 0.2$$

However, when both temperature and pressure approach the critical values (i.e. in the near-critical region) a simple modification of Equation 100 appears to be no longer valid. Under such conditions it may be desirable to employ relations analogous to subcritical boiling for the prediction of heat transfer coefficients. A number of authors [43, 44] have commented on the similarity of the near-critical and subcritical heat transfer regions. Hendricks and co-workers recommend Equation 105 as a possible means of correlating data in the near-critical region:

$$Nu_f = Nu_1 \frac{1}{0.7 + 2.4\, X_{TT,x}} + 0.15 \tag{105}$$

where

$$Nu_1 = 0.021\, P_{r_f}^{0.4}\, R_e^{0.8} \tag{106}$$

R_e = Reynolds number based on film viscosity and mean film density

and, Martinelli two-phase flow parameter $X_{TT,x}$:

$$X_{TT,x} = \left(\frac{w_\ell}{w_g}\right)^{0.9} \left(\frac{\mu_\ell}{\mu_g}\right)^{0.1} \left(\frac{\rho_g}{\rho_\ell}\right)^{0.5}$$

The subscripts ℓ and g refer to liquid and gas. The mean film density is obtained from

$$\frac{1}{\rho_{mf}} = \frac{x_2}{\rho_f} + \frac{1 - x_2}{\rho_\ell} \tag{107}$$

where x_2 refers to the "pseudo quality" calculated from the equilibrium density, the ideal gas density, and an extrapolation of the liquid density.

Effect of Heat Transfer Coefficient on Stability Prediction

The heat transfer coefficient enters through the transfer time τ. Increasing the heat transfer coefficient will reduce τ and generally result in an increased stability number prediction. The influence of transfer time on the Nyquist diagram for Cleveland run 20 slice 70 is illustrated in Figure 28. The crossover point is increased by increasing the heat transfer coefficient. The starting point, however, is unaffected by any change in h'. A graph of the effect of τ on stability number is given in Figure 29. Heat transfer coefficients in the region 500 to 1000 Btu/(hr ft^2 °F) ex-

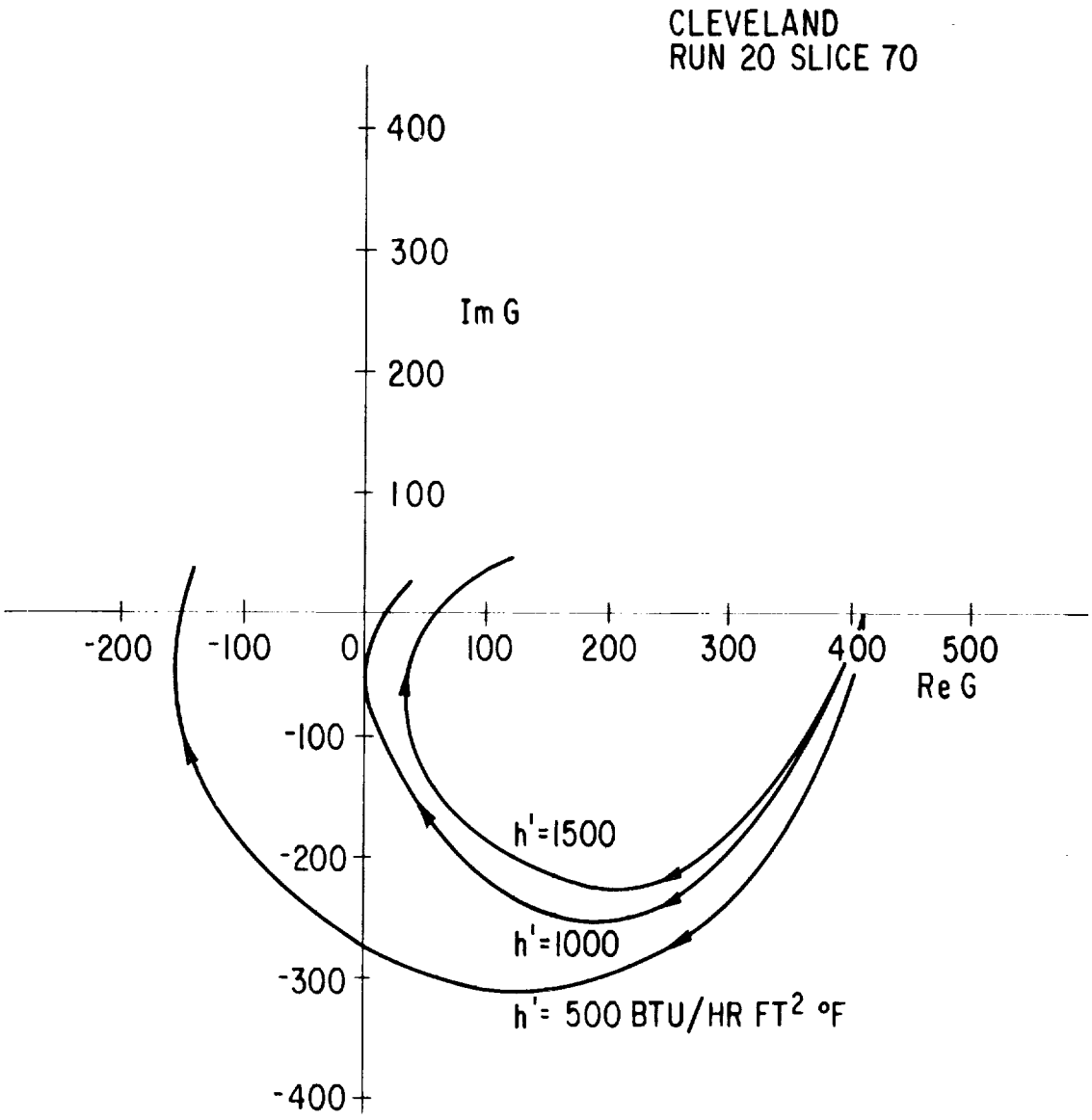

Figure 28. Effect of Heat Transfer Coefficient on Nyquist Diagram, Cleveland Run 20/70

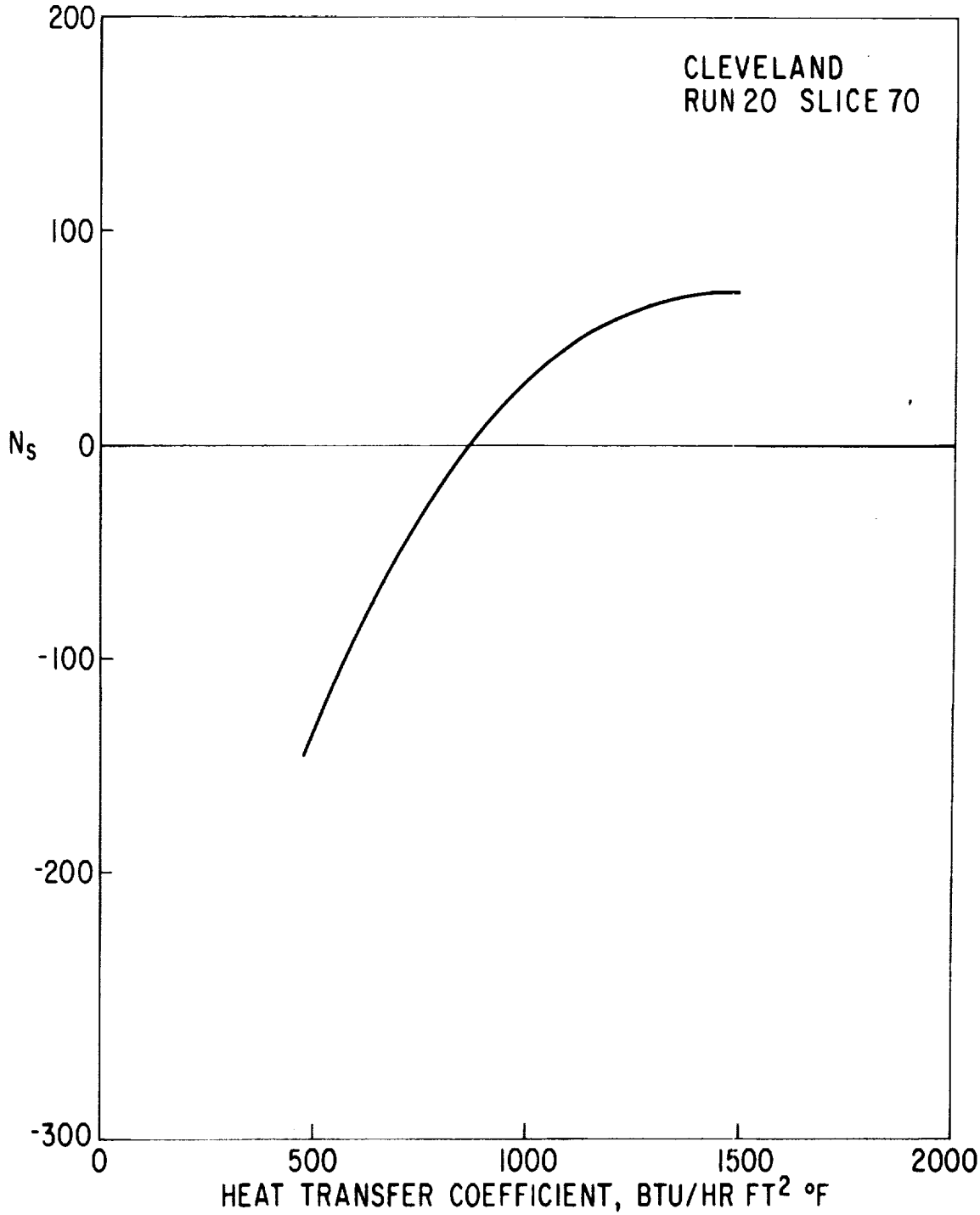

Figure 29. Effect of Heat Transfer Coefficient on Stability Number, Cleveland Run 20/70

hibit the greatest influence on the stability predictions. For heat transfer coefficients greater than about 1250 Btu/(hr ft^2 °F) (at least for this particular run) there is relatively small effect on N_s.

That increasing the heat transfer coefficient tends to be stabilizing is seen to be physically reasonable. Any perturbation in the fluid temperature causes a fluid volume change and a corresponding change in heat transfer area; but this would be compensated by increased or decreased rate of heat transfer from the wall. The greater the heat transfer coefficient from the wall to the fluid, the faster will be the thermal compensation effect of the wall.

The importance of the heat transfer coefficient in determining the stability prediction can vary according to the other parameters of the experiment. Predictions made for Thurston's hydrogen data, for example, were less affected by changes in the heat transfer coefficient than were those for the Cleveland data.

Section 8

SIMPLIFIED CRITERIA

ZUBER'S THIRD-ORDER EQUATION

The use of the full characteristic equation (Equation 73) and the Nyquist diagram to predict stability for these systems is at best a cumbersome procedure. Although it is true that the procedure can be automated for the computer as it has been done here, it is still desirable from the point of view of the design engineer to be able to apply a much simpler criterion. From the point of view of the researcher a simpler criterion is desirable for greater ease in understanding the physical phenomena of the instabilities.

Zuber[1] was able to make reasonable assumptions on his characteristic equation and greatly reduce the order of the problem. The simplified criteria he obtained agreed quite well qualitatively with general experimental observations. Thurston[3] has reformulated Zuber's first-order characteristic equation and has had a great deal of success in correlating instability data with it. This will be discussed in more detail in the following pages.

As stated in Section 5, the model used here is identical with Zuber's except that the effect of heat transfer to the wall has been included. Although this effect complicates the problem considerably, it is shown in the Appendix that the approximate solution obtained in Section 5 (page 21) for the characteristic equation and Zuber's exact fifth-order equation* are of the same form. In spite of the similarily it is not possible to simplify Equation 73 to the same degree that Zuber did.

The reasons lies in an assumption which Zuber made to simplify the exact fifth-order characteristic equation down to the third-order equation. Since Zuber's simpler criteria were based on the third-order equation, its validity will be discussed here. It will be shown that the third-order equation will always fail to predict stability as compared with the more exact fifth-order equation.

Zuber's first simplification was made in the integration of the momentum equation in the light region. In the acceleration, body force, and friction pressure drop perturbations (Equations 56, 58, and 59) the velocity $\bar{u}(z)$ was replaced by its upper bound $\bar{u}_3$. This simplified the integration and resulted in the third-order characteristic equation. It is listed along with the fifth-order equation for comparison in the Appendix.

*The exact fifth-order equation is only implied in Zuber's report. An approximation is made to reduce the order by two before the characteristic equation is written.

The effect of this simplification on the stability prediction is investigated by writing the characteristic equations of the fifth- and third-order in the following way:

$$K + G_5(s) = 0 \qquad \text{and} \qquad K + G_3(s) = 0$$

where K and G are defined as in Equation 76. The order of the equation, indicated by the subscript, differs only because different expressions are used for $\delta\Delta p_\ell / \delta u_1$. It may be readily shown that the G functions have the following three properties:

1. G_5 has no pole in the right-half s plane, but G_3 has a single first order pole there (at $s = \Omega$).
2. $G_5(0) = G_3(0)$
3. As $s \to \infty$, $G_5(s) \to G_3(s) \to s\tau_{13}$

Of the possible configurations of Nyquist diagrams mapped by functions with these three properties, there are two categories to be considered. The starting point of the diagram [G(0)] is either at the right of the operating point (-K) or at the left. On Figure 30, diagrams for these two categories are labelled R and L. Because of Property 2, the starting point for G_3 and G_5 will be the same. Because of Property 3, both will circle the right half plane as s does for large s. In category R, when the starting point lies to the right of the operating point, there are essentially only three possible ways for the Nyquist diagrams to look. These are labelled as Cases R-1, R-2, and R-3 in Figure 30. The diagram can fail to circle the operating point (R-1); it can circle in the counter clockwise direction an even number of times (R-2); and it can circle the clockwise direction an odd number of times (R-3).

Table 11 summarizes the information concerning these cases and the conclusions to be drawn from them. The second column gives the minimum net number of rotations about the operating point for each case. The last two columns give the conclusions to be drawn from these diagrams for the fifth-order and the third-order equations. As discussed in Section 5, the number of zeros in the right half plane is given as the sum of the rotations and the poles, $Z = R + P$. For Case R-1, $Z = 0 + 0 = 0$ for the fifth-order equation; therefore, it is stable. For G_3 it is $Z = 0 + 1 = 1$, indicating instability. Case R-2 is physically impossible because it indicates a negative number of zeroes. This configuration can only result when there are more poles in the right half plane. Case R-3 has a positive number of rotations for both G_5 and G_3, making both unstable.

The significance of these three cases is that in Category R (that is, when the Ledinegg criterion is satisfied) the fifth-order equation can predict stability, as in case R-1, but the third-order equation cannot predict stability in any case. Similar arguments can be employed for Category L when the Ledinegg criterion is not satisfied. Here, there are essentially

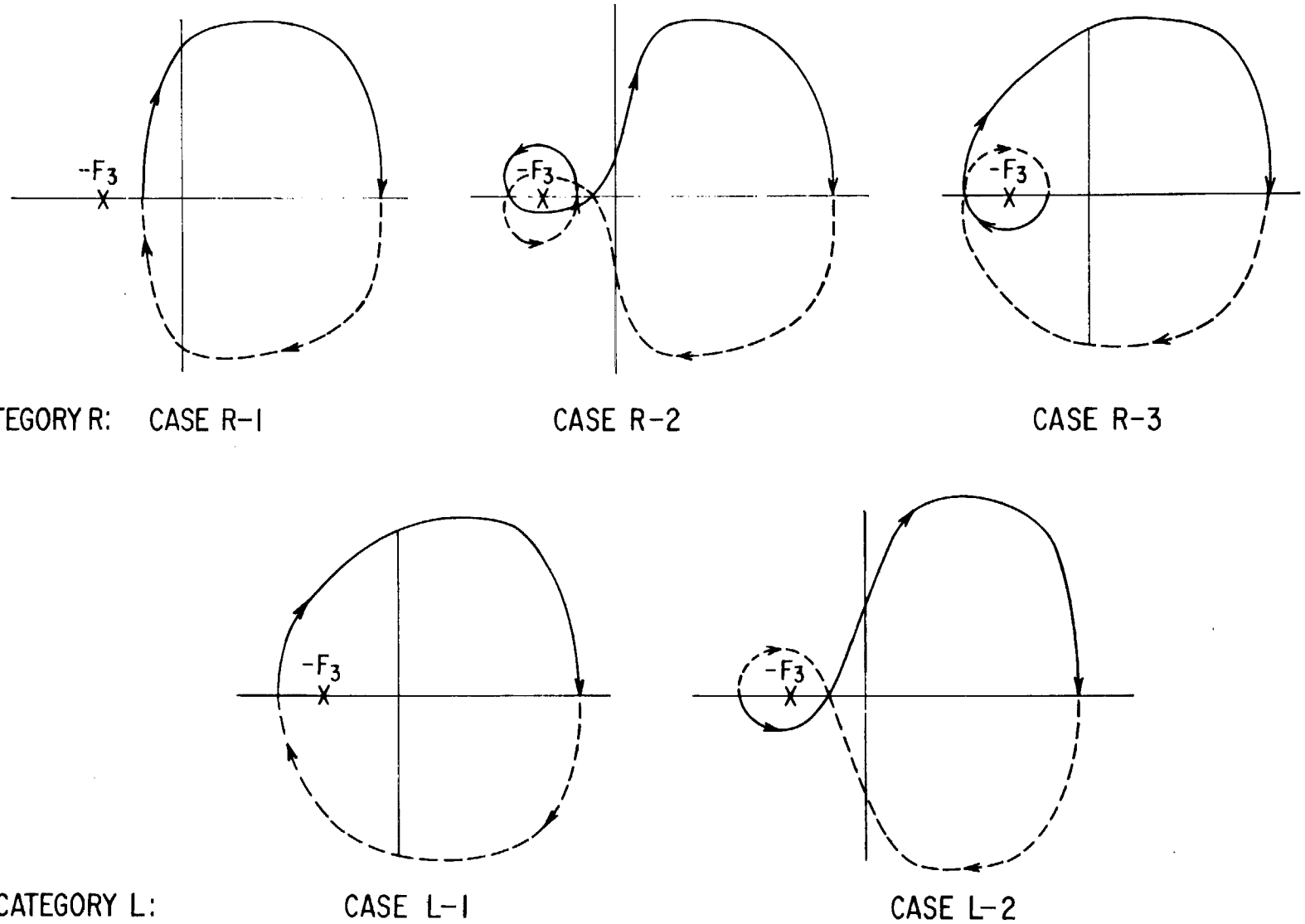

Figure 30. Possible Configurations for the Nyquist Diagrams

two configurations, L-1 and L-2. The conclusion then is that the fifth-order equation cannot be stable, but the third-order can in Case L-2.

Table 11

POSSIBLE STABILITY PREDICTIONS
BY THE CHARACTERISTIC EQUATIONS

		Fifth Order $G_5(s)$	Third Order $G_3(s)$
	Poles, P:	0	1
Case	Rotations, R		
R-1	0	Stable	Unstable
R-2	-2	Not Possible	Not Possible
R-3	1	Unstable	Unstable
L-1	1	Unstable	Unstable
L-2	-1	Not Possible	Stable

The third-order equation with the pole at $s = \Omega$ cannot predict stability correctly. When it can be stable, in Category L, the fifth-order cannot be. When the fifth-order equation can be stable, the third cannot be. Therefore, any simplifications derived from the third-order equation cannot be expected to give quantitative stability predictions.

This should be true for equations of both the second and first order which Zuber derived from the third. The fact that Zuber's third-order equation can be expected to give incorrect results has kept similar simplifications from being made to the characteristic equation developed here in Equation 73.

ZUBER'S FIRST-ORDER EQUATION

Thurston[3] has shown that Zuber's first-order stabilizing criterion (Equation VII-29, Reference 1) can be written in terms of dimensionless parameters to yield

$$(N_{BO})_{iZu} = \frac{D'}{4L'_e\left(\frac{N_{GLP}}{2} - 1\right)}\left[\frac{1}{N_{SV}} - \frac{N_{SUB}\,N_{GLP}}{2}\right] \qquad (108)$$

where $L'_e = \ell'(1-\tau_{12})$ and the other quantities are defined by Equations 109 to 111.

$$N_{SV} = \frac{\Delta v^*_{fg}}{v^*_f} \qquad (109)$$

$$N_{SUB} = \frac{\tau_{12}\Delta i_{13}}{\lambda^*} = \frac{4\ell'\tau_{12}}{D'} N_{BO} \quad (110)$$

$$N_{GLP} = \frac{0.5\,(1-\tau_{12})\,\varphi_{23}\,(1+\bar{u}_3) + k_e\,\bar{u}_3}{\tau_{12}\,\varphi_{12} + k_i} \quad (111)$$

The starred quantities are pseudo-two-phase properties defined by Thurston[3] The incipient boiling number is computed from Equation 108 which appears to give the proper qualitative dependence of boiling number at the inception of oscillation $(N_{BO})_{iZu}$ on the system parameters. Table 12 illustrates the effect of parameter variation according to Equation 108 on system stability.

Table 12

INFLUENCE OF PARAMETER VARIATION ON $(N_{BO})_{iZu}$

	Parameter Variations (Other Parameters Remaining Constant)	$(N_{BO})_{iZu}$	Effect
1.	ℓ' increases	decreases	destabilizing (if $N_{BO})_{iZu} > 0$)
2.	D' increases	increases	stabilizing (if $(N_{BO})_{iZu} > 0$)
3.	N_{SV} increases	decreases	destabilizing
4.	N_{SUB} increases	decreases	destabilizing

These effects agree fairly well with experimental data. While such agreement is a necessary condition to show the validity of a prediction it is not sufficient.

Table 13 summarizes results obtained from Thurston's data using Zuber's first-order equation.

Three cases were considered:

1. Exit pressure drop calculated from given orifice diameter; no upstream pressure drop.
2. Ignore exit pressure drop; no upstream pressure drop.
3. Ignore exit pressure drop, and take upstream coefficient to be $k_i = 2.4$

Case 1 represents the worst conditions for stable operation since the effect of an inlet pressure drop is ignored; in addition, in computing the exit pressure drop from the given orifice diameter, the stabilizing influence of the plenum is neglected.

Table 13

PREDICTIONS FROM ZUBER'S FIRST ORDER EQUATION

Run Number*	N_{SV}	N_{SUB}	Case 1 N_{GLP}	Case 1 $(N_{BO})_i \times 10^4$	Case 2 N_{GLP}	Case 2 $(N_{BO})_i \times 10^4$	Case 3 N_{GLP}	Case 3 $(N_{BO})_i \times 10^4$
- 7	1.75	0.118	44230	-0.62	351.2	-0.615	28.8	-0.450
+ 9	0.85	0.55	3420	-3.41	19.0	-2.96	7.1	-1.91
+10	0.85	0.471	14105	-2.63	81.8	-2.54	15.4	-2.05
-11	0.83	0.00	0	-6.26	0.0	-6.26	16.0	+0.89
-17	2.25	0.365	5986	-2.03	145.8	-2.03	82.4	-2.02
+18	2.60	0.269	1538	-1.55	46.7	-1.52	29.9	-1.50
-28	0.80	0.811	8682	-4.43	302.6	-4.41	40.3	-4.31
+29	0.80	0.812	4307	-4.52	162.7	-4.49	30.9	-4.36
+30	.45	0.831	520	-5.62	19.3	-5.73	9.3	-5.88
-31	1.65	0.656	3315	-3.73	130.3	-3.74	31.7	-3.75
-46	3.00	0.316	2606	-1.71	484.4	-1.71	26.2	-1.71
+47	3.00	0.500	454	-3.11	54.9	-3.15	4.7	-3.86
-48	1.20	0.578	4006	-3.09	632.6	-3.09	18.7	-2.93
+50	1.25	0.542	1842	-2.93	297.9	-2.92	13.6	-2.69
+51	1.30	0.0	∞	0.0	∞	0.0	21.7	0.405
-57	1.80	0.306	6969	-1.63	1071.2	-1.62	27.9	-1.52
+59	1.85	0.273	2452	-1.47	388.9	-1.46	15.2	-1.25
-65	2.75	0.516	902	-3.03	107.9	-3.04	9.9	-3.25
+66	2.75	0.425	128	-5.61	0.8	-4.13	0.0	-4.77
-69	1.40	0.0	∞	0.0	∞	0.0	39.2	0.199
+70	1.40	0.0	∞	0.0	∞	0.0	33.3	0.236
-71	1.90	0.0	∞	0.0	∞	0.0	92.1	0.0607
+72	2.65	0.0	∞	0.0	∞	0.0	61.2	0.0662
-97	1.45	0.44	6893	-2.36	541.3	-2.35	50.6	-2.30
+98	1.45	0.71	587	-4.59	25.9	-4.60	7.5	-4.63
-139	0.80	1.04	1393	-6.23	67.2	-6.19	13.4	-6.02
+140	0.80	1.12	944	-7.25	26.6	-7.19	5.4	-6.78

Case 1: $k_e \neq 0$, $k_i = 0$

Case 2: $k_e = 0$, $k_i = 0$

Case 3: $k_e = 0$, $k_i = 2.4$

* + = stable

\- = unstable

In progressing from Case 1 to Case 3 the gas-to-liquid pressure drop ratio is caused to decrease; this should generally cause the system stability to increase. Table 13 shows that decreasing the N_{GLP} can cause $(N_{BO})_{iZu}$ either to increase or to decrease algebraically, although not to a very great extent. For example, Runs 29 and 30 show an increase and decrease, respectively, of $(N_{BO})_{iZu}$. More important, with the exception of a few cases, the values of the incipient boiling numbers calculated from Equation 108 are negative. This, of course, is physically unrealistic.

For the two limits $N_{GLP} \to 0$ and $N_{GLP} \to \infty$, it can be seen that $(N_{BO})_{iZu}$ as calculated from Equation 108 will usually be negative.

1. Take $N_{GLP} \to 0$

In this case Equation 108 quickly gives

$$\lim_{N_{GLP} \to 0} (N_{BO})_{iZu} = - \frac{D'}{4L'_e N_{SV}} \tag{112}$$

which is always negative. However, small values of N_{GLP} would tend to correspond to high subcooling, and in this region the first-order equation does not apply.

2. Take $N_{GLP} \to \infty$

This case can occur when $k_i = 0$ and $k_e \neq 0$ or $k_e = 0$. As $\tau_{12} \to 0$, it is seen from Equations 110 and 111 that $N_{GLP} \to \infty$ and $N_{SUB} \to 0$. The product of these parameters results in a finite number:

$$N_{GLP} N_{SUB} = \frac{[0.5\, \varphi_{23} (1 + \bar{u}_3) + k_e \bar{u}_3]\, \Delta i_{23}}{\varphi_{12} \lambda^*} \tag{113}$$

Consider the data of Run 29, where

$\bar{u}_3 = 22.6$ $\qquad$ $k_e = 103$

$\varphi_{12} = \varphi_{23} = 8.3$ $\qquad$ $N_{SV} = 0.8$

$\lambda^* = 73$ Btu/lb

$\Delta i'_{13} = 875$ Btu/lb

Inserting these values in Equation 113 gives

$$N_{GLP} N_{SUB} = 3500$$

Therefore, Equation 108 will yield a negative $(N_{BO})_{iZu}$. Even under the more favorable circumstances where $k_e = 0$, it is found that $N_{GLP} N_{SUB} = 142$ and hence would still cause $(N_{BO})_{iZu}$ to be negative.

Figure 31 is a plot of the actual boiling number for a run versus the negative incipient boiling number as predicted from Equation 108. Although the stable points tend to cluster in the lower right region there certainly is not a clear division between two regions. The points along the vertical axis, i.e., $(N_{BO})_{iZu} = 0$, were obtained when there was no subcooling, i.e., $\tau_{12} = 0$ and $N_{GLP} \rightarrow \infty$.

A better separation of stable and oscillatory points is obtained if the product of the boiling and specific volume numbers is plotted. Figure 32 is a graph of the $N_{SV}\ N_{BO}$ versus $N_{SV}(N_{BO})_{iZu}$. With the exception of two points all of the stable points lie in the region $N_{SV}\ N_{BO} < 0.005$ and conversely for the unstable points. Edeskuty and Thurston [3] note that Rogers [9] was able to correlate his data by such a criterion. As seen in Figures 31 and 32, though, there is no apparent effect of the boiling number at inception, as calculated from Equation 108, on the stability of the system. There is no clear evidence of a relationship between $N_{SV}\ N_{BO}$ and $N_{SV}(N_{BO})_{iZu}$.

Recently, Rogers [9] has analyzed data obtained from low vapor quality, subcritical hydrogen in terms of Zuber's first-order equation. However, the data did not permit an estimation of N_{GLP}.

In summary, although the qualitative dependence of the Zuber first-order equation on the system parameters is in general agreement with experiment, its value as a predictive tool appears limited. The parameters which are generated in the first-order analysis are certainly pertinent to the stability of the system, and, as such, can be used in correlating data. The utility of empirical equations such as Thurston has derived for his system cannot be questioned. However, it is felt the applicability of these correlations as a predictive, rather than a correlating, technique would be of less generality than the approach being followed in this program.

DERIVATION OF NEW CRITERION

On the basis of the experience gained in calculating the Nyquist diagrams for a wide variety of test conditions, a greatly simplified criterion for stability will be developed here from the full characteristic equation, Equation 73. Approximations will be made to the characteristic equation near the crossover frequency ω_c to obtain the stability number N_s. This then will serve as the criterion.

It is convenient to start with a very simple system and then gradually broaden the applicability of the criterion. Assume first that the inlet and exit pressure drops are very large in comparison with the test section pressure drop. This is generally true for both the NASA and the Cleveland data. Neglecting the test section momentum equation, Equation 73 becomes

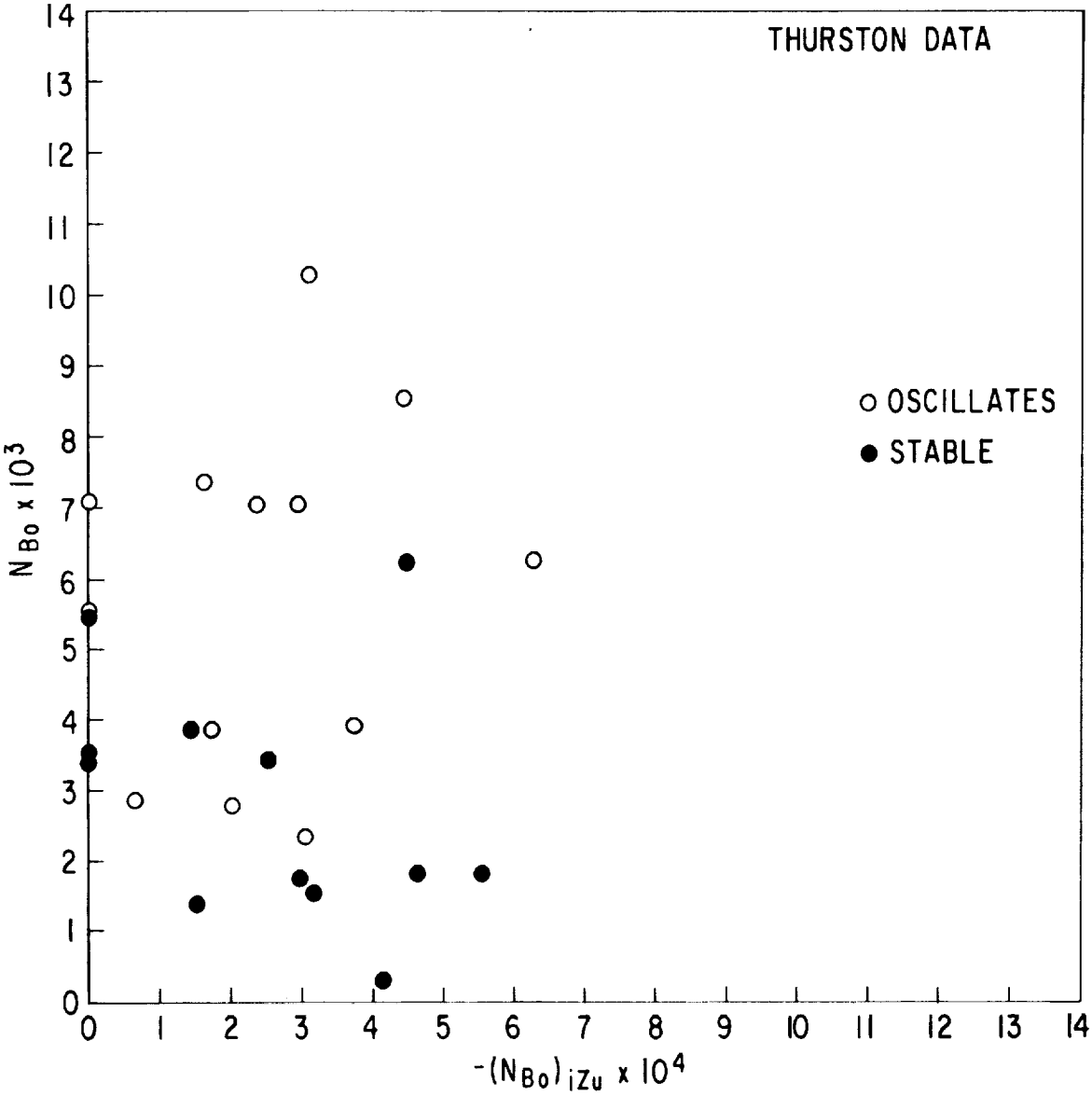

Figure 31. Actual Boiling Number Versus Incipient Boiling Number Predicted by Zuber's First Order Equation

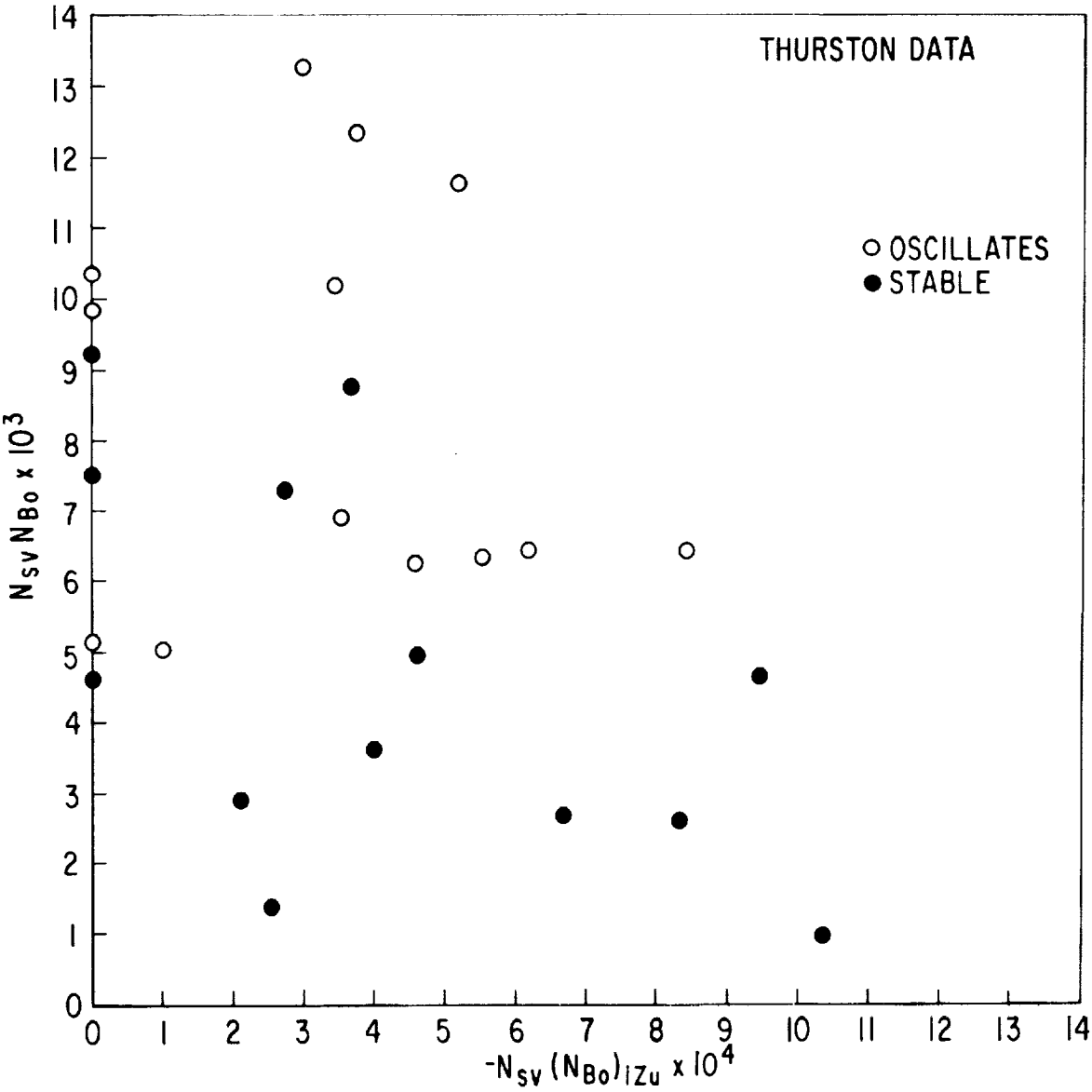

Figure 32. Actual N_{SV} N_{BO} Versus N_{SV} (N_{BO}) i Predicted by Zuber's First Order Equation

$$\frac{\delta \Delta p_{o1}}{\delta u_1} + \frac{\delta p_3}{\delta u_1} = 0$$

Using Equations 62 and 69 this can be written simply as

$$2k_i + k_e \left(\bar{u}_3^2 \frac{\delta \rho_3}{\delta u_1} + 2 \frac{\delta u_3}{\delta u_1} \right) = 0 \qquad (114)$$

when there is no plenum ($c_3 = 0$). The density and velocity perturbations are given by Equations 49 and 44.

In an attempt to simplify Equation 114 further consider the expressions for $\delta \rho_3$ and δu_3. Suppose the wall heat transfer effect W is small. If it is zero, the problem reduces, of course, to Zuber's fifth-order characteristic equation. If it is small, the expressions for $m_{1,2}$ of Equation 43 can be expanded to give

$$m_{1,2} \rightarrow \frac{R - s}{2} \pm \frac{R - s}{2} \left[1 + 2 \frac{\Omega(\Omega - R)}{(R - s)^2} + \cdots \right]$$

$$\rightarrow R - s + \frac{\Omega(\Omega - R)}{R - s}, \quad - \frac{\Omega(\Omega - R)}{R - s}$$

$$\rightarrow R - s, \quad 0 \qquad (115)$$

Suppose now that W can be neglected completely, except when it appears in an exponential. If this is done, Equations 49 and 44 can be written as

$$\delta \rho_3 \approx - \bar{\rho}_3^2 \Omega \tau_{12} \left(A e^{(R - s)\tau_{23}} + B \right) \qquad (116)$$

and

$$\delta u_3 \approx \tau_{12} B(\Omega - s) \qquad (117)$$

and the constants A and B from Equation 48 become

$$\left. \begin{aligned} A &\approx \frac{\delta u_1 - s \, \delta \lambda}{\tau_{12}(s - \Omega)} \\ B &\approx - \frac{\delta u_1 - \Omega \, \delta \lambda}{\tau_{12}(s - \Omega)} \end{aligned} \right\} \qquad (118)$$

The expression for the transition point perturbation Equation 36 becomes

$$\delta \lambda \approx \delta u_1 \frac{1 - e^{-(s+W)\tau_{12}}}{s} \qquad (119)$$

An additional simplification will be made to W, which from its definition in Equation 29 has the limits

$$\text{as } \mathcal{T}_w \to 0$$

$$W \to \frac{C_w s}{1+\mathcal{T}s} = \frac{C_w}{\mathcal{T}} \frac{1}{1+\frac{1}{\mathcal{T}s}}$$

and $$\text{as } \mathcal{T}_w \to \infty$$

$$W \to \frac{\left(C_w/\sqrt{\mathcal{T}_w}\right)\sqrt{s}}{1+\left(\mathcal{T}\sqrt{\mathcal{T}_w}\right)\sqrt{s}} = \frac{C_w}{\mathcal{T}} \frac{}{1+\frac{\sqrt{\mathcal{T}_w}}{\mathcal{T}\sqrt{s}}}$$

Therefore, if s is large enough W may be considered independent of the wall conduction time for a very wide range of $\mathcal{T}_w$. This is substantially true for the data which have been considered in Section 6. W will therefore be replaced by

$$W \approx \frac{C_w}{\mathcal{T}} \equiv H \tag{120}$$

From the definitions of C_w and $\mathcal{T}$, H is a dimensionless heat transfer coefficient. It is completely independent of the properties of the wall.

The approximations made above should not be too serious. The strongest effect of W, where it appears in an exponential, has been retained. An alternate way of deriving the same result is to assume s is large. This may then be thought of as the next step in applying the asymptotic approximation which was used in Section 5 to obtain the solution. Results contained in Reference 12 indicate that the approximation may be carried this far with the essence of the system dynamic response still retained.

Continuing, Equations 116 to 120 may be combined into Equation 114 to give

$$2k_i + k_e \left[-\Omega \frac{e^{-(s+H)\tau_{12}}}{s-\Omega} e^{(\Omega-s)\tau_{23}} + (2s-\Omega)\frac{1-\frac{\Omega}{s}(1-e^{-(s+H)\tau_{12}})}{s-\Omega} \right] \approx 0$$

On rearranging this becomes

$$2k_i + k_e \left\{ 2 - \frac{\Omega}{s} \left[1 + \left\{ \frac{1-(2-\Omega/s)e^{(s-\Omega)\tau_{23}}}{1-\Omega/s} \right\} e^{\Omega\tau_{23} - H\tau_{12} - s\tau_{13}} \right] \right\} \approx 0 \tag{121}$$

When the frequency in $s = i\omega$ equals the crossover frequency ω_c, Equation 121 by definition should approximate the stability number. At the crossover frequency the imaginary part of Equation 121 must be zero. An attempt will then be made to choose ω_c so that the imaginary part of Equation 121 is zero. The real part will be the stability number and must be greater than zero for the system to be stable.

Note first that the definition of $\Re$ in Equation 38 and the time in Equation 41 require that

$$e^{\Re \tau_{23}} = e^{(\Omega - H/\bar{\rho}_{ave})\tau_{23}} = \bar{u}_3 e^{-(H/\bar{\rho}_{ave})\tau_{23}} \tag{122}$$

In all the runs considered $\bar{u}_3$ is a fairly large number, of the order of 5 or greater. Therefore it would be expected that $e^{(s-\Re)\tau_{23}}$ would be of relatively small magnitude. Assume then that the term

$$\frac{1 - (2 - \Omega/s)e^{(s-\Re)\tau_{23}}}{1 - \Omega/s}$$

is a real number and can be approximated by the magnitude of the numerator divided by that of the denominator

$$\frac{1 - (2 - \Omega/s)e^{(s-\Re)\tau_{23}}}{1 - \Omega/s} \approx \frac{1}{\sqrt{1 + (\Omega/\omega_c)^2}}$$

Here s has been replaced by $i\omega_c$ and $e^{(s-\Re)\tau_{23}}$ has been considered small. With this, Equation 121 can be written as the stability number

$$2k_i + k_e \left\{ 2 - \frac{\Omega}{i\omega_c} \left[1 + \frac{\bar{u}_3}{\sqrt{1 + (\Omega/\omega_c)^2}} e^{-\hat{H}} e^{-i\omega_c \tau_{13}} \right] \right\} \approx N_S \tag{123}$$

where $\hat{H} = H(\tau_{12} + \tau_{23}/\bar{\rho}_{ave})$.

Equation 122 has been used to introduce $\bar{u}_3$ into Equation 123. If Equation 123 is to have a zero imaginary part, the real part of the bracketed expression must be zero.

$$\mathrm{Re}\left[1 + \frac{\bar{u}_3}{\sqrt{1 + (\Omega/\omega_c)^2}} e^{-\hat{H}} e^{-i\omega_c \tau_{13}} \right] =$$

$$1 + \frac{\bar{u}_3}{\sqrt{1 + (\Omega/\omega_c)^2}} e^{-\hat{H}} \cos \omega_c \tau_{13} \approx 0$$

If $\bar{u}_3$ is large, this must be true when $\cos \omega_c \tau_{13} \approx 0$ or when

$$\omega_c \approx \frac{\pi}{2\tau_{13}} (1 + 2n), \quad n = 0, 1, 2 \ldots \tag{124}$$

The real part of the expression, Equation 123, will then be

$$N_S = 2k_i + k_e \left\{ 2 + \frac{\Omega}{\omega_c} \frac{\bar{u}_3}{\sqrt{1 + (\Omega/\omega_c)^2}} e^{-\hat{H}} \sin \omega_c \tau_{13} \right\} \tag{125}$$

If the sign of $\sin \omega_c \tau_{13}$ is positive, the stability number is positive and the system is stable. If it is negative, N_s could possibly be negative. Therefore n = 1, 3, . . . corresponds to the successive crossover points of the Nyquist diagram of Figure 4, and n = 0, 2, . . . must then correspond to the places where the loops cross the real axis on the right. The crossover frequency occurs then at the first crossing with 180 degree phase lag, n = 1.

$$\omega_c \approx \frac{3\pi}{2\tau_{13}} \tag{126}$$

That this is a good approximation for the crossover frequency can be seen on Figure 33, where the observed crossover frequency for the Nyquist diagram has been plotted against the total residence time τ_{13}. (The line is Equation 126.) The agreement is good, but generally trails off at the larger residence times. This results from the fact that $\bar{u}_3$, as well as other factors of $\cos \omega_c \tau_{13}$, are no longer dominantly large. A better approximation to ω_c might be

$$\omega_c \approx \frac{3\pi}{2\tau_{13}} - \frac{\sqrt{1 + \left(\frac{2\Omega\tau_{13}}{3\pi}\right)^2}}{\bar{u}_3} e^{+\hat{H}}$$

However, in view of other approximations to be made this hardly appears to be justified.

Using Equation 126 for the crossover frequency, the stability number Equation 125 can be written

$$N_s \approx 2k_i + 2k_e - k_e \frac{\bar{u}_3}{\sqrt{1 + (\omega_c/\Omega)^2}} e^{-\hat{H}} \tag{127}$$

The criterion for oscillatory stability is that $N_s > 0$. Therefore a system which is strongly choked upstream and downstream will be stable if

$$1 + \frac{k_i}{k_e} > \frac{\bar{u}_3}{\sqrt{1 + (\omega_c/\Omega)^2}} \frac{e^{-\hat{H}}}{2} \equiv \Sigma \tag{128}$$

Equation 128 may be interpreted as follows. The left side may be thought of as a ratio of stabilizing to destabilizing pressure drops, properly weighted. The system upstream pressure drop is k_i and the exit pressure drop is $k_e \bar{u}_3$. $k_i + k_e$ is the stabilizing force and k_e is the destabilizing force. It is interesting that the exit pressure drop contributes both to stability and instability. As discussed in Section 5, the inlet pressure drop is only stabilizing. Σ, the right-hand side of Equation 128, may be thought of as a measure of the size or the expansion of the principle loop of the Nyquist diagram. The larger the loop the less likely the system is stable, though it still may still be stable if the upstream pressure drop k_i is large enough. The loop expansion Σ is proportional to the overall fluid expansion

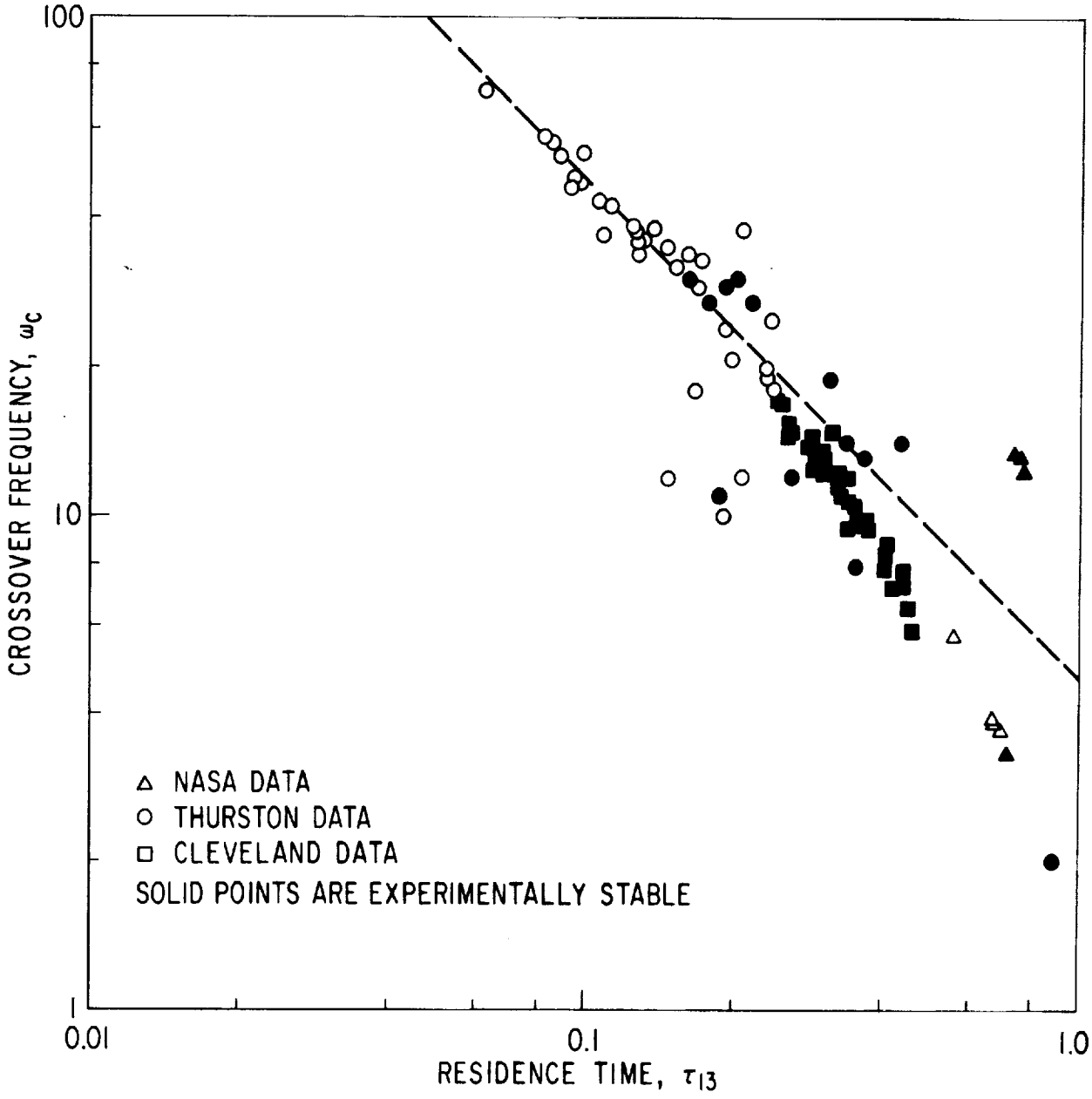

Figure 33. Nyquist Crossover Frequency as a Function of Residence Time

$\bar{u}_3$. $\bar{u}_3$ depends on the energy input relative to the flow rate and the subcooling; however, Σ is damped by the heat transfer rate in the exponential. The denominator provides the proper scale factor.

Friction Pressure Drop

Equations 127 and 128 apply when the inlet and exit pressure drops dominate the system. The effect of the friction pressure drop in the test section will be considered here in much the same way. The heavy-region friction pressure drop from Equation 52 is

$$\frac{\delta \Delta p_{12}}{\delta u_1} = \varphi_{12} \left(\frac{\delta \lambda}{\delta u_1} + 2\tau_{12} \right) \tag{129}$$

The light-region friction pressure drop is given by Equation 59. Using the same approximations as before, Equations 115 to 120, this may be simplified to

$$\frac{\delta \Delta p_{23}}{\delta u_1} = \varphi_{23} \left[-\delta\lambda - \frac{\Omega}{2\Omega - s} \frac{e^{-(s+H)\tau_{12}}}{s-\Omega} \left(\bar{u}_3 e^{(\mathcal{R}-s)\tau_{23}} - 1 \right) \right.$$

$$\left. - \left(1 - \frac{2s}{\Omega} \right) \frac{1 - \frac{\Omega}{s}(1 - e^{-(s+H)\tau_{12}})}{s - \Omega} (\bar{u}_3 - 1) \right]$$

It can then be rearranged to give

$$\frac{\delta \Delta p_{23}}{\delta u_1} = \varphi_{23} \left[\frac{\delta\lambda}{\delta u_1} + \frac{2}{\Omega}(\bar{u}_3 - 1) - \frac{1}{s}(\bar{u}_3 - 1) - \frac{\Omega}{s} \frac{F_{13}\bar{u}_3 e^{\mathcal{R}\tau_{23} - H\tau_{12} - s\tau_{13}}}{\Omega} \right] \tag{130}$$

where

$$F_{23} = \frac{1 - \left[5 - 2(\Omega/s + s/\Omega) + 2/\bar{u}_3 (s/\Omega + \Omega/s - 2) \right] e^{(s-\mathcal{R})\tau_{23}}}{(2 - s/\Omega)(1 - \Omega/s)}$$

As before, since $e^{(s-\mathcal{R})\tau_{23}}$ is a small number F_{23} will be assumed real and nearly equal to

$$F_{23} \approx \frac{1}{3\sqrt{1 + \frac{1}{9}\left(\frac{\omega_c}{\Omega} - \frac{2\Omega}{\omega_c} \right)^2}}$$

at the crossover frequency. The friction pressure drops may then be treated in the same manner as the downstream pressure drop. The crossover frequency may be taken as Equation 126. Then the real part of the resulting expression in Equation 129 and 130 can be added to the stability number of Equation 127 as the friction pressure drop contributions. These will be

$$\mathrm{Re}\left\{\frac{\delta\Delta P_{12}}{\delta u_1} + \frac{\delta\Delta P_{23}}{\delta u_1}\right\} \approx 2\varphi_{12}\tau_{12} + 2\varphi_{23}\frac{\bar{u}_3 - 1}{\Omega} - \frac{\varphi_{23}\bar{u}_3}{\Omega}(\Omega/\omega_c)\frac{\bar{u}_3 e^{-\hat{H}}}{3\sqrt{1 + \frac{1}{9}\left(\frac{\omega_c}{\Omega} - 2\frac{\Omega}{\omega_c}\right)^2}}$$

if the term $(\varphi_{12} - \varphi_{23})\,\delta\lambda$ can be neglected. It is perhaps more convenient to write the third term of this expression in terms of the expansion factor Σ appearing in Equation 128.

$$\mathrm{Re}\left\{\frac{\delta\Delta P_{12}}{\delta u_1} + \frac{\delta\Delta P_{23}}{\delta u_1}\right\} \approx 2\varphi_{12}\tau_{12} + 2\varphi_{23}\frac{\bar{u}_3 - 1}{\Omega} - \frac{\varphi_{23}\bar{u}_3}{\Omega}\,2\,w_{23}\,\Sigma \qquad (131)$$

where w_{23} is the weighting factor

$$w_{23} = \frac{1}{3}\sqrt{\frac{1 + (\Omega/\omega_c)^2}{1 + \frac{1}{9}(\omega_c/\Omega - 2\Omega/\omega_c)^2}} \qquad (132)$$

Adding this contribution to the expression for the stability number, Equation 129 becomes

$$N_s \approx 2k_i + 2\varphi_{12}\tau_{12} + 2\varphi_{23}\frac{\bar{u}_3 - 1}{\Omega} + 2k'_e - 2\left(k_e + \frac{\varphi_{23}\bar{u}_3}{\Omega}\,w_{23}\right)\Sigma \qquad (133)$$

The heavy-region pressure drop is seen to be only stabilizing. The light-region pressure drop, like that for the downstream orifice, contributes some to both stabilizing and destabilizing forces.

Acceleration Pressure Drop

The same general procedure will again be used to add the effect of the acceleration pressure drop into Equation 133. Using Equations 115 through 120, the acceleration pressure drop, Equation 57, can be simplified to

$$\frac{\delta\Delta P_{12}}{\delta u_1} \approx -\Omega\left[\frac{1 - e^{-(s+H)\tau_{12}}}{s}\right] - \Omega\left[\frac{\Omega}{\Omega - s}\,\frac{e^{-(s+H)\tau_{12}}}{s - \Omega}\left(e^{(\Omega - s)\tau_{23}} - 1\right)\right.$$
$$\left. - s\tau_{23}\,\frac{1 - \frac{\Omega}{s}\left(1 - e^{-(s+H)\tau_{12}}\right)}{s - \Omega}\right]$$

This can be rearranged into a form similar to the heavy-region friction and downstream orifice pressure drops.

$$\frac{\delta \Delta p_a}{\delta u_1} = \Omega \tau_{23} - \frac{\Omega}{s} - \frac{\Omega}{s} F_a \, e^{R\tau_{23} - H\tau_{12} - s\tau_{13}} \tag{134}$$

where

$$F_a = \frac{1 - \left[1 - \frac{\Omega}{s} \left(\frac{s-\Omega}{\Omega} \right)^2 - \Omega \tau_{23} \left(\frac{s-\Omega}{\Omega} \right) \right] e^{(s-R)\tau_{23}}}{(1 - \Omega/s)\ (1 - s/\Omega)}$$

As before, assume F_a to be approximated, at the crossover frequency, by

$$F_a \approx \frac{1}{2 \sqrt{1 + \frac{1}{4} \left(\frac{\Omega}{\omega_c} - \frac{\omega_c}{\Omega} \right)^2}}$$

The real part of Equation 134 should then be nearly equal to

$$\mathrm{Re} \left\{ \frac{\delta \Delta p_a}{\delta u_1} \right\} = \Omega \tau_{23} - w_a \Sigma \tag{135}$$

where the weighting factor w_a is given by

$$w_a = \sqrt{\frac{1 + (\Omega/\omega_c)^2}{1 + \frac{1}{4} (\Omega/\omega_c - \omega_c/\Omega)^2}} \tag{136}$$

The contribution of the acceleration pressure drop, Equation 135, added to the stability number expression, Equation 133, gives

$$N_s \approx 2k_i + 2\varphi_{12}\tau_{12} + 2\varphi_{23} \frac{\bar{u}_3 - 1}{\Omega} + \Omega \tau_{23} + 2k_e - 2 \left(k_e + \varphi_{23} \frac{\bar{u}_3}{\Omega} w_{23} + \frac{w_a}{2} \right) \Sigma \tag{137}$$

From Equation 137 the criterion for stability can then be written

$$\frac{k_i + \varphi_{12}\tau_{12} + \varphi_{23} \frac{\bar{u}_3 - 1}{\Omega} + \frac{\Omega \tau_{23}}{2} + k_e}{\frac{w_a}{2} + \varphi_{23} \frac{\bar{u}_3}{\Omega} w_{23} + k_e} > \Sigma \tag{138}$$

Equation 132 represents a simplified stability criterion for the system. It includes the effects of upstream and downstream orifice and the acceleration and friction pressure drops in the test section. It does not include the inertia or body force pressure drops. Since these have been found to be completely negligible or zero for the sets of data analyzed they will be omitted in this approximate analysis. Equation 138 is valid only when there is no outlet plenum.

Outlet Plenum

A correction will be developed here to account for an outlet plenum when it is present in the system. The plenum acts to damp out oscillations which enter it before they reach the outlet orifice. It is convenient then to define an effective orifice coefficient to account for the plenum's behavior.

Consider the exit pressure perturbation again as given by Equation 69. Assume that the factor $(1/\gamma)\,(1+2c_3s)/(1+c_3s)$ in the denominator is nearly unity. Write Equation 69 as

$$\delta p_3 \approx \frac{k_e}{(1+c_3s)^2}\left[\bar{u}_3^2\ \delta\rho_3 + (1+c_3s)\ \delta u_3\right] \tag{139}$$

As the factor of the $\bar{u}_3^2\,\delta\rho_3$ term take as the effective orifice coefficient, $(k_e)_{eff}$, k_e divided by the magnitude of the damping factor, ignoring the phase differences:

$$(k_e)_{eff} \approx \frac{k_e}{1+(c_3\omega_c)^2} \tag{140}$$

The contribution of the plenum on the δu_3 term is slightly different. From the original assumptions of Equations 115 to 120 the δu_3 term can be written

$$\frac{k_e}{1+c_3s}\ \frac{\delta u_3}{\delta u_1} \approx \frac{k_e}{1+c_3s}\left[1-\frac{\Omega}{s}+\frac{\Omega}{s}\ e^{-(s+H)\tau_{12}}\right]$$

By comparison with Equation 121 and the earlier development without the plenum it can be shown that the exponential term here contributed an insignificant amount to the destabilizing effect of the downstream orifice. The real constant 1 was responsible for the stabilizing effect. If the exponential term is again neglected and the real part of the remainder is considered at the crossover frequency,

$$\mathrm{Re}\left\{\frac{k_e}{1+ic_3\omega_c}\left(1-\frac{\Omega}{i\omega_c}\right)\right\} = \frac{k_e}{1+(c_3\omega_c)^2}\ (1+c_3\Omega) = (k_e)_{eff}\,(1+c_3\Omega)$$

Therefore the contribution to the stabilizing forces can be written as the effective coefficient times the factor $(1+c_3\Omega)$.

Complete Criterion

Incorporating the effect of the plenum into Equation 137 for the stability number, the final expression can be written

$$N_s \approx 2k_i + 2\varphi_{12}\tau_{12} + 2\varphi_{23}\,\frac{\bar{u}_3-1}{\Omega} + \Omega\tau_{23} + 2(k_e)_{eff}\,(1+c_3\Omega) - 2\left((k_e)_{eff} + \varphi_{23}\,\frac{\bar{u}_3}{\Omega}\,w_{23} + \frac{w_a}{2}\right)\ \Sigma \tag{141}$$

The criterion for stability can then be written

$$\Psi \equiv \frac{k_i + \varphi_{12}\tau_{12} + \frac{\Omega\tau_{23}}{2} + \varphi_{23}\frac{\bar{u}_3 - 1}{\Omega} + (k_e)_{eff}(1+c_3\Omega)}{\frac{w_a}{2} + \varphi_{23}\frac{\bar{u}_3}{\Omega}\, w_{23} + (k_e)_{eff}} > \frac{\bar{u}_3}{\sqrt{1+\left(\frac{\omega_c}{\Omega}\right)^2}}\,\frac{e^{-\hat{H}}}{2} \equiv \Sigma \tag{142}$$

As discussed above for Equation 128 the criterion can be interpreted in terms of the ratio of stabilizing to destabilizing pressure drops, Ψ, and the Nyquist diagram loop size, Σ. Using the steady-state pressure drop expressions of Equations 52, 57, 59, 62, and 68, Ψ can be written as

$$\Psi = \frac{\Delta\bar{p}_{01} + \Delta\bar{p}_{12} + \Delta\bar{p}_a\left[\frac{\ell n\,\bar{u}_3}{2(\bar{u}_3-1)}\right] + \Delta\bar{p}_{23}\left[\frac{2}{\bar{u}_3+1}\right] + \Delta\bar{p}_{34}\left[\frac{(k_e)_{eff}(1+c_3\Omega)}{k_e\,\bar{u}_3}\right]}{\Delta\bar{p}_a\left[\frac{w_a}{2(\bar{u}_3-1)}\right] + \Delta\bar{p}_{23}\left[\frac{2\bar{u}_3 w_{23}}{\bar{u}_3^2-1}\right] + \Delta\bar{p}_{34}\left[\frac{(k_e)_{eff}}{k_e\bar{u}_3}\right]} \tag{143}$$

For convenience the criterion Equation 142 and all expressions required to evaluate it are collected together in Table 14.

APPLICATION TO DATA AND DISCUSSION

Figure 34 shows the pressure drop ratio Ψ plotted against the Nyquist loop expansion Σ for all three sets of data. The solid line is Equation 142 written as an equality. If the points fall above the line they are predicted to be stable. The values of Ψ and Σ for each run considered are also tabulated in Tables 2, 4, and 9 for reference.

For the most part the agreement between the criterion and the data is good. There are about ten data points which fall on the wrong side of the line further than about 20 to 25 percent away. As can be seen from the tabulated results, the points generally agree well with the Nyquist results. The runs with the smallest stability numbers are the closest to the line on Figure 34. There are exceptions however. The most notable series of runs which has wide discrepancies is Thurston's early series with the smaller plenum and the smaller orifices. These runs contribute four of the incorrect points of Figure 34, and they contributed three incorrect points on Figure 6; however, the incorrect points are not necessarily the same ones. This is a peculiarity without an adequate explanation at present.

There are several interesting points about the criterion in Equation 142. The ratio of the stabilizing to destabilizing pressure drops Ψ shows that all of the pressure drops contribute to some extent toward stability; on the other hand, only those downstream from the transition point are

Table 14

SIMPLIFIED STABILITY CRITERION

Stabilizing to destabilizing pressure drop ratio > Nyquist loop size

$$\Psi > \Sigma \quad \text{for stability} \tag{1}$$

where

$$\Psi = \frac{\Delta\bar{p}_{01} + \Delta\bar{p}_{12} + \Delta\bar{p}_a \frac{\ell n\, \bar{u}_3}{2(\bar{u}_3-1)} + \Delta\bar{p}_{23} \frac{2}{\bar{u}_3+1} + \Delta\bar{p}_{34} \frac{(k_e)_{eff}(1+c_3\Omega)}{k_e\, \bar{u}_3}}{\Delta p_a \frac{w_a}{2(\bar{u}_3-1)} + \Delta\bar{p}_{23} \frac{2\bar{u}_3 w_{23}}{\bar{u}_3^2-1} + \Delta\bar{p}_{34} \frac{(k_e)_{eff}}{k_e\, \bar{u}_3}} \tag{2}$$

$$\Sigma = \bar{u}_3 \frac{\exp\left[-\frac{C_w}{\mathcal{J}} (\tau_{12} + \frac{2\bar{u}_3}{\bar{u}_3+1} \tau_{23})\right]}{2\sqrt{1+\left(\frac{\omega_c}{\Omega}\right)^2}} \tag{3}$$

$$\Delta\bar{p}_{01} = k_i \tag{4}$$

$$\Delta\bar{p}_{12} = \varphi_{12}\, \tau_{12} \tag{5}$$

$$\Delta\bar{p}_a = \bar{u}_3 - 1 \tag{6}$$

$$\Delta\bar{p}_{23} = \varphi_{23} \frac{\bar{u}_3^2 - 1}{2\Omega} \tag{7}$$

$$\Delta\bar{p}_{34} = k_e\, \bar{u}_3 \tag{8}$$

$$(k_e)_{eff} = \frac{k_e}{1+(c_3\omega_c)^2} \tag{9}$$

$$\omega_c = \frac{3\pi}{2\tau_{13}} \tag{10}$$

$$w_a = \sqrt{\frac{1+(\Omega/\omega_c)^2}{1+\frac{1}{4}(\Omega/\omega_c - \omega_c/\Omega)^2}} \tag{11}$$

$$w_{23} = \frac{1}{3}\sqrt{\frac{1+(\Omega/\omega_c)^2}{1+\frac{1}{9}(\omega_c/\Omega - 2\Omega/\omega_c)^2}} \tag{12}$$

Additional relations:

$$\bar{u}_3 = 1 + \Omega(1 - \tau_{12}) \tag{13}$$

$$\tau_{23} = \frac{\ell n\, \bar{u}_3}{\Omega} \tag{14}$$

$$\tau_{13} = \tau_{12} + \tau_{23} \tag{15}$$

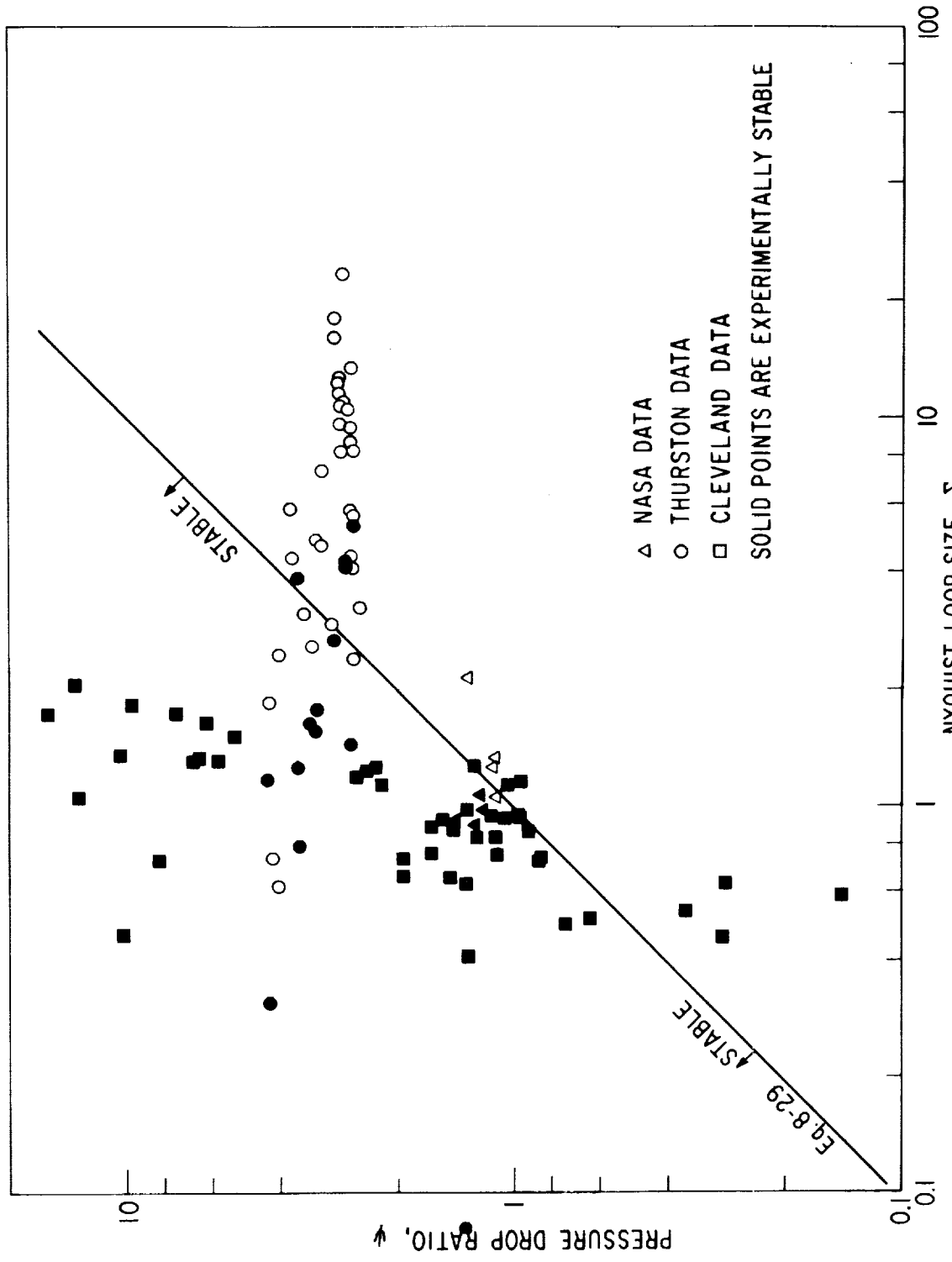

Figure 34. Simplified Stability Criterion

destabilizing. This agrees with the general comments made in Section 5 (page 27), where it was reasoned that those pressure drops downstream of the transition point feed back delayed signals which cause the instability. The criterion indicates the same thing. The Nyquist loop size is determined from the factors of the delay $e^{-sT_{13}}$. This delay appears in the acceleration, friction, and downstream pressure drop terms. Therefore these, with the appropriate weighting factors, are destabilizing.

The Nyquist loop size factor Σ shows the importance of the fluid expansion $\bar{u}_3$, the heat transfer rate $C_W/\mathcal{J}$ and the residence time τ_{13}. The latter enters into both the exponential and the scale factor in the denominator: the shorter the delay time τ_{13} the more the loop size is reduced by the denominator.

Since the heat transfer rate appears in the exponential, its effect is the strongest. A small error in the prediction of the heat transfer coefficient can make a big difference in the loop size and the stability prediction. Since the effect is the largest when the factor $\tau_{12} + (2\bar{u}_3/(\bar{u}_3+1))\tau_{23}$ is largest, the heat transfer would generally have its greatest damping effect when the fluid residence time $\tau_{13} = \tau_{12} + \tau_{23}$ is largest. The NASA runs generally had the largest residence times, Thurston's the shortest.

The relation between the residence time and the heat transfer damping effect can be explained physically as follows. It was shown in Equation 37 that the heat transfer rate diminished the fluid reaction frequency. If the fluid is rising in temperature and is expanding it will tend to receive more energy from the augmented heat transfer area. This will increase the temperature even further. On the other hand, as the temperature rises heat will be transferred back to the wall at a certain rate, thus diminishing the further increase in temperature. But if the rate (or frequency) of the original rise is much faster, the heat will have less time to be transferred back to the wall. Therefore the heat transfer effect will be relatively smaller. As indicated by Equation 126, the lower the fluid residence time the higher the frequency of the oscillations will be. Consequently the heat transfer effect is less when the residence time is less, just as indicated by the exponential in Σ.

The simplified criterion Equation 142 is also interesting in comparison with Thurston's correlation, discussed earlier in this section. Thurston wrote the fluid expansion $\bar{u}_3$ in terms of his boiling number and specific volume number as

$$\bar{u}_3 = 1 + N_{BO}\, N_{SV}\, \frac{4\ell'}{D'}\, (1 - \tau_{12})$$

Putting this into the expression for the Nyquist loop size in Equation 142 and solving for the boiling number yields

$$N_{BO} < \frac{D'}{4\ell'(1-\tau_{12})} \left(\Psi\, \frac{\bar{u}_3}{\Sigma} - 1 \right) \frac{1}{N_{SV}}$$

This is quite similar to Thurston's reformulation of Zuber's first-order equation (Equation 108). The boiling number is inversely proportional to the specific volume number. Thurston had a constant subtracted from the right side, but it was essentially negligible. The magnitude of the coefficient can be estimated in the following way.

At the stability limit $\Psi = \Sigma$. It can be seen from Figure 6 that $\bar{u}_3 \approx 15$ roughly separates Thurston's stable and unstable points. τ_{12} is of the order of 0.05 for most of Thurston's runs. From Table 3, $D'/4\ell' = 1/1920$ except for a few runs. Using these numbers gives a coefficient of about 0.0075, as compared with 0.0045 from Thurston's correlation. From the NASA data take $\bar{u}_3 \approx 6.5$ from Figure 5, $\tau_{12} \approx 0.6$, and $D'/4\ell' \approx 0.001$. This gives

$$\frac{D'}{4\ell'(1-\tau_{12})} \left(\Psi \frac{\bar{u}_3}{\Sigma} - 1 \right) \approx 0.009$$

Therefore the coefficient is roughly constant for both sets of data. The difference between the coefficients predicted here and Thurston's could well be the different approaches used to evaluate Ω here and N_{BO} and N_{SV} by Thurston. It is concluded that Equation 142 provides a fairly firm theoretical basis for Thurston's correlation. Furthermore, it should permit the coefficient to be calculated in advance.

Section 9

RESULTS AND CONCLUSIONS

APPLICATION OF MODEL TO DATA

The figures in Section 6 indicate how well the approximate analytical solution to the model predicts the instability observed experimentally by three different investigators. The agreement is reasonably good. The model is quite good in differentiating between members of a series of runs which are the least stable. However, the value of the stability number at incipient instability tended to be slightly conservative. The predicted stability number was generally negative in the range of -15 to -25 when the experimental stability limit was reached.

There are isolated exceptions. The most notable general exception appeared to be Cleveland's runs with the upstream orifice. Thurston's runs with the smaller plenum and downstream orifices tended to give a larger proportion of questionable results. There is no conclusive explanation for these discrepancies. For the former a great deal of scatter in the values of the orifice coefficients was obtained; having to back-calculate the upstream pressure drop from the entire system pressure drop probably contributed a great deal to the scatter. For the latter, these runs tended to be exceptionally sensitive to the parameters used. Future experimental studies could emphasize runs with similar operating conditions.

Experience with the applications has indicated several desirable measurements which should be included in any experimental program. The analysis has shown the importance of participation of the entire system in the instability phenomenon. Therefore pressure drops should be carefully measured both upstream and downstream of the test section. The measurements should be taken as closely as possible to incipient instability to determine the stability limit. Finally the importance of simultaneous heat transfer measurements is discussed in this section.

The results presented in Section 6 were obtained using the approximate solution to the system equations. Figure 27 indicates how well that asymptotic approximation predicts the actual system stability number. The trend indicates that the approximation gives stability numbers somewhat closer to zero. In general the exact solutions confirmed the asymptotic approximation's ability to correctly order a series of runs, from the most to the least stable. It is concluded, then, that the asymptotic approximation is a useful tool in obtaining a closed-form solution to this problem. The results obtained are close to quantitative, and it is felt that the advantages of a closed-form solution greatly outweigh the numerical discrepancies. The development of a simplified criterion in Section 8 is a case in point.

The comparison between the model and the data indicates that there may be limitations on the model. The rather consistent tendency to be conservative in the stability predictions suggests the possible omission of a stabilizing force. If so, it is believed to be minor. It is felt the known limitations of the model can be at least as important; therefore it would be most fruitful to determine experimentally or theoretically conditions under which the present model clearly fails rather than to attempt to tighten the prediction for these data.

Experience gained in using the two-region approximation to the $1/\rho$-i curve suggests that this is not a serious limitation to the model. It is recommended that the two-region approximation be applied in such a way as to yield the correct fluid residence time. Therefore the approximation should closely match the area under the ρ-i curve. This approach is not necessarily consistent with choosing the transposed critical temperature for the transition point as was suggested by Zuber[1] and by Thurston.[2] Applied as recommended, the two-region approximation should not contribute errors of more than 10 to 15 percent in the stability number. Consistently applied, it should always give the correct relative stability prediction among several runs.

There are a number of other possible limitations on the model. Experience with the treatment of the heat transfer to the wall is discussed in detail below. Other assumptions implicit in the analysis have not been investigated. The model is one-dimensional even though there are large temperature variations in the radial direction. The model formulation basically ignores the large variations in physical properties as the fluid passes through the transposed critical temperature. It is not known how this would influence the friction factor and the heat transfer characteristics used. The assumption that the energy equation is independent of pressure may be questioned in some of both Thurston's and Cleveland's runs in which the pressure changed considerably over the test section. Even though the specific volume versus enthalpy or distance was adjusted to agree with this pressure drop, expansion work in the energy equation could be significant. In a few runs, expecially in Cleveland's data, the pressure fell sufficiently so that the fluid would pass through a subcritical, two-phase region. The runs were treated as if this had not occurred. It is not known how any of these effects might influence the stability prediction.

Zuber noted that the model as originally developed should apply to subcritical, two-phase systems when there is no slip between the phases.[1] Attempts to use the analysis at low pressures, $p_r \approx 0.1$ were consistently unsuccessful. The model predicted that the systems were much more unstable than observed experimentally. However, the slip velocity was estimated to have a large effect on the mixture specific volume. It is concluded that slip must be accounted for. Zuber has recently published[4] an extension of the basic model used here which includes the effect of slip, but it has apparently not yet been compared with experimental data.

EFFECT OF WALL HEAT TRANSFER

It has been shown in this analysis that the heat transfer to the test section wall is a very important stabilizing influence in supercritical systems. From the three sets of data considered here it is not adequate to assume that the test section wall is negligibly thin. It is not believed that it will be negligible in any system.

So long as the wall has a sufficiently large thermal capacitance the dynamics of the heat transfer to and from the wall must be included. The effect can be explained physically as follows. As the fluid temperature increases, it expands and is exposed to more heating surface area; therefore the fluid will receive more energy and rise higher in temperature. If the wall is infinitely thin its temperature will rise the same amount to maintain the transfer of all the energy to the fluid. If the wall has a finite thermal capacitance, its temperature will not rise instantaneously; therefore the temperature difference and consequently the energy transferred will be diminished. For a given fluid temperature rise, the higher the film heat transfer coefficient the greater the decrease in energy received by the fluid. Since the resultant enthalpy and density changes are diminished, the system tends to be more stable.

The above argument and the model used suggest that this heat transfer effect would not be present in subcritical, two-phase systems. Neglect of the wall capacitance may therefore be entirely justifiable except when the fluid is single-phase. If the heat transfer is expressed as the product of a constant coefficient and the temperature difference between the wall and the bulk fluid, the energy transferred should stay constant in spite of fluctuations in the two-phase bulk properties. Eventhough the bulk enthalpy may change, the temperature should remain at the saturation temperature. However, the heat transfer coefficient may well fluctuate with physical properties and flow rates in both single- and two-phase systems. This possibility was not considered in the present analysis; it is not known how it would affect the predicted stability number.

Since the supercritical stability number strongly depends on the heat transfer effect, the results are particularly sensitive to the value of the heat transfer coefficient used. A given percentage change in the heat transfer coefficient might make an even larger change in the predicted stability number. This is shown most clearly by the simplified criterion developed in Section 8. Generally, the larger the residence time of the fluid the more sensitive is the stability number to changes in the heat transfer coefficient. Prediction of heat transfer coefficients for supercritical fluids does not appear to be on firm ground; property variations both with radius and length make it difficult to select the proper average value to be used in the analysis. It is concluded that this lack of certainty on the heat transfer coefficient is the major limitation on the analysis as it stands now. Uncertainty in h' could easily account for the differences observed between the calculated stability numbers and the experimental

results. This is true even for Thurston's data, which included sufficient data to calculate the coefficient as a function of distance for one run.*

In view of the importance of the heat transfer coefficient more work needs to be done to determine exactly the reliability of the prediction of h'. Clearly any experimental work on instabilities should include the measurement of heat transfer coefficients.

SIMPLIFIED CRITERION

A simplified stability criterion has been developed from the full characteristic equation for the system. The criterion,and the parameters needed to apply it, are included in Table 14. Figure 34 shows how well it applies to all three sets of data considered. Considering the simplicity of the criterion and the diverse experimental conditions, the agreement is thought to be very good.

The criterion is in the form of a simple equation. It states that a ratio of stabilizing to destabilizing pressure drops, when properly weighted, must exceed a measure of the Nyquist loop size. All parameters in the criterion are theoretically based on the model used here and can be predicted in advance. There are no parameters which must be adjusted to fit sets of experimental data. The criterion includes the effects of upstream and downstream pressure drops, as well as the acceleration and friction pressure drops in the test section. Pressure drops upstream from the transition point are stabilizing; all those downstream contribute to both stabilizing and destabilizing forces. The Nyquist loop size depends on the energy input relative to the flow rate through the factor $\bar{u}_s$, the overall fluid expansion. The loop size is strongly affected by the heat transfer coefficient for the system.

Since the criterion was derived with few explicit limitations on the size of any of the important parameters, the criterion should have a fairly broad applicability. The effect of gravity and body forces has been omitted because it was quite negligible in the forced convection systems considered. Therefore the criterion should not apply to natural circulation loops. Otherwise there are ostensibly no limitations.

Although the data to which the criterion has been applied are faily diverse, there are undoubtedly regions where it will fail. The available data do not clearly indicate where these might be. Certainly the criterion should fail when the complete analytical model fails. There is an indication also that the criterion might be weak when the total fluid residence time grows large. One result that falls out of the simplification is that the crossover

*A recent paper by Thurston[26] indicates that the heat transfer coefficient in the heavy region tends to be somewhat higher near the unstable conditions than would be normally predicted. This just emphasizes the lack of confidence in heat transfer predictions for these fluids.

frequency, or the oscillation frequency at the stability limit, should be inversely proportional to the residence time. This, incidently, is a result found experimentally by Stenning and Veziroglu.[8] Figure 33 shows that at the larger values of τ_{13} this is less likely to be true. Although the predictions of the criterion on Figure 34 do not appear to be significantly less valid at the larger residence times, this is a possibility which could be investigated. Other limitations of the criterion will have to be determined by comparison with additional experimental data.

In view of the simplicity and wide applicability of the criterion of Table 14 it is recommended that it be used as a guideline in designing stable-operating supercritical heat exchangers. Since the available data do not seem to point out all the limitations of the criterion, more data are needed. It is recommended that controlled laboratory experimentation be performed to further confirm or disprove the utility of the criterion.

CONTROL OF OSCILLATORY BEHAVIOR

The results obtained from the full characteristic equation, the Nyquist diagrams, the simplified criterion, and even the signal flow diagram of Figure 3 all indicate that the pressure drops upstream of the transition point are stabilizing. This is a generally accepted experimental fact as well.[1] This observation can be used as a basis for a feedback control scheme to eliminate any oscillatory behavior.

As discussed in Section 5, the instabilities are caused by the feedback of delayed signals by the pressure drops downstream of the transition point. Therefore, it should be expected that if any signal at the outlet of the exchanger, such as the temperature or velocity, were measured and fed back to control the upstream pressure or velocity, the instabilities would only be aggravated. The control signal would only add to the inherent pressure drop feedback of delayed signals. However, if any signal were measured near or upstream from the transition point the feedback would be stabilizing. What is measured and what is controlled is largely a matter of convenience for the particular application. The important point is that the measuring point should be upstream of the transition point, or at least close enough to it that the delay is minimized.

This same idea has been successfully applied experimentally by Hill and McCann.[11] In controlling a reactor preheater for supercritical propane they observed that the control was poor when outlet measurements were used for the feedback signal. Control improved considerably when measurements were made at an intermediate position in the heater. Although instabilities as such were not observed, the point is well illustrated.

Section 10

NOMENCLATURE

(MLT$\tilde{\theta}$ System of Units Used with H Defined by $H=ML^2T^{-2}$)

Note: Throughout the report dimensioned variables have been identified by a prime. The nomenclature lists all variables in dimensionless form, however, with their corresponding dimensions included.

A	Coefficient defined in Equation 48
A_c	Cross-sectional area of tube [L^2]
A_w	Cross-sectional area of tube wall [L^2]
B	Coefficient defined in Equation 48
C_w	Thermal capacitance of the wall, defined in Equation A-30
c_p, c_v	Specific heat at constant pressure and volume [$HM^{-1}\theta^{-1}$]
c_w	Wall specific heat [$HM^{-1}\theta^{-1}$]
c_3	Plenum volumetric capacitance, defined by Equation A-26
D	Tube diameter [L]
F_a, F_{23}	Functions in Equations 130 and 134
f	Friction factor
G	Mass flow rate [$ML^{-2}T^{-1}$]
G(s), G_3, G_5	Complex portion of characteristic equation defined in Equation 76; subscripts refer to the order of the characteristic equation.
g	Gravitational constant [LT^{-2}]
H	$C_w/\mathcal{J}$
$\hat{H}$	$H(\tau_{12} + \tau_{23}/\bar{\rho}_{ave})$
h	Film heat transfer coefficient [$\theta L^{-2}T^{-1}$]
i, Δi	Enthalpy, enthalpy rise [HM^{-1}]
K	Negative of operating point on Nyquist diagram, defined for Equation 75

k	Conductivity $[\theta L^{-1}T^{-1}]$
k_i, k_e, $(k_e)_{eff}$	Inlet and exit orifice coefficients; effective k_e defined in Equation 140
L_e	$\ell (1 - \tau_{12})$
ℓ	Test section length [L]
ℓ_w	Wall thickness [L]
$m_{1,2}$	Parameters defined in Equation 43
N_{BO}	Boiling number, defined in Equation 110
N_{GLP}	Gas-to-liquid pressure drop ratio, defined by Equation 111
N_s	Stability number, defined by Equation 75
N_{SUB}	Subcooling number, defined by Equation 110
N_{SV}	Specific volume number, defined by Equation 109
N_u	Nusselt number
P	Number of poles
P_r	Prandtl number
p, p_c	Pressure, critical pressure $[ML^{-1}T^{-2}]$
Δp	Pressure drop $[ML^{-1}T^{-2}]$
Δp_{12}, Δp_{23}	Friction pressure drop in heavy and light regions
q	Input energy flux $[HL^{-2}T^{-1}]$
q_w	Energy transferred from wall to fluid $[HL^{-2}T^{-1}]$
R	Gas constant; also used as number of rotations of Nyquist diagram
R_e	Reynolds number
$\mathcal{R}$	Reaction frequency, defined in Equation 38
s	Operator for time derivative or parameter in Laplace transformation

T, T_c	Temperature, critical temperature [θ]
t	Time [T]
$\mathcal{J}$	Heat transfer time, defined by Equation A-31
$\mathcal{J}_w$	Conduction time, defined by Equation A-32
u	Velocity [LT^{-1}]
V	Plenum volume [L^3]
v	Specific volume [L^3M^{-1}]
v_f^*, Δv_{fg}^*	Pseudo-liquid specific volume and volume change in pseudo-vaporization used by Thurston [L^3M^{-1}]
W	Function of wall energy storage, defined by Equation 29
w_g, w_ℓ	Vapor and liquid mass flow rates [MT^{-1}]
x_2	Pseudo-quality
y	Distance coordinate in wall [L]
Z	Number of zeroes
z	Distance [L]

Greek Letters

γ	Ratio of specific heats in plenum
$\delta( )$	Perturbation variable
ζ	Distance or residence time coordinate, defined by Equation 41
λ_{12}	Length of the heavy region, = τ_{12} [L]
λ^*	Pseudo-latent heat used by Thurston
μ	Viscosity [$ML^{-1}T^{-1}$]
ξ	Tube perimeter [L]
ρ	Density [ML^{-3}]
Σ	Nyquist loop size parameter, defined in Table 14

τ_{12}, τ_{23}, τ_{13} Residence time in heavy region, light region, total test section

φ Dimensionless friction coefficient, defined in Equation A-28

$\chi_{TT,x}$ Martinelli two-phase flow parameter

Ψ Ratio of stabilizing to destabilizing pressure drops defined in Table 14

Ω Reaction frequency defined by Equation A-23

ω, ω_c Frequency in Nyquist diagram, crossover frequency

Subscripts

a Acceleration

bg Body force in light Region

ex. External

f Liquid or heavy fluid

g Vapor

h Heavy region

I Inertia

ℓ Light region

p Plenum

w Wall

o, 1, 2, 3, 4 Positions on Figure 1

Superscripts

()' Dimensioned variable

$\bar{()}$ Steady-state variable

Section 11

REFERENCES

1. Zuber, N., "Analysis of Thermally Induced Flow Oscillations in the Near Critical and Supercritical Thermodynamic Region" Final Report NAS 8-11422, Marshall Space Flight Center, Huntsville, Ala., May 1966.

2. Thurston, R. S.,"Thermal-acoustic Oscillations Induced by Forced Convection Heating of Dense Hydrogen," Los Alamos Scientific Laboratory Report LA-3543, August 1966.

3. Edeskuty, F. J., and Thurston, R. S., "Similarity of Flow Oscillations Induced by Heat Transfer in Cryogenic Systems," paper presented at Symposium on Two-Phase Flow Dynamics, Eindhoven, September 1967.

4. Zuber, N., "Flow Excursions and Oscillations in Boiling Two-phase Flow Systems with Heat Addition," paper presented at Symposium on Two-Phase Flow Dynamics, Eindhoven, September 1967.

5. Platt, G. K., and Wood, C. C., "Saturn Booster Liquid-Oxygen Heat Exchanger Design and Development," Adv. in Cryogenic Eng, Vol. 7, 1962, p. 296.

6. Crocco, L., and Cheng, S.-I., Theory of Combustion Instability in Liquid Propellent Rocket Motors, Pergamon Press, Oxford, 1956.

7. Thurston, R. S., and Rogers, J. D., "Avoidance of Thermal-acoustic Oscillations Induced by Forced Convection Film Boiling in Tubes," paper presented at American Society of Mechanical Engineers Vibrations Conference, Boston, March 1967.

8. Stenning, A. H., and Veziroglu, T. N., "Density-wave Oscillations in Boiling Freon-11 Flow," American Society of Mechanical Engineers paper 66-WA/HT-49, New York meeting, November 1966.

9. Rogers, J. D., "Oscillations in Flowing and Heated Subcritical Hydrogen," paper presented at Cryogenic Engineering Conference, Stanford August 1967; also Los Alamos Scientific Laboratory Report LA-DC-8726, August 1967.

10. Sanathanan, C. K., "On the Synthesis of Space Dependent Transfer Functions," IEEE Transactions, Vol. AC-11, 1966, p. 724.

11. Hill, W. S., and McCann, M. J., "Direct Digital Control of a Preheater for a Supercritical Fluid," Proceedings, 1966 Joint Automatic Control Conference (Seattle) June 1966, p. 754.

12. Friedly, J. C., "Asymptotic Approximations to Plug Flow Process Dynamics", Proceedings 1967 Joint Automatic Control Conference (Philadelphia) June 1967, p. 216.

13. Gilliland, E. R.; Gould, L. A; and Rinard, I. H., "A Series Method for the Analysis of Plug-flow Process Dynamics," paper presented at American Institute of Chemical Engineers meeting, February 1961.

14. Lamb, D. E., and Simkins, C. R., "Frequency Domain Analysis of Multivariable Lumped and Distributed Parameter Systems," Proceedings 1963 Joint Automatic Control Conference (Minneapolis), p. 486.

15. Koppel, L. B., "Dynamics of a Flow-forced Heat Exchanger," I/EC Fund, Vol. 1, 1962, p. 131; also "Dynamics and Control of a Class of Nonlinear, Tubular, Parametrically Forced Heat Exchangers and Chemical Reactors", I/EC Fund., Vol. 5, 1966, p. 403.

16. Bird, R. B.; Stewart, W. E.; and Lightfoot, E. N., Transport Phenomena, John Wiley & Sons, Inc., New York, 1960.

17. Campbell, D. P., Process Dynamics, John Wiley & Sons, Inc., New York, 1958.

18. Friedly, J. C., and Kroeger, P. G., "Stability Investigation of Thermally Induced Flow Oscillations in Cryogenic Heat Exchangers," First Quarterly progress report on contract NAS 8-21014, February 1967.

19. Coughanowr, D. R., Koppel, L. B., Process Systems Analysis and Control, McGraw-Hill Book Company, New York, 1965.

20. Newton, G. C.; Gould, L. A.; Kaiser, J. F., Analytical Design of Linear Feedback Controls, John Wiley & Sons Inc., 1958.

21. Ledinegg, M.; "Flow Distribution in Forced circulation Boilers," Engineer's Digest, Vol. 10, No. 3, 1949, p. 85; also in Maschinenbau and Warmerwirtschaft, Vol. 3, No. 4, 1948, p. 49.

22. Fleming, R. B. and Staub, F. W., "Investigation of the Nature of Cryogenic Fluid Flow Instabilities in Heat Exchangers," Final Report on Contract NAS 8-11422, May 1966.

23. Dittus, D. G., and Boelter, L. M. K., University of California (Berkeley) Publ. Eng., Vol. 2, 1930, p. 443.

24. "Thermodynamic-transport and Related Properties of Para-hydrogen from 36 to 5000°R at Pressure to 5000 psia," Los Alamos Scientific Laboratory Report LA-3405-MS, December 31, 1965.

25. Cleveland, J. R., Internal Letter, Rocketdyne, North American Aviation, Inc., DCR 4121-2000, January 15, 1964.

26. Thurston, R. S., "Hydrogen Heat Transfer in the Presence of Thermal Acoustic Oscillations," paper presented at the Cryogenic Engineering Conference, Stanford, California August 1967; also Los Alamos Scientific Laboratory Report LA-DC 8587, August 1967.

27. Thurston, R. S.,"The Effect of Self-induced Thermal-acoustic Oscillations on Heat Transfer to Hydrogen," Los Alamos Scientific Laboratory Report LA-3616, December 1966.

28. Williamson, K. D., Jr., Los Alamos Scientific Laboratory Report, to be published; also paper presented at AIChE meeting, New York (1967)

29. Johnson, W. J., A Compendium of the Properties of Materials at Low Temperature (Phase 1), Part 1, WADD Technical Report 60-56, 1960.

30. Shitsman, M. E., "Impairment of the Heat Transmission at Supercritical Pressures," Translation from Teplofizika Vysokikh Temperatur, Vol. 1, 1963, p. 267.

31. Friedly, J. C., and Kroeger, P. G.,"Stability Investigation of Thermally Induced Flow Oscillations in Cryogenic Heat Exchangers," Second Quarterly Progress Report on contract NAS 8-21014, May 1967.

32. Zuber, N., and Staub, F. W.,"Steady State and Transient Void Fraction in Two-phase Flow Systems,"Final Report, Program of Two-Phase Flow Investigation, GEAP 5417, January 1967.

33. Harriott, P., Process Control, McGraw-Hill Book Company, New York, 1964.

34. McAdams, W. H., Heat Transmission, McGraw-Hill Book Company, New York, 1954.

35. Richards, R. J.; Steward, W. G.; and Jacobs, R. B.,"A Survey of the Literature on Heat Transfer from Solid Surfaces to Cryogenic Fluids," Boulder Laboratories, NBS Tech. Note 122, 1961.

36. Dickinson, N. L., and Welch, C. P., "Heat Transfer to Supercritical Water," American Society of Mechanical Engineers Transactions, Vol. 80, 1958, p. 746.

37. Miropolskii, L., and Shitsman, M. E., "Heat Transfer to Water and Steam at Variable Specific Heat (in Near-Critical Region)" Sov. Phys., Tech-Phys., Vol. 2, 1957, p. 2196.

38. Bringer, R. P., and Smith, J. M., "Heat Transfer in the Critical Region," American Institute of Chemical Engineers Journal, Vol. 1, 1957, p. 49.

39. Monroe, A. G.; Bristow, H. A. S.; and Newell, J. E. "Heat Transfer to Boiling Liquids at Low Temperatures and Elevated Pressures," Journal of Applied Chemistry, Vol. 2, 1952, p. 613.

40. Hendricks, R. C.; Graham, R. W.; Hsu, Y. Y., and Madeiros, A. A., "Correlation of Hydrogen Heat Transfer in Boiling and Supercritical Pressures States," ARS Journal, Vol. 32, 1962, p. 244.

41. Hendricks, R. C.; Graham, R. W.; Hsu, Y. Y.; and Friedman, R., "Experimental Heat Transfer Results for Cryogenic Hydrogen Flowing in Tubes at Supercritical and Subcritical Pressures to 800 psia.", National Aeronautics and Space Administration, TN D-3095, 1966.

42. McCarthy, K. R., and Wolf, H., "Forced Convection Heat Transfer to Gaseous Hydrogen at High Heat Flux and High Pressure in a Smooth, Round Electrically Heated Tube.", ARS Journal, Vol. 30, 1960, p. 423.

43. Goldman, K., "Heat Transfer to Supercritical Water at 5000 psia Flowing at High Mass Rates Through Round Tubes," Int. Dev. Heat Transfer, American Society Mechanical Engineers, 1961, p. 561.

44. Griffith, J. D., and Sabersky, R. H., "Convection in a Fluid at Supercritical Pressures," ARS Journal, Vol. 30, 1960, p. 289.

APPENDIX

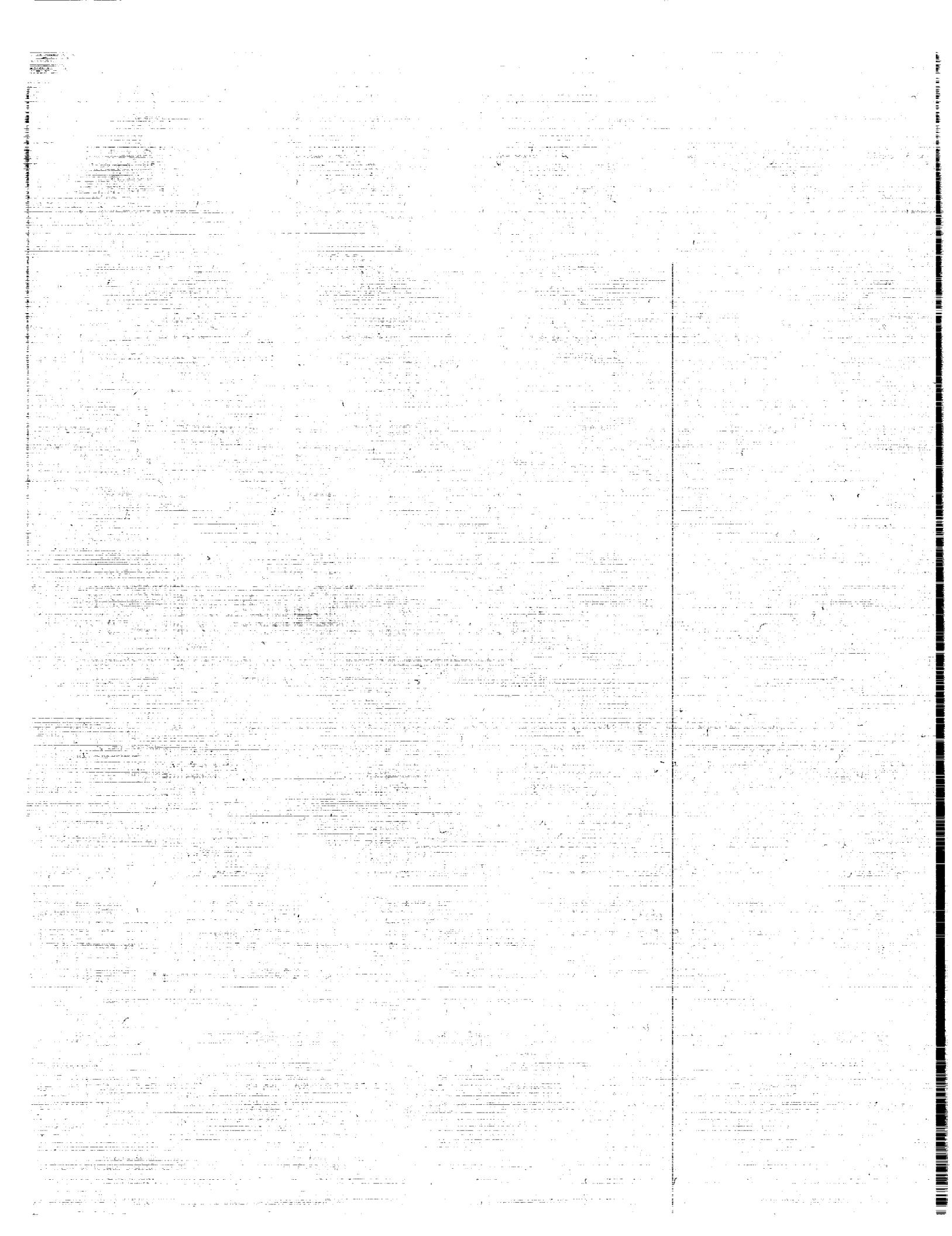

Appendix

CHARACTERISTIC EQUATIONS

The relationships derived in Section 5 to obtain the characteristic equation will be collected here. It will then be compared with Zuber's fifth and third order characteristic equations.

The characteristic equation from Equation 73 is:

$$\frac{\delta \Delta p_{o1}}{\delta u_1} + \frac{\delta \Delta p_h}{\delta u_1} + \frac{\delta \Delta p_\ell}{\delta u_1} + \frac{\delta p_3}{\delta u_1} = 0 \tag{A-1}$$

where

$$\frac{\delta \Delta p_{o1}}{\delta u_1} = 2\, k_i \tag{A-2}$$

$$\frac{\delta \Delta p_h}{\delta u_1} = (g + \varphi_{12}) \frac{\delta \lambda}{\delta u_1} + (s + 2\varphi_{12})\, \tau_{12} \tag{A-3}$$

$$\frac{\delta \Delta p_\ell}{\delta u_1} = \frac{\delta \Delta p_I}{\delta u_1} + \frac{\delta \Delta p_a}{\delta u_1} + \frac{\delta \Delta p_{bg}}{\delta u_1} + \frac{\delta \Delta p_{23}}{\delta u_1} \tag{A-4}$$

$$\frac{\delta p_3}{\delta u_1} = \frac{k_e \left[\frac{\bar{u}_3^2\, \delta \rho_3}{1 + c_3 s} + 2\, \delta u_3 \right]}{1 + \frac{c_3 s}{\gamma} \left[\frac{1 + 2 c_3 s}{1 + c_3 s} \right]} \tag{A-5}$$

and

$$\frac{\delta \Delta p_I}{\delta u_1} = s \tau_{12} \left[\frac{m_2}{m_1} \frac{A}{\delta u_1} \left(e^{m_1 \tau_{23}} - 1 \right) + \frac{m_1}{m_2} \frac{B}{\delta u_1} \left(e^{m_2 \tau_{23}} - 1 \right) \right] \tag{A-6}$$

$$\frac{\delta \Delta p_a}{\delta u_1} = \Omega \frac{\delta \lambda}{\delta u_1} + \Omega \tau_{12} \left[\left(\frac{m_2}{\Omega} + \frac{m_2}{m_1} - \frac{\Omega}{m_1} \right) \frac{A}{\delta u_1} \left(e^{m_1 \tau_{23}} - 1 \right) + \right.$$

$$\left. \left(\frac{m_1}{\Omega} + \frac{m_1}{m_2} - \frac{\Omega}{m_2} \right) \frac{B}{\delta u_1} \left(e^{m_2 \tau_{23}} - 1 \right) \right] \tag{A-7}$$

$$\frac{\delta \Delta p_{bg}}{\delta u_1} = -g \left\{ \frac{\delta \lambda}{\delta u_1} + \Omega \tau_{12} \left[\frac{A/\delta u_1}{m_1 - \Omega} \left(\frac{e^{m_1 \tau_{23}}}{\bar{u}_3} - 1 \right) + \right. \right.$$

$$\left. \left. \frac{B/\delta u_1}{m_2 - \Omega} \left(\frac{e^{m_2 \tau_{23}}}{\bar{u}_3} - 1 \right) \right] \right\} \qquad \text{(A-8)}$$

$$\frac{\delta \Delta p_{23}}{\delta u_1} = \varphi_{23} \left\{ - \frac{\delta \lambda}{\delta u_1} + \tau_{12} \left[\left(\frac{2m_2 - \Omega}{m_1 + \Omega} \right) \frac{A}{\delta u_1} \left(\bar{u}_3 \, e^{m_1 \tau_{23}} - 1 \right) + \right. \right.$$

$$\left. \left. \left(\frac{2m_1 - \Omega}{m_2 + \Omega} \right) \frac{B}{\delta u_1} \left(\bar{u}_3 \, e^{m_2 \tau_{23}} - 1 \right) \right] \right\} \qquad \text{(A-9)}$$

The expressions for $\delta\lambda$, $\delta\rho_3$, and δu_3 are given by

$$\frac{\delta \lambda}{\delta u_1} = \frac{1 - e^{-(s+W)\tau_{12}}}{s + W} \qquad \text{(A-10)}$$

$$\frac{\delta \rho_3}{\delta u_1} = \frac{\Omega \tau_{12}}{\bar{u}_3^2} \left(\frac{A}{\delta u_1} e^{m_1 \tau_{23}} + \frac{B}{\delta u_1} e^{m_2 \tau_{23}} \right) \qquad \text{(A-11)}$$

$$\frac{\delta u_3}{\delta u_1} = \tau_{12} \left(m_2 \frac{A}{\delta u_1} e^{m_1 \tau_{23}} + m_1 \frac{B}{\delta u_1} e^{m_2 \tau_{23}} \right) \qquad \text{(A-12)}$$

Other parameters are

$$A/\delta u_1 = \frac{1 - (\Omega - m_1)\, \delta\lambda/\delta u_1}{\tau_{12} (m_2 - m_1)} \qquad \text{(A-13)}$$

$$B/\delta u_2 = -\frac{1 - (\Omega - m_2)\, \delta\lambda/\delta u_1}{\tau_{12} (m_2 - m_1)} \qquad \text{(A-14)}$$

$$m_{1,2} = \frac{\mathcal{R} - s}{2} \pm \sqrt{\frac{\mathcal{R} - s}{2} + \Omega (\Omega - \mathcal{R})} \qquad \text{(A-15)}$$

$$\mathcal{R} = \Omega - \frac{1}{\bar{\rho}_{ave}} W \qquad \text{(A-16)}$$

$$W = \frac{(C_W / \mathcal{J}_W) \sqrt{s \mathcal{J}_W} \tanh \sqrt{s \mathcal{J}_W}}{1 + (\mathcal{J} / \mathcal{J}_W) \sqrt{s \mathcal{J}_W} \tanh \sqrt{s \mathcal{J}_W}} \qquad \text{(A-17)}$$

$$\bar{\rho}_{ave} = \frac{1 + \bar{\rho}_3}{2} \qquad \text{(A-18)}$$

Some steady-state relations required are

$$\bar{\rho}_3 = 1/\bar{u}_3 \tag{A-19}$$

$$\bar{u}_3 = 1 + \Omega\,(1 - \tau_{12}) \tag{A-20}$$

$$\tau_{23} = \frac{\ln \bar{u}_3}{\Omega} \tag{A-21}$$

To evaluate the characteristic equation, Equation A-1, with the set of Equations A-2 to A-21, twelve dimensionless parameters are required. These are τ_{12}, Ω, k_e, k_i, c_3, γ, φ_{12}, φ_{23}, g, C_w, $\mathcal{J}$, and $\mathcal{J}_w$. These are defined in terms of more readily available experimental parameters.

$$\tau_{12} = \frac{i_2' - i_1'}{i_3' - i_1'} = \frac{i_2' - i_1'}{q'\,\xi'\,\ell'}\,A_c'\,\bar{\rho}_1'\,\bar{u}_1' \tag{A-22}$$

where the choice of i_2' is discussed in Section 7.

$$\Omega = \left(\frac{\partial v'}{\partial i'}\right)_p \frac{q'\,\xi'\,\ell'}{A_c'\,\bar{u}_1'} \tag{A-23}$$

$$k_e = \frac{\bar{\rho}_3'\,\bar{\rho}_3'}{(\bar{\rho}_1'\,\bar{u}_1')^2} \tag{A-24}$$

$$k_i = \frac{\Delta p_{01}'}{\bar{\rho}_1'\,u_1'^2} \tag{A-25}$$

$$c_3 = \frac{V'}{A_c'\,\ell'}\,\frac{\bar{\rho}_3'}{\bar{\rho}_1'} \tag{A-26}$$

$$\gamma = (c_p'/c_v') \text{ at position 3} \tag{A-27}$$

$$\varphi_{12} \text{ or } \varphi_{23} = \frac{f\,\ell'}{2D'} \tag{A-28}$$

$$g = \frac{g'\,\ell'}{u_1'^2} \tag{A-29}$$

$$C_w = \frac{A_w'\,\rho_w'\,c_w'}{A_c'\,\bar{\rho}_1'\,c_p'} \tag{A-30}$$

$$\mathcal{J} = \frac{A_w'\,\rho_w'\,c_w'}{h'\,\xi'} \tag{A-31}$$

$$\mathcal{J}_w = \frac{\ell_w'\,\rho_w'\,c_w'}{k_w'}\,\frac{\bar{u}_1'}{\ell'} \tag{A-32}$$

COMPARISON WITH ZUBER'S FIFTH-ORDER CHARACTERISTIC EQUATION

Zuber's most general fifth-order equation[1] can be written when there is no plenum, i.e., $c_3 = 0$, just as Equation A-1. The pressure drops, Equations A-2 to A-5, are also the same for Zuber's fifth-order equation. The difference comes only in the pressure drops in the test section in Equations A-6 and those following. For Zuber's fifth-order equation these expressions are:

$$\frac{\delta \Delta P_I}{\delta u_1} = s\,\tau_{12}\,(\Omega - s)\frac{B}{\delta u_1}\,\tau_{23} \tag{A-33}$$

$$\frac{\delta \Delta p_a}{\delta u_1} = -\Omega\frac{\delta \lambda}{\delta u_1} + \Omega_{12}\left[-\frac{\Omega}{\Omega - s}\,\frac{A}{\delta u_1}\left(e^{(\Omega - s)\tau_{23}} - 1\right) - s\frac{B}{\delta u_1}\,\tau_{23}\right] \tag{A-34}$$

$$\frac{\delta \Delta p_{bg}}{\delta u_1} = -g\left\{\frac{\delta \lambda}{\delta u_1} + \Omega\,\tau_{12}\left[-\frac{1}{s}\,\frac{A}{\delta u_1}\left(\frac{e^{(\Omega - s)\tau_{23}}}{\bar{u}_3} - 1\right) - \frac{1}{\Omega}\,\frac{B}{\delta u_1}\left(\frac{1}{u_3} - 1\right)\right]\right\} \tag{A-35}$$

$$\frac{\delta \Delta p_{23}}{\delta u_1} = \varphi_{23}\left\{-\frac{\delta \lambda}{\delta u_1} + \tau_{12}\left[\frac{-\Omega}{2\Omega - s}\,\frac{A}{\delta u_1}\left(\bar{u}_3\, e^{(\Omega - s)\tau_{23}} - 1\right) + \right.\right.$$

$$\left.\left. + \frac{\Omega - 2s}{\Omega}\,\frac{B}{\delta u_1}\,(\bar{u}_3 - 1)\right]\right\} \tag{A-36}$$

$$\frac{\delta \lambda}{\delta u_1} = \frac{1 - e^{-s\tau_{12}}}{s} \tag{A-37}$$

$$\frac{\delta \rho_3}{\delta u_1} = \frac{\Omega \tau_{12}}{\bar{u}_3^2}\left(\frac{A}{\delta u_1}\,e^{(\Omega - s)\tau_{23}} + \frac{B}{\delta u_1}\right) \tag{A-38}$$

$$\frac{\delta u_3}{\delta u_2} = \tau_{12}\,(\Omega - s)\,\frac{B}{\delta u_1} \tag{A-39}$$

$$A/\delta u_1 = \frac{1 - s\,\delta\lambda/\delta u_1}{\tau_{12}\,(s - \Omega)} \tag{A-40}$$

$$B/\delta u_1 = -\frac{1 - \Omega\,\delta\lambda/\delta u_1}{\tau_{12}\,(s - \Omega)} \tag{A-41}$$

Zuber's fifth-order equation has been written this way to emphasize the similarity between it and the results from the current model. The equations compare term by term. The only difference is that Zuber assumed the wall heat capacity zero, making $W = 0$. By taking $W = 0$ in Equations A-6 to A-17 it may be immediately shown that

$$\mathcal{R} = \Omega$$

$$m_{1,2} = \Omega - s,\ 0$$

and Equations A-33 to A-41 follow immediately from Equations A-6 to A-14. In a sense, then, the current model may be thought of as a fifth-order exponential polynomial. Only the radicals in $m_{1,2}$ and the expression for W keeps it from being one.

ZUBER'S THIRD-ORDER CHARACTERISTIC EQUATION

Zuber's third-order characteristic equation differs from the fifth-order only in the expressions for the acceleration, body force, and friction pressure drops in the light region, Equations A-34 to A-36. These were simplified by letting the velocity $\bar{u} = \bar{u}_3$ while integrating these pressure drop perturbations across the light region. The resulting expressions are:

$$\frac{\delta \Delta p_a}{\delta u_1} = -\Omega \frac{\delta \lambda}{\delta u_1} + \Omega \tau_{12} \left[\frac{-\Omega (1 - \tau_{12})}{\bar{u}_3} \frac{A}{\delta u_1} e^{(\Omega - s)\tau_{23}} - s \frac{B}{\delta u_1} \tau_{23} \right] \qquad \text{(A-42)}$$

$$\frac{\delta \Delta p_{bg}}{\delta u_1} = -g \left\{ \frac{\delta \lambda}{\delta u_1} - \Omega \tau_{12} \left[\frac{-\tau_{23}}{\bar{u}_3} \frac{A}{\delta u_1} e^{(\Omega - s)\tau_{23}} - \frac{1}{\Omega} \frac{B}{\delta u_1} \left(\frac{1}{\bar{u}_3} - 1 \right) \right] \right\} \qquad \text{(A-43)}$$

$$\frac{\delta \Delta p_{23}}{\delta u_1} = \varphi_{23} \left\{ -\frac{\delta \lambda}{\delta u_1} + \tau_{12} \left[-\frac{\bar{u}_3 - 1}{2 u_3 \Omega} \frac{A}{\delta u_1} e^{(\Omega - s)\tau_{23}} + \right. \right.$$

$$\left. \left. + \frac{\Omega - 2s}{\Omega} \frac{B}{\delta u_1} (\bar{u}_3 - 1) \right] \right\} \qquad \text{(A-44)}$$

where the remaining expressions are the same as before.

Comparing Equations A-42 to A-44 with Equations A-34 to A-36 shows that factors of $1/s$, $1/(\Omega - s)$, and $1/(2\Omega - s)$ have been eliminated from the second terms. The omission of the latter two result in the lowering of the order of the characteristic equation by two orders in s. Also, it may be readily shown by comparing any of the three Equations A-42 to A-44 with its fifth-order counterpart, that the third-order equation has a pole at $s = \Omega$. The fifth does not. As shown in Section 8 this leads to difficulties for the third-order equation.

DISTRIBUTION LIST FOR FINAL REPORT

Copies	Recipient	Designee
	NASA Marshall Space Flight Center Huntsville, Alabama 35812	
1	Office of Technical Information, M-MS-IPC	(x)
1	Purchasing Office, PR-CH	(x)
1	Patent Office, M-PAT	(x)
1	Keith Chandler, R-P&VE-PA	(x)
4	Chief, Liquid Propulsion Technology, RPL Office of Advanced Research and Technology NASA Headquarters Washington, D. C. 20546	(x)
25	NASA Scientific and Technical Information Facility P. O. Box 33 College Park, Maryland 20740	(x)
1	Mr. Vincent L. Johnson Director, Launch Vehicles and Propulsion, SV Office of Space Science and Applications NASA Headquarters, Washington, D. C. 20546	(x)
1	Mr. Edward Z. Gray Director, Advanced Manned Missions, MT Office of Manned Space Flight NASA Headquarters, Washington, D. C. 20546	(x)
1	Mr. Clarence A. Syvertson Mission Analysis Division NASA Ames Research Center Moffett Field, California 24035	(x)
1	(Technical Monitor) Max E. Nein R-P&VE-PT Marshall Space Flight Center Huntsville, Alabama 35812	(x)

NASA FIELD CENTERS

Copies	Recipient	Designee
2	Ames Research Center Moffett Field, California 94035	Harold Hornby Mission Analysis Div.
2	Goddard Space Flight Center Greenbelt, Maryland 20771	Merland L. Moseson Code 620
2	Jet Propulsion Laboratory California Institute of Technology 4800 Oak Grove Drive Pasadena, California 91103	Henry Burlage, Jr. Propulsion Div., 38
2	Langley Research Center Langley Station Hampton, Virginia 23365	Dr. Floyd L. Thompson Director
2	Lewis Research Center 21000 Brookpark Road Cleveland, Ohio 44135	Dr. Abe Silverstein Director
2	Marshall Space Flight Center Huntsville, Alabama 35812	Hans G. Paul Code R-P&VED
2	Manned Spacecraft Center Houston, Texas 77001	Dr. Robert R. Gilruth Director
2	Western Operations Office 150 Pico Boulevard Santa Monica, California 90406	Robert W. Kamm Director
2	John F. Kennedy Space Center, NASA Cocoa Beach, Florida 32931	Dr. Kurt H. Debus

GOVERNMENT INSTALLATIONS

Copies	Recipient	Designee
1	Aeronautical Systems Division Air Force Systems Command Wright-Patterson Air Force Base Dayton, Ohio 45433	D. L. Schmidt Code ASRCNC-2
1	Air Force Missile Development Center Holloman Air Force Base, New Mexico	Maj. R. E. Bracken Code MDGRT
1	Air Force Missile Test Center Patrick Air Force Base, Florida	L. J. Ullian
1	Air Force Systems Division Air Force Unit Post Office Los Angeles 45, California	Col. Clark Technical Data Center
1	Arnold Engineering Development Center Arnold Air Force Station Tullahoma, Tennessee	Dr. H. K. Doetsch
1	Bureau of Naval Weapons Department of the Navy Washington, D. C.	J. Kay RTMS-41
1	Defense Documentation Center Headquarters Cameron Station, Building 5 5010 Duke Street Alexandria, Virginia 22314 ATTN: TISIA	
1	Headquarters, U.S. Air Force Washington 25, D. C.	Col. C. K. Stambaugh AFRST
1	Picatinny Arsenal Dover, New Jersey 07801	I. Forsten, Chief Liquid Propulsion Laboratory, SMUPA-DL
1	Air Force Rocket Propulsion Laboratory Research and Technology Division Air Force Systems Command Edwards, California 93523	RPRR/Mr. H. Main

GOVERNMENT INSTALLATIONS

Copies	Recipient	Designee
1	U. S. Atomic Energy Commission Technical Information Services Box 62 Oak Ridge, Tennesse	A. P. Huber Oak Ridge Gaseous Diffusion Plant (ORGDP) P. O. Box P
1	U. S. Army Missile Command Redstone Arsenal Alabama 35809	Dr. Walter Wharton
1	U. S. Naval Ordnance Test Station China Lake California 93557	Code 4562 Chief, Missile Propulsion Div.

CPIA

1	Chemical Propulsion Information Agency Applied Physics Laboratory 8621 Georgia Avenue Silver Spring, Maryland 20910	Neil Safeer

INDUSTRY CONTRACTORS

Copies	Recipient	Designee
1	Aerojet-General Corporation P. O. Box 296 Azusa, California 91703	L. F. Kohrs
1	Aerojet-General Corporation P. O. Box 1947 Technical Library, Bldg. 2015, Dept. 2410 Sacramento, California 95809	R. Stiff
1	Aeronautronic Philco Corporation Ford Road Newport Beach, California 92663	D. A. Carrison
1	Aerospace Corporation 2400 East El Segundo Boulevard P. O. Box 95085 Los Angeles, California 90045	John G. Wilder MS-2293 Propulsion Dept.
1	Arthur D. Little, Inc. 20 Acorn Park Cambridge, Massachusetts 02140	E. Karl Bastress
1	Astropower Laboratory Douglas Aircraft Company 2121 Paularino Newport Beach, California 92663	Dr. George Moc Director, Research
1	Astrosystems International, Inc. 1275 Bloomfield Avenue Fairfield, New Jersey 07007	A. Mendenhall
1	Atlantic Research Corporation Edsall Road and Shirley Highway Alexandria, Virginia 22314	A. Scurlock
1	Beech Aircraft Corporation Boulder Division Box 631 Boulder, Colorado	J. H. Rodgers
1	Bell Aerosystems Company P.O. Box 1 Buffalo, New York 14240	W. M. Smith

INDUSTRY CONTRACTORS

Copies	Recipient	Designee
1	Bendix Systems Division Bendix Corporation 3300 Plymouth Road Ann Arbor, Michigan	John M. Brueger
1	Boeing Company P. O. Box 3707 Seattle, Washington 98124	J. D. Alexander
1	Missile Division Chrysler Corporation P. O. Box 2628 Detroit, Michigan 48231	John Gates
1	Wright Aeronautical Division Curtiss-Wright Corporation Wood-Ridge, New Jersey 07075	G. Kelley
1	Missile and Space Systems Division Douglas Aircraft Company, Inc. 3000 Ocean Park Baulevard Santa Monica, California 90406	R. W. Hallet Chief Engineer Advanced Space Tech.
1	Aircraft Missiles Division Fairchild Hiller Corporation Hagerstown, Maryland 10	J. S. Kerr
1	General Dynamics/Astronautics Library & Information Service (128-00) P. O. Box 1128 San Diego, California 92112	Frank Dore
1	Re-Entry Systems Department General Electric Company 3198 Chestnut Street Philadelphia, Pennsylvania 19101	F. E. Schultz
1	Advanced Engine & Technology Dept. General Electric Company Cincinnati, Ohio 45215	D. Suichu
1	Grumman Aircraft Engineering Corp. Bethpage, Long Island New York	Joseph Gavin

INDUSTRY CONTRACTORS

Copies	Recipient	Designee
1	Ling-Temco-Vought Corporation Astronautics P. O. Box 5907 Dallas, Texas 75222	Warren C. Trent
1	Lockheed California Company 2555 North Hollywood Way Burbank, California 91503	G. D. Brewer
1	Lockheed Missiles and Space Co. ATTN: Technical Information Center P. O. Box 504 Sunnyvale, California 94088	Y. C. Lee
1	Lockheed Propulsion Company P. O. Box 111 Redlands, California 92374	H. L. Thackwell
1	The Marquardt Corporation 16555 Saticoy Street Van Nuys, California 91409	Warren P. Boardman, Jr.
1	Baltimore Division Martin Marietta Corporation Baltimore, Maryland 21203	John Calathes (3214)
1	Denver Division Martin Marietta Corporation P. O. Box 179 Denver, Colorado 80201	J. D. Goodlette (A-241)
1	McDonnell Aircraft Corporation P. O. Box 516 Municipal Airport St. Louis, Missouri 63166	R. A. Herzmark
1	Space & Information Systems Division North American Aviation, Inc. 12214 Lakewood Boulevard Downey, California 90241	H. Storms

INDUSTRY CONTRACTORS

Copies	Recipient	Designee
1	Rocketdyne (Library 586-306) North American Aviation, Inc. 6633 Canoga Avenue Canoga Park, California 91304	E. B. Monteath
1	Northrop Space Laboratories 3401 West Broadway Hawthorne, California	Dr. William Howard
1	Astro-Electronics Division Radio Corporation of America Princeton, New Jersey 08540	S. Airweather
1	Reaction Motors Division Thiokol Chemical Corporation Denville, New Jersey 07832	Arthur Sherman
1	Republic Aviation Corporation Farmingdale Long Island, New York	Dr. William O'Donnell
1	Space General Corporation 9200 East Flair Avenue El Monte, California 91734	C. E. Roth
1	Stanford Research Institute 333 Ravenswood Avenue Menlo Park, California 94025	Lionel Dickinson
1	TRW Systems Group One Space Park Redondo Beach, California 90278	G. W. Elverum
1	TAPCO Division TRW, Incorporated 23555 Euclid Avenue Cleveland, Ohio 44117	P. T. Angell
1	Thiokol Chemical Corporation Huntsville Division Huntsville, Alabama	John Goodloe

INDUSTRY CONTRACTORS

Copies	Recipient	Designee
1	Research Laboratories United Aircraft Corporation 400 Main Street East Hartford, Connecticut 06108	Erle Martin
1	United Technology Center 587 Methilda Avenue P. O. Box 358 Sunnyvale, California 94088	B. Abelman
1	Aerospace Operations Walter Kidde and Company, Inc. 567 Main Street Belleville, New Jersey 07109	R. J. Hanville Director of Research Engineering
1	Florida Research and Development Pratt and Whitney Aircraft United Aircraft Corporation P. O. Box 2691 West Palm Beach, Florida 33402	R. J. Coar
1	Rocket Research Corporation 520 South Portland Street Seattle, Washington 98108	Foy McCullough, Jr.